THE MODULATION OF SHORT WAVES RIDING ON NON-UNIFORM VELOCITY FIELDS (SOLITARY WAVES AND LONG WAVES)

I-FAN SHEN

DOCTOR OF PHILOSOPHY

UNIVERSITY OF EDINBURGH

JULY 1994

DECLARATION

This thesis has been composed by myself and, except where stated, is entirely of my own research.

ACKNOWLEDGEMENTS

I would like to thank the following people for their help and advice on the work. Dr. W.J. Easson and Prof. C.A. Greated, my supervisors, encourage and support me with their patience in my Ph.D. study. They also open the interesting fields in fluid dynamics and wave mechanics for me to approach and to enjoy. Dr. W.A.B. Evans and Dr. Kai-ming She are kind of sharing their numerical programmes to be used in this thesis, and Mr. Wei-Dong Peng gives me many mathematical and methodological advices as well as his kind friendship.

I was supported by Overseas Research Student Awards (ORS) and Cowan House Scholarships for two years. I express thanks and appreciation to the two bodies.

Finally I would like to thank my parents and my sister, for their support and encouragement. During these three and half years, they have paid enormous attention to my work. Lian, my wife, shares my feeling in getting through this Ph.D. work. To them the thesis is dedicated.

ABSTRACT

This work studies the modulation and kinematics of short waves riding on non-uniform velocity fields (solitary waves and long waves) and achieves theoretical and experimental conclusions.

For the interactions between short waves and solitary waves, short waves and long waves, this research shows that the wavenumber, frequency and amplitude of short waves riding on solitary waves and long waves are strongly modulated. It also demonstrates that the maximum values of the modulated short wavenumber, frequency, and amplitude always occur at the crests of solitary waves and long waves. By increasing either the amplitudes of solitary waves or the steepnesses of long waves the main conclusion--- that the modulated short wavenumber, frequency, and amplitude increase on the crest of solitary waves and long waves--- is achieved.

The kinematics of two component waves (short waves and long waves) has been measured by PIV (Particle Image Velocimetry). Comparison of the results with linear theory and various stretching methods is also carried out.

The mechanism of the modulation of short waves riding on solitary waves or long waves, as studied in this thesis, provides a useful base line for work on more general and complex local water wave breaking.

Contents

Declaration i

Acknowledgments ii

Abstract iii

1 Introduction. 1

1.1 General Description of Wave Interaction 1

1.2 Literary Review 6

1.3 Aims 12

1.3.1 Mathematical Aspect: development of a mathematical model and determination of the modulation of short waves riding on non-uniform velocity fields 15

1.3.2 Experimental Aspect: combination of water motion from short waves and long waves and prediction of kinematics within waves 16

2 Mathematical Wave Theories. 19

2.1 Introduction 19

2.1.1 Basic Assumptions 20

2.1.2 Governing Equations 21

2.2 Solitary Waves 24

2.3 Stokes' Waves 25

2.4 Linear Theory and Modified Methods 26

2.4.1 Linear Theory 26

2.4.2 Modified Methods 27

2.4.2.1 Linear Extrapolation 28

2.4.2.2 The Wheeler Stretching Method 29

2.4.2.3 The Chakrabarti Stretching Method 31

2.4.2.4 The Superposition Stretching Method 31

2.4.2.5 The Delta Stretching Method 32

2.5 The Boundary Integral Method 33

2.6 Regions of Validity 34

3 Short Wave Modulation by Non-Uniform Velocity Fields. 38

3.1 Introduction 38

3.2 The Modulation Theory 42

3.2.1 Governing Equation for Short Waves Riding on a Solitary Wave 42

3.2.2 Governing Equations in Orthogonal Curvilinear Co-ordinates 43

3.2.3 Multiple-Scale Perturbation Method 46

3.2.4 The Nonlinear Schrödinger Equation and Wave Action Conservation 47

3.2.5 The Numerical Scheme for Solitary Waves 48

3.2.6 The Modulation of Short Waves Riding on a Long Solitary Waves 51

3.2.7 Numerical Results 54

3.3 Discussions 60

4 Experimental Facilities for Water Waves. 63

4.1 The Wave Tank and the Wave Generator 63

4.1.1 Wave Tank 63

4.1.2 Wavemaker 64

4.1.3 Wave Generation Software 65

4.1.4 Reflection and Resonance 66

4.2 Surface Measurement Techniques: Wave Gauges 67
4.3 Internal Kinematics Measurement 69
4.3.1 The Particle Image Velocimetry Acquisition 69
4.3.1.1 Camera, Lens and Film 71
4.3.1.2 Laser and Scanning Beam System 73
4.3.2 PIV Acquisition Errors and Limitations 75
4.3.2.1 System Error in the Scanning Beam System 75
4.3.2.2 System Error in Time Between Pulses 76
4.3.3 The PIV Analysis System 78
4.3.3.1 Young's Fringe and Autocorrelation Calculation . 78
4.3.4 PIV Analysis Errors and Limitations 83
5 Short Wave Modulation by Long Waves. 86
5.1 Introduction 86
5.2 The Modulation: Frequency 88
5.2.1 Experimental Frequency Modulation 100
5.2.2 Theoretical Approaches 107
5.2.3 Comparisons 114
5.3 Kinematics of Waves 115
5.3.1 Comparisons with Linear Theory 117
5.3.2 Comparisons with the Wheeler Stretching Method 119
5.3.3 Comparisons with the Chakrabarti Stretching Method 121
5.3.4 Comparisons with the Superposition Stretching Method .. 122
5.3.5 Comparisons with the Time-Stepping Technique 124
5.3.6 Comparisons Between Theories 128

6 Further Work. 130

6.1 The Stability of Solitary Waves 131

6.2 Internal Solitary Waves 133

6.2.1 Governing Equations 134

6.2.1.1 Generalized Stokes' Formula 136

6.2.1.2 Green's Theorem 137

6.2.1.3 Constrained Flat-Topped Internal Solitary Waves 140

7 Conclusion. 142

7.1 Summary 143

7.1.1 The Modulation of Short Waves 144

7.1.1.1 The Modulation of Short Waves Riding on a long solitary wave 144

7.1.1.2 The Modulation of Short Waves Riding on long regular waves 144

7.1.2 Wave Kinematics 145

7.1.2.1 Kinematics of Monochromatic Long Waves 146

7.1.2.2 Kinematics of Short Waves Riding on Long Waves 147

7.1.2.3 General Assessment of Wave Modelling 147

7.2 Suggestions for Further Research 148

Bibliography. 151

Appendix A The Conservations. 159

A.1 The Phase Conservation 159

A.2 The Conservation of Wave Action 161

A.3 Dean's Stream Function 162

Chapter 1

INTRODUCTION

1.1 General Description of Wave Interaction

Scientists have long been trying to understand the mechanics of the ocean, particularly the motion of waves, currents and tides. In the past the main reason for this scientific pursuit has been the safety of ships. Recently, in coastal and offshore engineering, some urgent tasks have been encountered: the design of offshore oil rigs, problems of coastal erosion and impact, and so on. The need to understand and interest in the mechanics of waves has greatly increased. In particular the study of water wave interaction plays an important role in oceanography and coastal engineering. The design of offshore structures is significantly affected by the perceived impact of extreme storm environmental loading which is even more unpredictable in multi-component wave interaction. Although for any space-frame structure the calculation of the

extreme wave loading is likely to be dominated, according to the universally used Morison's equation (Morison et al. 1950), by a drag term proportional to the square of the calculated local wave velocity, the large discrepancy in local velocities occurs from the contribution of high-frequency waves. From another point of view, the recent development of remote sensing from satellites is used to measure the ocean wave spectrum. Also microwave radar images of the ocean surface give a mapping of wind speed. Therefore, based on the improvement of the empirical methods, the demand for a sound knowledge of wave interaction has been stimulated so as to ensure the integrity of offshore structures, the safety of the personnel manning them and the safety design of oil platforms. Analyzing wave energy exchange quantitatively resulted from wave interaction is also necessary. Meanwhile, the measurement of wave kinematics plays a key role in the development of the mathematical theories of wave kinematics and wave loading models used in the design of offshore structures. Furthermore kinematics of extreme waves and wave interaction are particularly relevant to the extreme loading case.

Without doubt, the accurate prediction of the kinematics of irregular ocean surface waves is essential to offshore and coastal engineering, and it is also a challenging and sophisticated task in the study of nonlinear wave mechanics. Usually particle velocities in irregular waves have been approximated using the fast Fourier transform (FFT) spectral method. This is a traditional method used to linearly decompose the record of wave elevations into many regular component waves and superpose kinematics of such regular waves. Unfortunately, the process of linear decomposition and superposition ignores the nonlinear interaction of waves.

Part of this thesis can be treated as a basic study of the interaction between two monochromatic waves, a short wavetrain and a long wavetrain. Such interaction forms the simplest case in irregular waves. A previous doctoral work undertaken by Sutherland (1992) considered a similar interaction, in which his two monochromatic waves are comparable.

In recent years there has been great interest in the study of the interaction of short waves riding on long waves (Zhang and Melville 1990). The evolution of short waves, generated both by wind and by gravity, riding on long ocean waves or currents has also long been an area of active research in wave mechanics (Miller, Shemdin and Longuet-Higgins 1991). While short waves riding on long waves are modulated by and interact with long waves, they tend to break on the crest of the long waves. By the breaking forms of spilling and plunging, they then transfer momentum to long waves. More detailed quantitative knowledge of the modulation of short waves, and of energy transfer to long waves, is required to understand the processes by which energy is relocated to the ocean surface.

This thesis will discuss the modulation of short waves riding on non-uniform velocity fields. Long waves can be treated as one of specific non-uniform velocity fields for short waves riding on. There are two main reasons for studying mechanics of short waves riding on non-uniform velocity fields. Firstly, short waves can be considered as infinitesimal perturbations of deformed free surfaces. From the mathematical point of view, such perturbations can be linearized on the free surfaces and further derivation and discussion have been made (Zhang and Melville 1990). Secondly, large discrepancies are found between predicted and measured velocities near the

free surface, where the contribution is from the large wavenumber (high frequency) tail of the wave spectrum. An explanation of such discrepancies is called for.

Basic Description of Waves

A basic description of waves can be helpful as a starting point in considering their behaviour in other complicated cases. Those most commonly used are described below:

Solitary waves form a useful limit, that where the period tends to infinity and the necessarily two-dimensional wave is fully described by its height to depth ratio and the bed slope (usually zero). Solitary waves with long troughs and peaky crests are totally different from periodic waves. This is a mainly mathematical limit though the shoaling of small steep waves comes into this category.

Shallow water waves are taken to be those in which the water depth is small compared to the wavelength, that is when their ratio is less than 1/20. The cnoidal theory is designed for describing shallow water waves.

Deep water waves are taken to be where the depth to wavelength ratio exceeds 1/2. In this limit the sea bed can be ignored, thus slope and depth become irrelevant and the waves are completely defined by their period, amplitude and direction.

Monochromatic waves are waves of a single period. They are purely sinusoidal having only an infinitesimal amplitude. Finite-amplitude monochromatic waves can be artificially reduced to many sinusoidal components, which means a fundamental period wave followed with a series of harmonics. These harmonics are termed 'bound harmonics'. To avoid confusion, the term 'monochromatic' is used rather than single period.

Two-component waves are two monochromatic waves. In this thesis, the two monochromatic waves embody two different characteristics: one is the high-frequency waves, i.e. short waves, and the other is the low-frequency waves, i.e. long waves. Small-wavelength disturbances may ride on large-amplitude long gravity waves, as orbital velocities of fluid particles provide a variable surface current through which the short waves propagate.

Meanwhile, the non-uniformed current is comparable with the propagation velocity of the short waves relative to the long ones; actually their interaction is no longer weak. This is true of non-uniformed currents where the entire effect is that of a shift in reference frame and a subsequent Doppler shift in the short wave period. Short waves may be either gravity or capillary waves. In this thesis short waves are gravity waves; capillary waves generated by surface tension are beyond the study of this thesis.

Fourier approach (Fast Fourier Transform FFT) is usually assumed to be a linear model. It analyses the sea state in terms of the sinusoidal components from time series of the surface, and transfers the wave energy from time domain into frequency domain. The fully spectral description includes energy as well as phase information and the direction of travel of each component. This is an assumption made in many measurements of sea spectra. Energy at any frequency is taken to represent a free wave of that frequency. However, much of the higher order harmonic energy is actually associated with the bound harmonics of lower frequency fundamental waves (Laing 1986).

Spectral models based on substantial quantities of real sea data have been developed to predict the two-dimensional form of any sea state as functions of the wind fetch and history (The SWAMP Group 1985). The two models most

widely used are Pierson and Moskowitz (1964) and the JONSWAP (Hasselman et al. 1973). For waves of, or above, moderate height, non-linear effects become very important. Some properties, such as the description of the behaviour of the high crest, including the internal kinematics given by the simpler models, are entirely inadequate. Further modification, based on FFT, such as stretching, is desirable.

Conservation of wave energy: a general concept appears to be conservation of 'wave action', which in the simplest linear cases is energy flux divided by an appropriate frequency. The conservation of wave action is originally given by an average variational principle and is a general result valid when involving slowing varying media. The average variational principle involves a Lagrangian and takes the variations of the variational equations averaged by one wavelength, i.e. averaged-Lagrangian equation.

1.2 Literary Review

With the general description of waves as the starting point for all modelling in the above section, there are three substantial simplifications: (i) wave interaction behaviour can be studied separately from the interaction of wind and waves, and of structures and waves; (ii) the water is assumed to be an inviscid and incompressible fluid of uniform density; (iii) waves are assumed to be gravity waves by ignoring the effects of surface tension.

Unna (1941, 1942) first attacked the problem and came to the striking conclusion that for the modulation of secondary (short) waves riding on primary (long)

waves; the short waves become shorter in wavelength and larger in amplitude on the crests of the long waves; and conversely, become both longer and smaller on the troughs of the long waves. That is, the steepnesses of short waves are steeper on the crest and flatter on the trough of the long waves.

The studies of interaction for one short wavetrain riding on a long wavetrain became active almost thirty years ago. Short waves riding on long waves can be viewed as if they are travelling on currents with a varying horizontal velocity field, provided that the wavelength ratio of long waves to short waves is significant.

Longuet-Higgins and Stewart (1960, 1964) based their approach on the weakly nonlinear wave assumption. They first explored the interaction between a linear short wavetrain and a weakly nonlinear long wavetrain by using the perturbation method. The phenomenon was first predicted by using the perturbation method (Longuet-Higgins and Stewart 1960) based on the assumption that both short and long waves are weakly nonlinear. The phenomenon was also found in investigating the superharmonic instability (disturbances with short wavelength) of a finite-amplitude periodic wavetrain (Longuet-Higgins 1978 a). Even in the ideal situation, namely, in the absence of wind, viscosity and wave breaking, the analysis of the interaction between finite-amplitude short and long waves is still very complicated (Phillips 1979). Phillips (1981) and Longuet-Higgins (1987) computed the modulation of linear short waves riding on a finite-amplitude long wave. Based on the assumption of small wavelength ratio, Phillips (1981) extended the study of Longuet-Higgins and Stewart (1960) to a long wave with finite amplitude and applied the wave action conservation theory to a short wave riding on a finite-amplitude long wave.

Whitham (1965) first introduced the theory of the conservation of wave action. Bretherton and Garrett (1968) applied the wave action conservation theory to study the modulation of short waves travelling on long waves. Their results confirmed the modulation of a short wave on a long wave by Longuet-Higgins and Stewart (1960, 1964). As the velocity field of a finite-amplitude long wave can be accurately computed through the numerical schemes developed by Schwartz (1974), the modulation of the short wave on the finite-amplitude long wave can be quantitatively predicted, with the assumption that the envelope of the short wave amplitude is steady with respect to the long wave surface. Although the long wave is of finite amplitude in Phillips' study (1981), the short wave is essentially linear.

Most related work concentrated on the modulation of short waves riding on long waves. References on the topic of short waves riding on long solitary waves are very scarce. So far, most of theoretical and experimental research investigation has been focused on how short waves may be trapped by internal waves, see Hughes and Grant (1978), Lewis, Lake and Ko (1974) and Kwoh, Lake and Rungaldier (1988). However, it is expected that the mechanism of short waves riding on long solitary waves is similar to that of short waves riding on internal waves.

Gargett and Hughes (1972) showed that short gravity waves may be trapped by long internal waves, thus caustic formation and local wave breaking may occur. The study by Shen, Evans, Easson and Greated (1994) gave the modulation of short waves riding on a long free-surface solitary wave and provided a new insight into local wave breaking.

West, Brueckner and Janda (1987) employed a set of free surface boundary conditions (Zakharov 1968) and expanded a numerical technique developed by Watson and West (1975) for solving the nonlinear partial differential equations describing the evolution of wave interaction. They used this technique to compute the simplest case of interaction between strongly nonlinear short and finite-amplitude long waves with a ratio of 8 in wavenumber and amplitude. Short wave amplitude was smaller than long wave amplitude. From their numerical computation they arrived at two main conclusions. Firstly, the location of the maximum modulation of short waves may be unsteady instead of being fixed at the crest of the long wave. Secondly, short waves appear to be phase locked to the long waves instead of being free travelling waves.

The two conclusions above in the paper by West, Brueckner and Janda (1987) were questioned by Zhang (1987). He pointed out the contradiction caused by different assumptions made in studying long and short wave interactions. The different assumptions provided acceptable explanations to the contradictions mentioned above and the Watson-West method used by West, Brueckner and Janda (1987) was based on Taylor's expansion which was powers of wave amplitude (or wave slope) at the calm water level. The expansion may be poor if waves of quite different wavelengths and amplitudes were present. Therefore, the poor convergence of the Taylor's expansion was expected in the context of long and short wave interactions. It is possible that their observations may result from the poor convergence in evaluating the vertical velocity at the free surface. But from another point of view, the computations of West, Brueckner and Janda (1987) considered the wave slopes of short and long waves to be 0.314 and 0.157 respectively, these being strongly nonlinear. However, their numerical technique included both resonant and non-resonant random wave interaction.

Unfortunately, Zhang (1987) did not report any numerical correction for supporting his criticism. Nevertheless the combination of the Hamiltonian system and probabilistic methods in approaching the dynamical system of complicated wave motions in open seas is suitable.

Zhang and Melville (1990) studied the steady modulation of weakly nonlinear short waves riding on a finite-amplitude long wave taking into account the surface tension. The instability of short waves riding on long waves has been discussed by Zhang and Melville (1992). They adapted the nonlinear Schrödinger equation which was derived in the paper of Zhang and Melville (1990). Furthermore, the study of the stability of a short wavetrain riding on a long wavetrain shows that the strong assumption of the steady envelope of the short wave amplitude is valid when the short wave train is weakly nonlinear. Naciri and Mei (1992) also studied the stability of short waves riding on long waves, but they gave another Schrödinger equation and applied the inverse transformation to the nonlinear Schrödinger equation. The comparison between the stability of both cases is not clear, since different assumptions and simplifications have been employed in both studies.

Besides these theoretical approaches, there are also a few experimental studies discussing on the modulation of short waves riding on long waves.

Zhang, Randall and Spell (1991) measured a regular and a two-component wave field and compared the results to Wheeler stretching, linear extrapolation and a nonlinear numerical scheme developed in the paper of Zhang and Melville (1990). The two-component waves were generated by the separate generation of two monochromatic wavetrains. The higher frequency (short) waves were generated first and were then overtaken by the low frequency (long) waves. The

periods and amplitudes were in the ratio 1:3 with the higher frequency having the lower amplitude. The wave profiles and kinematics were measured using wave gauges and LDA. Linear theory and the Wheeler stretching method were calculated from the measured wave spectrum.

In contrast to their findings in the regular wave case, they found and concluded that Wheeler stretching underpredicted crest and trough velocities and linear extrapolation and numerical theory (Zhang and Melville 1990) were very close to the measured results for the regular case; Wheeler stretching and linear theory were more accurate and linear extrapolation overestimated crest and trough velocities significantly for the two-component case. In the regular wave case the cut-off frequency was chosen to exclude the second and higher harmonics. For the two-component waves the cut-off frequency was just above double the higher frequency. The higher harmonics shall make a real contribution to wave kinematics in deep water depending on the bandwidth of spectrum of the sea being measured, the choice of filter cut-off frequency therefore plays an important role.

Miller, Shemdin and Longuet-Higgins (1991) and Chu, Long and Phillips (1992) studied steady wind-generated short waves riding on long wave groups. They all concluded and confirmed the short wind-generated waves are strongly modulated by long wave groups, i.e. the steepness of short waves are a function of the long wave phase when wind-generated short waves are riding on the long waves. The results of Miller, Shemdin and Longuet-Higgins (1991) were compared with the linear and non-dissipative theory of Longuet-Higgins and Stewart (1960), which described the modulation of short wave groups by long waves as due to the orbital motions of the long waves. The theory fitted the experiments well while the short waves were not too steep; i.e. the wind speed was well below 10 ms^{-1}. In the

work of Chu, Long and Phillips (1992), they described pre-existing statistically steady wind waves which were taken over by long wave groups. The long wave groups were mechanical-generated. Their frequency range of short wind-generated waves was from 2.5 Hz to 7.5 Hz depended on the fetch.

1.3 Aims

The purpose for the research presented here lies in the desire to determine the modulation of short waves riding on any given non-uniform velocity fields (long waves and solitary waves). The present work approaches the interaction of weakly nonlinear short waves riding on non-uniform velocity fields both in shallow water (solitary waves) and deep water (long waves). As the previous analyses cannot be applied to study the modulation of a weakly nonlinear short wavetrain travelling on a long solitary wave with finite amplitude, the study in this thesis reveals useful guidelines for the formulation of the relevant numerical scheme. Also it may provide the quantitative information which might then be used to check the corresponding numerical computation.

There are three main reasons for the present work. Firstly, the recent development of remote sensing from satellites makes it possible to measure the ocean wave spectrum and infer the wind velocity from microwave radar images of the ocean surface. Accurate measurements require more detailed quantitative knowledge of the modulation of short waves. The new technique in remote-sensing to detect, from Synthetic Aperture Radar (SAR), radar waves Bragg-scattered by the sea free surface in the range from a few centimetres (X-band) to

a few metres (L-band), makes it possible to measure wave interaction phenomena in the ocean. From the empirical point of view the images of microwave radar on the ocean surface also help in an understanding of the interaction between wind and waves (Allan 1983; Stewart 1985). It is important to have a sound knowledge of oceanographic wave interaction in order to understand the exchange of energy among waves. Usually, multi-component waves have been approximated by using the fast Fourier transform (FFT) spectral method, which linearly decomposes the time series of wave elevation into monochromatic waves and superposes the kinematics of such monochromatic waves (Sutherland, Easson and Greated 1990). Under the linear wave superposition assumption, the nonlinear wave interaction is not clear. Therefore, the long-term objectives are to understand in depth the nonlinear interaction of two-component waves and of multi-component finite-amplitude waves.

Secondly, in this world there is a large proportion of oil reserves situated below the sea bed in areas of deep and unpredictable wave environment. Even though the technology to build offshore structures exists, the design procedure has to make very large allowances for the uncertainty in the environmental loading because of the interaction of waves. There are also several other sources of uncertainty resulting from wave motions. The aim of this present research is to reduce these uncertain factors by increasing the knowledge of free surface fluid mechanics and the behaviour of wave interaction in particular.

Thirdly, the mathematical modelling of wave breaking behaviour is an area of active research. For example, an initial long wave is deformed by applying a non-uniform dynamic pressure distribution on the free surface with time-stepping technique (Longuet-Higgins and Cokelet 1976). Meanwhile some methods of

extrapolation are in favour of the more extreme measured waves and do not directly describe the mechanics of breaking (Department of Energy 1986). From another point of view, the distinction between spilling and plunging breakers is noted by Longuet-Higgins (1987) who mentioned the former being caused by short waves travelling forward to long waves, and the latter by perturbations of short waves travelling in the opposite direction of long waves. The design method does not include the mechanics of breaking. Also the mechanics of short waves riding on long waves and the instability of steep long waves are believed to be of the same family of breaking. These would have to include studies which focus on the factors causing wave breaking.

The occurrence of breaking is a limited case which determines the extreme wave conditions at any location. The extreme sea state is the result of the energy balance between incoming wind force and outgoing dissipation through breaking. This is particularly important in the extrapolation of wave height. If the data includes waves that are predominantly non-breaking, then the extrapolation will not reflect the effect of wave breaking. Only if the extrapolated wave height exceeds either 0.78 times the water depth, or 0.143 times the wave length is the design wave thought to be breaking. It is worth noting that it is precisely because waves in storms do break and they do not have heights in excess of the above limits which cause them to be regarded in design as non-breaking (Kuo and Kuo 1974). The breaking of extreme waves is a source of concern to offshore designers. Therefore the mechanism of local wave breaking and caustics is still worth approaching.

The present research bears on both mathematical and experimental aspects of this problem of short waves riding on non-uniform velocity fields (solitary waves and long regular waves).

1.3.1 Mathematical Aspect: development of a mathematical model and determination of the modulation of short waves riding on non-uniform velocity fields

The flow of the non-uniform velocity field can be considered as potential flow. Consequently the free surface of the non-uniform velocity field is treated as a streamline in the conformal mapping plane when the non-uniform velocity field is in steady state, if short waves are not imposed. In the presence of short waves, it is assumed that the velocity field and profile of non-uniform velocity fields are subject to a very small perturbation. Therefore, the free surface boundary conditions constituted by short waves and the non-uniform velocity fields can be expanded along the surface of the non-uniform velocity field. That means the expansion is on the calm water level of the mapping plane. In this thesis solitary waves in shallow water and long waves in deep water are chosen as the non-uniform velocity fields. Furthermore using the traditional multi-scale perturbation method, a non-linear Schrödinger equation is derived to describe the evolution of the short wavetrain riding on the non-uniform velocity field (solitary waves and long waves). Furthermore, a simplification of the nonlinear Schrödinger equation results in a conservation of wave action. Based on the conservations of wave action and phase, the short wave modulation by a non-uniform velocity field is determined. Besides, there are two strong assumptions in discussing the short wave modulation: 1) solitary waves and long waves are weakly nonlinear, i.e. solitary waves and long waves are of finite amplitude, and short waves are linear, and 2) the envelope of the short wave amplitude is steady (time-invariant) with respect to the surface of solitary waves and long waves.

1.3.2 Experimental Aspect: combination of water motion from short waves and long waves and prediction of kinematics within waves

The two-component waves generated by the wavemaker are linearly superposed. It is assumed from signal inputs that there is negligible interaction between the two. The combination of short waves with long waves is an area where laboratory work is necessary. Before this work there was no systematic laboratory study of internal kinematics within the interaction between short waves and long waves. Some mathematical models can incorporate the interaction of short waves with long waves, but it is most critical in the extreme high crest region where breaking makes the flow behaviour difficult to measure and model.

First, the wave elevations are recorded by a wave gauge for the cases of long waves, and short waves riding on long waves. The wave records will be used in a function fitting scheme for short wave frequency modulation and also be used in fast Fourier transform for predicting wave kinematics. Full detailed descriptions will be shown in Chapter 5. Secondly, the role of wave kinematics research cannot be overestimated in the development of offshore design practice. In fact the general theoretical development of fluid kinematics has consistently relied on measurements for verification and simulated areas of research. In fluid dynamics the flow velocity is the most useful physical property; whiles many devices, such as Pitot tubes, hot-wire anemometers and Laser Doppler Anemometry, have been used to provide point velocity measurements in the past. Also accurate experimental data has rarely been obtained near the crest of long waves, and they are in this region that velocities and free surface errors are greatest; therefore this is the most important region in the calculation of wave-induced forces. Therefore, part of the aim of this research is to test current theoretical predictions (linear

theory, the stretching methods and the time-stepping technique are concerned in this study) and to accurately measure kinematics close to the free surface. The chosen method is to make a set of accurate measurements of wave kinematics on different combinations of design waves using the particle image velocimetry technique developed at Edinburgh. These measurements of wave kinematics concentrate on the crest region of long waves, considering whether or not short waves exist, and cover a number of different wave conditions.

In Chapter 2 there is a basic introduction for various contemporary mathematical models of design waves including solitary waves, Stokes' waves, linear theory and stretching modifications, the time-stepping method and then a discussion for the validity of various theory. In Chapter 3, by following the methodology given by Zhang and Melville (1990), orthogonal curvilinear coordinates are applied to study the modulation of a weakly nonlinear short wavetrain riding on a long solitary wave with finite amplitude. Using the multi-scale perturbation method, the nonlinear Schrödinger equation describing the evolution of the short wavetrain riding on the long solitary wave is derived. With the assumption of the steady envelop of the short wave amplitude and the conservation of the short wave action, the modulation of short waves riding on a long solitary wave is derived. The modulation contains the modulated short wave frequency, wavenumber and amplitude. Chapter 4 is the introduction for the experimental facilities which have been used in this thesis including wave gauges and the particle image velocimetry technique (PIV). PIV is the only experimental technique used for wave internal kinematics. All experimental results and theoretical comparisons are shown in Chapter 5. There are two sections shown in Chapter 6. Both sections are treated as extensions of this thesis work. The first section is to discuss the stability of solitary waves using the normal-mode

technique. The other section of Chapter 6 is to derive a new numerical scheme of internal solitary waves. Chapter 7 gives the summary and conclusions of the modulation of short waves riding on non-uniform velocity fields (solitary waves and long waves).

Here as presented below, is an outline of the main research objectives that helps constructing this work:

- To investigate the theoretical modulation of short waves riding on long solitary waves. Using the concept of conformal mapping, a nonlinear Schrödinger equation will be derived for describing a narrow-banded short wavetrain riding on a long solitary wave. Also a linear conservation of wave action can be given by approximating the nonlinear Schrödinger equation. By applying the steady-state conservations of wave phase and wave action, the modulated short wavenumber, frequency and amplitude will demonstrate how short waves are strongly modulated by a long solitary wave.

- To investigate the modulation of short waves riding on long regular waves from both the experimental and theoretical point-of-views. The theoretical aspect for the modulation of short waves riding on long regular waves is similar to that of short waves riding on a long solitary wave.

- To measure the kinematics within regular waves and within two-component waves, short waves and long waves, by the particle image velocimetry (PIV) technique, and to carry out assessment on linear theory, various stretching methods (the Wheeler, Chakrabarti and superposition stretching methods) and the time-stepping technique in predicting wave kinematics.

Chapter 2

MATHEMATICAL WAVE MODELLING

2.1 Introduction

The Chapter introduces contemporary wave theories in terms of their ability to represent the physical aspects of real waves. The regions of validity for the theories used are discussed in Section 2.6.

This chapter can be regarded as a background to Chapter 5. In Sections 2.2 and 2.3 there are basic introductions of solitary waves and Stokes' waves. Both waves are treated as the non-uniform velocity fields of shallow water waves and deep water waves in the modulation of short waves riding on them. Linear theory (Section 2.4), which deals with small perturbation on still water, is strictly applicable to waves of small amplitude, and provides some good results for surface properties, e.g. dispersion relation. Also a detailed introduction is given

for several commonly used stretching methods in Section 2.4. The boundary integral method is a well-known numerical scheme to simulate and describe plunging breaking waves. This method (Section 2.5) is applied to a parallel computing simulation scheme of numerical wave tanks as developed by She, Greated and Easson (1992) and mounted on AMT Distributed Array Processors (DAP) 608. This is a supplement to kinematics comparisons, as demonstrated in Section 5.3, of various modified theories for monochromatic long waves.

2.1.1 Basic Assumptions

The problem is that of describing gravity waves (interfacial gravity waves) which are travelling along the interface of two fluids of different densities in a uniform gravitational field. The density of the upper fluid (like air) is infinitesimal to that of the lower fluid (like water). Therefore the upper fluid is taken as influencing the lower fluid only through the static pressure it applies at the interface. Such waves are defined as surface waves. The lower fluid is assumed to be inviscid, incompressible and irrotational. An intention to discuss waves (internal waves) between two fluids with comparable densities will appear in Chapter 6.

First the flow can be represented by the velocity potential, as a direct assumption of the above characteristics, i.e. inviscid, incompressible and irrotational characteristics, of the water. The velocity of the fluid is by definition the gradient of the velocity potential. Traditionally either the velocity potential or the stream function, forms the basis for all wave models. They obey Laplace's equation and consequently have a useful property: once either the velocity potential or the stream function is known on the boundary of a potential flow, then any of the two is uniquely defined everywhere within the interior of the

fluid. Thus, for waves under the assumption of potential theory if the velocity potential is known at the free surface and on the bed, and the end boundary conditions can be specified, then the potential and the velocities can be calculated everywhere within the wave. Also a wave train is identical when travelling over a flat bed. That is, periodic boundary conditions can be assumed. The wave propagation will not change its form and the static pressure along the free surface keeps constant.

2.1.2 Governing Equations

Navier-Stokes equations (2.1~2.3) were derived as the equations of motion of a Newtonian fluid. The derivation can be found in textbooks of fluid mechanics.

$$\frac{Du}{Dt} = -\frac{1}{\rho}\frac{\partial}{\partial x}(p+\rho gh) + \nu\nabla^2 u \qquad \text{(EQ 2.1)}$$

$$\frac{Dv}{Dt} = -\frac{1}{\rho}\frac{\partial}{\partial y}(p+\rho gh) + \nu\nabla^2 v \qquad \text{(EQ 2.2)}$$

$$\frac{Dw}{Dt} = -\frac{1}{\rho}\frac{\partial}{\partial z}(p+\rho gh) + \nu\nabla^2 w \qquad \text{(EQ 2.3)}$$

where $\vec{u}$ = (u,v,w) represents the velocity vector and t is time.

ρ, p, ν and h are density, dynamic pressure, kinematic viscosity, and height above a horizontal datum line.

The principle of continuity is equal to the conservation of mass which means the divergence of the velocity vector being zero Eqn. (2.4). The rotational vector can be given by the curl of the velocity vector Eqn. (2.5).

$$\nabla \bullet \vec{u} = \frac{\partial u}{\partial x} + \frac{\partial v}{\partial y} + \frac{\partial w}{\partial z} = 0 \qquad \text{(EQ 2.4)}$$

$$\nabla \times \vec{u} = (2\omega_x, 2\omega_y, 2\omega_z) \qquad \text{(EQ 2.5)}$$

$$\omega_x = \frac{1}{2}\left(\frac{\partial w}{\partial y} - \frac{\partial v}{\partial z}\right) \qquad \text{(EQ 2.6)}$$

$$\omega_y = \frac{1}{2}\left(\frac{\partial u}{\partial z} - \frac{\partial w}{\partial x}\right) \qquad \text{(EQ 2.7)}$$

$$\omega_z = \frac{1}{2}\left(\frac{\partial v}{\partial x} - \frac{\partial u}{\partial y}\right) \qquad \text{(EQ 2.8)}$$

where ω_x, ω_y and ω_z are the components of the rotation vector (and give the intensity of the vorticity). The subscripts x, y and z represent the directions of the rotation vector.

The fluid can also be assumed to be irrotational, that is to say that the angles between diagonals of the fluid element structure keep constant during motion. Mathematically this can be expressed as

$$\omega_x = \omega_y = \omega_z = 0 \qquad \text{(EQ 2.9)}$$

Thus, no generation or loss of vorticity is allowed. From Cauchy-Riemann's equations Potential theory is applicable to potential flow. If the flow is assumed to be irrotational then it is possible to define a continuous, differentiable scale function, a potential function of position and time. So the gradients of the potential function satisfy the irrotational condition automatically. The gradients of the velocity potential, as is known, give the flow velocity at that time and place, i.e.

$$u = \frac{\partial \phi}{\partial x}, \; v = \frac{\partial \phi}{\partial y}, \; w = \frac{\partial \phi}{\partial z} \qquad \text{(EQ 2.10)}$$

Moreover, substituting into the continuity equation (2.4) results in a second order linear differential equation which is known as Laplace's equation:

$$\nabla^2\phi = \frac{\partial^2\phi}{\partial x^2} + \frac{\partial^2\phi}{\partial y^2} + \frac{\partial^2\phi}{\partial z^2} = 0 \qquad \text{(EQ 2.11)}$$

Laplace's equation (2.11) is the governing field equation. Any specified solution for it requires appropriate boundary conditions. These boundary conditions are the bed condition and the free surface kinematic and dynamic boundary conditions. The bed condition assumes that no flow crosses a flat horizontal bottom boundary at the bed (z=0 is the still water level, and h is the water depth);

$$\frac{\partial\phi}{\partial z} = 0 \text{ at } z = -h \qquad \text{(EQ 2.12)}$$

At the free surface (air/water interface) the kinematic boundary condition states that any particle at the free surface ($z = \eta(x, y, t)$) will not leave it. Mathematically this can be represented by Eqn. (2.13):

$$\frac{\partial\phi}{\partial z} = \frac{\partial\eta}{\partial t} + u\frac{\partial\eta}{\partial x} + v\frac{\partial\eta}{\partial y} \qquad \text{(EQ 2.13)}$$

Using the irrotational condition, the dynamic boundary condition can be determined from Bernoulli's equation (2.14):

$$\phi_t + \frac{1}{2}(\phi_x^2 + \phi_y^2 + \phi_z^2) + g\eta = 0, \text{for } z = \eta \qquad \text{(EQ 2.14)}$$

where in this case the subscript denotes differentiation. This equation (2.14) may also be derived from the unsteady Navier-Stokes' Equation by assuming irrotationality and no kinematic viscosity, expressing velocities in terms of the velocity potential and then integrating with respect to the spatial co-ordinates

Although Laplace's equation is linear, it is difficult to solve because its two free boundary conditions are fully nonlinear. The following sections aim to discuss some well-known models of water waves. In fact there are many mathematical models of waves, which vary in complex computation from the linear, sinusoidal

approximation, to the time-stepping methods which can model overturning waves with fast parallel computing.

2.2 Solitary Waves

Two models, cnoidal waves and solitary waves, are suitable and applicable to the waves in shallow water. The cnoidal method uses and takes the wave profile (measured vertically up from the mean water level) given by a general and complex Jacobian elliptical function. The first approximation from KdV equations was developed by Kortweg and de Vries (1895). Their attempt was to replace trigonometric functions in the representation of wave motion. In particular shallow waves with their peaky crests and long shallow troughs have obviously non-sinusoidal surface profiles. The waves with small amplitude and long wavelength limits were discussed by Boussinesq (1871) and Rayleigh (1876). These are two important limits that tie solitary waves with other periodic wave representations.

Solitary waves may be regarded as the limiting case of cnoidal waves for which the wavelength is infinitely long. Scott-Russell (1844) first introduced the phenomenon of shallow water waves and called 'the wave of translation'. Like the sinusoidal wave approach, the solution forms of solitary waves can be explored as the basis of an expansion method; for example, Fenton (1972 and 1979) extended the solution form to any high order. Byatt-Smith (1970) showed the 120° Stokes' cusp of the maximum wave and Stokes' formula. The most notable works for solitary waves were by Byatt-Smith (1970) and Evans and Ford

(1994). Both papers gave their own exact solutions for their respective integral equations. The more detailed discussion of free surface solitary waves will appear in Chapter 3. Solitary waves form the non-uniform velocity field used for the modulation.

2.3 Stokes' Waves

Stokes' waves are a kind of basic solution to the design wave problem. The method works by expressing the velocity potential, or the stream function, as a truncated Taylor's series expansion, which is called Stokes' series, in sinusoidal function of the horizontal coordinate. The dynamic boundary condition is applied by substituting terms of the velocities and the elevation derived from the series expansion of the velocity potential. These expressions are subsequently simplified by excluding all terms of higher order than that previously chosen for the expansion parameter in the expression of the velocity potential.

The work is involved in the mathematical manipulation for a set of nonlinear equations which are constituted by the expansion coefficients. The evaluation of the coefficients for higher orders from the set of nonlinear equations is based on the Newton-Raphson method. Originally Stokes (1847) developed the general case for second order and the simplified deep water case for third order. This has led to the very widespread use of Stokes' fifth in engineering practice. Using newly available computing resources the extension to high order has been presented by Schwartz (1974). Based on the high order expansions, subharmonic and superharmonic phenomena have been discussed (Longuet-Higgins 1978 a, b).

The instability of Stokes' waves has also been shown both in deep and shallow water by a numerical scheme of normal-mode perturbations of finite-amplitude Stokes' waves, McLean (1982 a, b). In large amplitude Stokes' waves, the two-dimensional instability (Benjamin-Feir type, Benjamin and Feir 1967) will become a three-dimensional perturbation, McLean (1982 a, b). A similar discussion for the stability of free surface solitary waves, which is also based on normal-mode perturbation, will appear in Chapter 6.

2.4 Linear Theory and Modified Methods

2.4.1 Linear Theory

This theory was first developed by Airy (1845), called Airy waves, it uses the assumption that the wave amplitude is much smaller than both the wavelength and the still water depth h. Both of the nonlinear free surface boundary conditions can become linear by discarding all terms above the first order of Taylor's expansions in wave amplitude. Explicitly, the linear free surface boundary conditions are:

$$\eta_t = \Phi_z \text{ at } z = 0 \qquad \text{(EQ 2.15)}$$

$$\Phi_t + g\eta = 0 \text{ at } z = 0 \qquad \text{(EQ 2.16)}$$

If the free surface elevation is periodic Eqn. (2.17) and the variables are separated in the velocity potential, then it transpires that the velocity potential has a periodic component Eqn. (2.18), that is:

$$\eta = Ae^{i(kx-\omega t)} \qquad \text{(EQ 2.17)}$$

$$\Phi = Z(z)\, e^{i(kx-\omega t)} \qquad \text{(EQ 2.18)}$$

These linear boundary conditions, Eqns. (2.15) and (2.16), are then applied at the still water level and they lead to the following results:

Velocity potential:

$$\Phi = -A\frac{ig}{\omega}\frac{\cosh(kz)}{\cosh(kh)}e^{i(kx-\omega t)} \qquad \text{(EQ 2.19)}$$

Linear dispersion relation:

$$\omega^2 = gk\tanh(kh) \qquad \text{(EQ 2.20)}$$

These results are only strictly applicable to infinitesimally small amplitude waves. In particular, the linear dispersion relation gives a basic assumption for other complicated wave circumstances, such as random seas.

2.4.2 Modified Methods

Linear theory is only valid for small-amplitude waves up to still water level and a kinematic prediction for finite-amplitude waves is required. Therefore, there is a need to modify linear theory in order to predict the kinematics of finite-amplitude waves on crests as well as on troughs. Furthermore there is a phenomenon known as high frequency contamination with a large tail of the wave spectrum whose contribution to kinematics is more intractable. Also short waves are waves of high frequency which may be said to be riding on top of long finite-amplitude waves. This leads to very high contribution from high frequency components in the long wave crests. So the contribution of short waves will lead to much larger discrepancy. Therefore a further explanation is needed. Only short gravity waves are covered in this thesis.

Before introducing the modification of linear theory for finite-amplitude waves, it is necessary to explain the traditional spectral method (FFT). Using a Fourier transform, a two dimensional wave elevation Eqn. (2.17) can be decomposed into a summation of single-component waves.

$$\eta_L(x,t) = \sum_{i=1}^{\infty} \eta_i(x,t) = \sum_{i=1}^{\infty} a_i \cos\theta_i \qquad \text{(EQ 2.21)}$$

$$\Phi_L(x,z,t) = \sum_{i=1}^{\infty} \Phi_i(x,z,t) = \sum_{i=1}^{\infty} g\frac{a_i}{\omega_i}\frac{\cosh k_i(z+d)}{\cosh k_i d}\cos\theta_i \qquad \text{(EQ 2.22)}$$

$$u_L(x,z,t) = \sum_{i=1}^{\infty} u_i(x,z,t) = \sum_{i=1}^{\infty} a_i\omega_i\frac{\cosh k_i(z+d)}{\sinh k_i d}\cos\theta_i \qquad \text{(EQ 2.23)}$$

$$w_L(x,z,t) = \sum_{i=1}^{\infty} w_i(x,z,t) = \sum_{i=1}^{\infty} a_i\omega_i\frac{\sinh k_i(z+d)}{\sinh k_i d}\sin\theta_i \qquad \text{(EQ 2.24)}$$

where $\theta_i = k_i x - \omega_i t + \delta\theta_i$ and the subscript L represents linear theory. $\delta\theta_i$ is the initial phase of the component wave with index i.

2.4.2.1 Linear Extrapolation

The simplest modified method is linear extrapolation that is taking a sinusoidal profile of the required amplitude and assuming that the expressions derived for the infinitesimal wave are transformable at all positions within the finite-amplitude wave. Performing a Taylor's series expansion about still water level allows values to be calculated up to an elevation. Linear extrapolation is applicable in the region under the long wave crests and above the still water level and is a modification of linear theory, which assumes that the vertical partial derivative of a kinematic variable is a constant above the still water level. The value of velocity at the surface is then:

$$u_{ex}(x, z, t) = u(x, 0, t) + z\frac{\partial}{\partial z}u(x, 0, t) \text{ for } 0 < z < \eta \qquad \text{(EQ 2.25)}$$

The vertical velocity w_{ex} has a similar equation of Eqn. (2.25) from (2.24).

Apparent discrepancies between measured and predicted linear theory values led Wheeler (1969) to suggest the first of several stretching approximations to linear theory. What is 'stretching'? Generally speaking, it is a co-ordinate transformation from mean water level to the instantaneous water level. There are four frequently used stretching methods:

2.4.2.2 The Wheeler Stretching Method

The stretching approximation of Wheeler (1969) is a linear filtering technique. The Wheeler stretching method maps the vertical co-ordinate z onto a computational vertical co-ordinate z_{ws}. This method assumes that the finite sinusoidal profile for each phase of the wave is stretched in the vertical direction so that the top value defined for z=0 becomes the value at the surface of the wave. All the values within the wave are similarly shifted.

It avoids the problems of high frequency contamination by stretching the vertical co-ordinate z so that the velocity value previously calculated for the still water level is now calculated for the surface. All other vertical co-ordinates are stretched or compressed from the bed by using the same transformation in z, namely:

$$z_{ws} + d = (z + d)\frac{d}{d + \eta} \qquad \text{(EQ 2.26)}$$

In deep water

$$z_{ws} = z \qquad \text{(EQ 2.27)}$$

$(z + d)\, d/(\eta + d)$ is an effective height which is always less than mean water level. It is the same ratio to mean water height as the actual height z to the free

surface. This is to reduce velocities above mean water level and to enhance velocities below mean water level. Forristall (1985) suggested that the results of the Wheeler stretching method provides a lower kinematic boundary condition error than linear wave theory does.

Therefore the equation for horizontal velocity (2.23) becomes:

$$u_{ws}(x, z, t) = \sum_{i=1}^{\infty} u_i(x, z_{ws}, t) = \sum_{i=1}^{\infty} a_i \omega_i \frac{\cosh k(z_{ws} + d)}{\sinh k_i d} \sin\theta_i \qquad \text{(EQ 2.28)}$$

The subscript ws denotes calculation by the Wheeler stretching method. The vertical velocity is derived using the same substitution. Figure 2.1 shows the diagram comparing linear theory, linear extrapolation and the Wheeler stretching method.

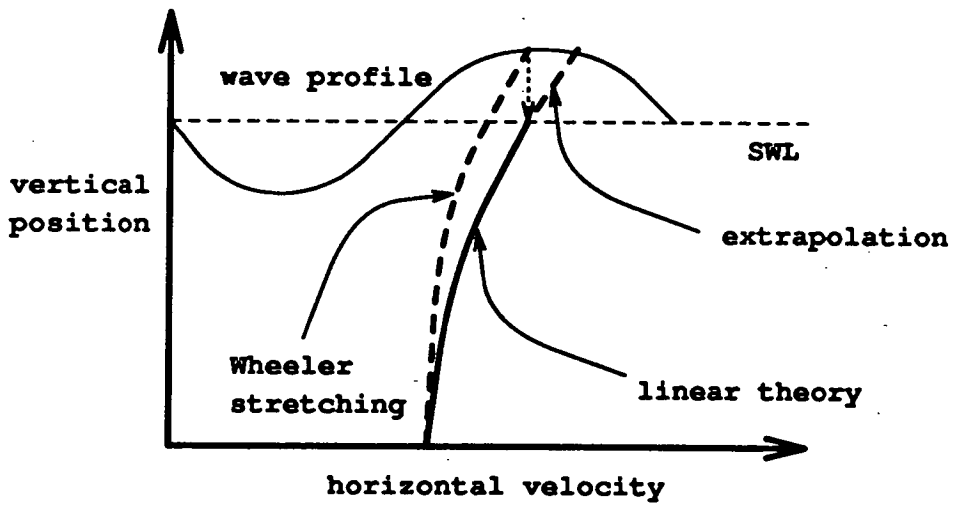

Fig. 2.1: Sketch for comparing linear theory with linear extrapolation and the Wheeler stretching method.

2.4.2.3 The Chakrabarti Stretching Method

The expression for the dynamic pressure term, which is derived from linear theory, is only valid for z<0. Inversely in the dynamic boundary condition the dynamic pressure term is not valid for z>0. Chakrabarti (1971) suggested that the dynamic pressure term should be changed so that a new expression for the dynamic pressure completely and exactly satisfies the dynamical boundary condition in any position within waves. The transformation in this case is in the denominator of the depth decay term of (2.22), (2.23) and (2.24), is

$$d_{cs} = \eta + d \qquad \text{(EQ 2.29)}$$

It results in a velocity potential of

$$\Phi_{cs}(x, z, t) = \sum_{i=1}^{\infty} g \frac{a_i}{\omega_i} \frac{\cosh k_i (z + d)}{\cosh k_i d_{cs}} \sin\theta_i \qquad \text{(EQ 2.30)}$$

This leads to an expression for the horizontal component of velocity u_{cs} given by:

$$u_{cs}(x, z, t) = \sum_{i=1}^{\infty} a_i \omega_i \frac{\cosh k_i (z + d)}{\sinh k_i d_{cs}} \cos\theta_i \qquad \text{(EQ 2.31)}$$

The vertical velocity is derived from using the same approximations.

2.4.2.4 The Superposition Stretching Method

This is a direct modification from linear theory and Wheeler stretching. Pawsey and Dello Stritto (1983) noted that while Wheeler stretching suppresses the extrapolation of high frequency components well above their region of theoretical applicability, it also suppresses the extrapolation of the dominant wave in an irregular sea state above the still water level. Each component wave is extended up to its own wave component amplitude. So it is proposed that each component could be stretched up to its instantaneous wave elevation rather than

stretching waves to the still water level. In other words instead of the elevations being altered in the ratio like Eqn. (2.26) in the calculation of the velocity potential, horizontal velocity and etc., it could be altered in the ratio, given in Eqn. (2.32). Both authors called the technique superposition stretching. The transformation in the vertical co-ordinate is

$$z_{ss} + d = (z + d)\frac{d + \eta_i}{d + \eta} \qquad \text{(EQ 2.32)}$$

where the subscript ss denotes superposition stretching and η_i is given by Eqn. (2.21). The velocity potential and horizontal component of velocity become:

$$\Phi_{ss}(x, z, t) = \sum_{i=1}^{\infty} \Phi_i(x, z_{ss}, t) = \sum_{i=1}^{\infty} g\frac{a_i}{\omega_i}\frac{\cosh k_i(z + d)\,(\frac{d + \eta_i}{d + \eta})}{\cosh k_i d}\sin\theta_i \qquad \text{(EQ 2.33)}$$

$$u_{ss}(x, z, t) = \sum_{i=1}^{\infty} u_i(x, z_{ss}, t) = \sum_{i=1}^{\infty} a_i\omega_i\frac{\cosh k_i(z + d)\,(\frac{d + \eta_i}{d + \eta})}{\sinh k_i d}\cos\theta_i \qquad \text{(EQ 2.34)}$$

The vertical velocity is derived using the same transformation.

2.4.2.5 The Delta Stretching Method

Linear theory, linear extrapolation and the above-mentioned stretching methods provide different validities to wave kinematics with respect to a lower bound and an upper bound, see Rodenbusch and Forristall (1986). They suggested combining the two bounds for predicting wave kinematics and they called such a combination 'delta stretching', in order to reduce the error.

The most commonly used stretching approximations have been detailed in the above paragraphs. No one can say which stretching method is better than any other, or indeed whether any of them are appropriate.

2.5 The Boundary Integral Method

The present model developed by She, Greated and Easson (1992) is established on the basis of the boundary integral method based on Green's Theorem with intention to model a laboratory wave flume. The boundary is set as the fluid boundary in a two-dimensional wave tank. The wave tank dimensions and geometries are the inputs to fit various environments. It has the advantage of a direct analogy between a numerical model and a real wave flume. Therefore such numerical simulation is close to the study of two-dimensional waves in the laboratory.

The work by Longuet-Higgins and Cokelet (1976) was the first successful numerical simulation in overturning steep gravity waves by the pressure variation of Bernoulli's equation on the free surface. Some of the most notable subsequent works is that of Dold and Peregrine (1985).

A two-dimensional numerical wave tank has been set up on AMT DAP-608 with the same dimensions as those of the short wave tank at Edinburgh. Two-dimensional waves are generated by a hinged wave maker at one end of the wave flume and are absorbed by a damper at the other end. In this thesis the model has been used to simulate long monochromatic waves, which are low frequency waves, for comparing with experimental measurements by PIV, but it is not successful in simulating the case of short waves riding on long monochromatic waves, because the local slope becomes too high during the simulation.

2.6 Regions of Validity

The different wave theories outlined above were derived under specific circumstances and assumption. The question of the most accurate solution for a given circumstance is important yet difficult to answer. In fact, there is no universal model for all design waves. Either a mathematical or empirical method has been used to establish the validity of its own wave theory. Ideally their predictions of internal kinematics should be compared with full scale waves over a range of conditions.

It is important to know which validity of the various water wave theories to apply to a particular problem, where the wave characteristics and water depth are specified. For example, should we prefer linear theory or the cnoidal theory? In fact the validity consists of two aspects: the mathematical verification and the physical verification. The mathematical validity is the ability of any given wave theory to satisfy the mathematically posed boundary condition problem. For example, the cnoidal theory only approximately satisfies Laplace's equation. Stokes' waves and solitary waves satisfy the dynamic free surface boundary approximately.

On the other hand, the physical validity refers to how well the predictions of the various theories agree with the actual measurements. It is difficult to draw a short conclusion regarding the physical validity due to the physical design and real measurement requirements. Experimental verification is usually performed by comparing the measured and the predicted values of the kinematics within the wave.

The validity of various wave theories has been examined by Dean (1970) and Le Méhauté (1976). Explicit comparisons between measured and theoretical results have been also made: Le Méhauté, Divoky and Lin (1968) compared the horizontal velocities below the crest for measured results and various theories. Comparisons for two-component waves (both components are comparable) have been done, see Sutherland (1992).

In terms of the design use of wave theories, there are a range of waves which need to be described. The three parameters, period, height and depth, determine a two-dimensional design wavetrain. The regions of validity have usually been drawn as areas on a graph with the y axis as the non-dimensional relative steepness (H/gT^2) and the x axis as the non-dimensional relative depth (d/gT^2), where H and T are wave heights and wave periods and g is the gravity acceleration. Figure 2.2 shows the boundaries of applicability of the various theories.

This decision for predicting wave mechanics can be made on the basis of comparison to experiments (as performed in the following chapters) or using theoretical considerations. Dean (1970) has compared several wave theories by seeing which has the lowest free surface dynamic boundary condition errors for each of a series of regular waves. He chose to use the dynamic boundary condition, as Laplace's equation and the bed boundary condition are linear and the kinematic boundary condition is always matched by the stream function solution. The results are included in fig. 2.2 and formed the basis of Sleath's diagram.

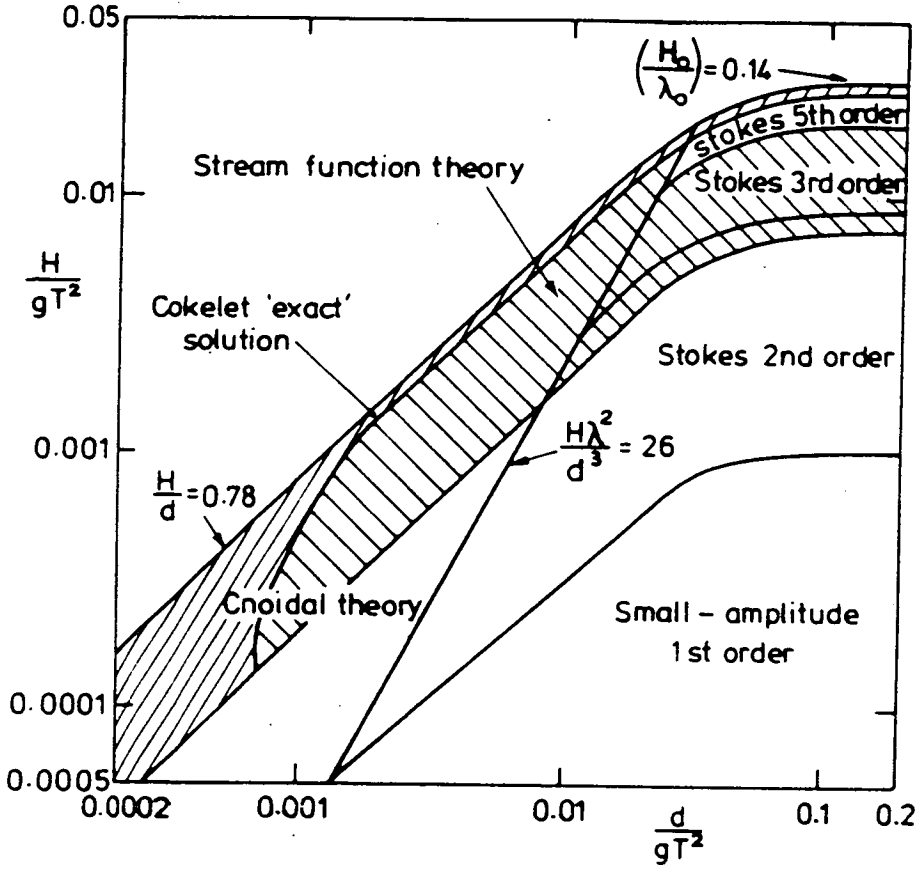

Fig. 2.2: The validity of wave theories (after Sleath 1984).

The process of determining which theory produces the lowest error in the dynamic free surface boundary condition does not necessarily determine which theory produces the lowest error in wave kinematics predictions. Moreover, all theories are based on specific idealisation, often centring on Laplace's equation thereby excluding viscosity, compressibility and vorticity. Hence even a highly accurate solution is only a good solution to a highly idealised wave condition.

Le Méhauté (1976) suggested that the cnoidal theory is preferable to small-amplitude theory for

$$\frac{H\lambda^2}{d^3} > 26 \qquad \text{(EQ 2.35)}$$

where H, λ and d are the wave height, wavelength and depth.

Dean (1965) gave two solutions for defined surface profiles and the design wave problems respectively. Then Dean (1970) showed that his stream function theory gave better results than the small-amplitude and shallow-water theories in the shaded region in fig. 2.2.

To sum up, the most common alternatives are the Stokes' fifth and the cnoidal theories. The cnoidal theory is derived to fit shallow water waves. While in deep water, Stokes' wave theory is recommended. It is surprising that the linear wave theory did well for the intermediate depths.

Furthermore, some very high order approximations have been made for predicting design wave kinematics. For example, Stokes', Dean's and cnoidal approaches of high order expansions have been developed by Schwartz (1974), Chaplin (1980) and Fenton (1979) respectively. There are also some investigations concerning numerical techniques for calculating irregular wave kinematics from the recorded free surface elevation record. To estimate the kinematics of irregular waves, Lambrakos (1981) was first to set up a double Fourier series expansion and reduced the errors in the kinematic and dynamical boundary conditions by the Newton-Gauss method, and Sobey (1992) gave a local Fourier approximation to estimate the kinematics of irregular waves and deduced the equivalent errors by a least-squares solution. Recently, Baldock and Swan (1994) developed a numerical technique, which is also a form of a double Fourier series expansion and reduces the errors in the kinematic and dynamical boundary conditions through the Newton-Raphson method and the least-squares algorithm, and provided good results to the comparison between prediction and measurements in wave kinematics.

Chapter 3

SHORT WAVE MODULATION BY NON-UNIFORM VELOCITY FIELDS

3.1 Introduction

The propagation of waves riding on non-uniform velocity fields is different from that of waves on uniform velocity fields. The difference results from the nonlinear kinematic and stress boundary conditions at the deformable boundary; while the role of these boundary conditions is governed by non-uniform velocity fields. In view of the difference, therefore, considerable modifications are necessary in dealing with weakly nonlinear waves riding on a free surface. It is usually reasonable to suppose that waves propagate through a known slowly-varying, depth-independent, horizontal current and that the depth also varies slowly for waves riding on non-uniform velocity fields. In this chapter a long solitary wave is treated as the major non-uniform velocity field; hence the

following discussion will be on the interaction between short waves and long solitary waves.

Solitary waves can be found in the sea, in deep water, and even in shallow water. For a long time this has been an attraction to mathematicians and engineers as an interesting subject of research, as a result of such research many insights into wave phenomena have been acquired. In the solution of the solitary wave it has been acceptably assumed that a solitary wave is of a two-dimensional potential flow and that the pressure is constant along the surface streamline. Scott-Russell (1844) first described this complicated phenomenon of solitary waves, and later Boussinesq (1871), Rayleigh (1876), and Korteweg and de Vries (1895) developed approximate descriptions applicable to the small amplitude and long wavelength limits. With the help of a computer programme, Byatt-Smith (1970) demonstrated that the form of his integral equation proved the physical properties of solitary waves assumed by Stokes, such as the 120° Stokes' cusp of the maximum wave and Stokes' formula, $F^2=\tan \mu / \mu$, for the exponential decay coefficient μ. Evans and Ford (1994) obtained an alternative exact integral equation for the solitary wave profile, which was considered a function of the distance x along the solitary wave rather than a function of velocity potential Φ along the surface (Byatt-Smith 1970). Both the above-mentioned integral equations describe exact solutions for the solitary wave profile. In following Evans' numerical scheme, it is necessary to know the velocity distribution U_0, the scale factor H_0 and the effective gravity acceleration g_1 along the free surface of solitary waves prior to beginning a discussion of the modulation of short waves riding on a solitary wave.

As a much-researched area in nonlinear wave dynamics, the interaction of short

waves riding on long regular waves/currents has been studied with emphasis. Short waves riding on long waves are strongly modulated by the long waves. This kind interaction is almost fully discussed by Zhang and Melville 1990 and Naciri and Mei 1992. Owing to the occurrence of new technique in remote sensing, to detect, with Synthetic Aperture Radar (SAR), radar waves Bragg-scattered by the free sea surface ranging from a few centimetres (X-band) to a few metres (L-band), it has become possible to measure the ocean wave spectrum and wave interaction phenomena in the ocean. From the empirical point of view, the images of microwave radar on the ocean surface also help the understanding of the interaction between wind and waves (Allan 1983; Stewart 1985). Having a sound knowledge of the oceanographic wave interaction is indispensable in realizing the energy exchange among waves. The problem of short waves interacted by long waves in shallow water is not thoroughly explored. Particularly shallow-water waves (sometimes called cnoidal waves) with their peaky crests and long shallow troughs are obviously not purely sinusoidal surface profiles. Seen from this view, sinusoidal waves will not be able to represent solitary waves which exist in the sea. A short wave is considered as a form of deep-water wave from the aspect of physical interpretation, and solitary waves as shallow-water waves; therefore it is of importance to study the modulation of short wavetrains riding on solitary waves.

By using the perturbation method, Longuet-Higgins and Stewart (1960) first explored the interaction between a linear short wavetrain and a weakly nonlinear long wavetrain; after that Phillips (1981) and Longuet-Higgins (1987) computed the modulation of linear short waves riding on finite-amplitude long waves. The conservation of wave action, as an alternative to a non-conservation equation which is involved with a radiation-stress tensor, was first introduced by Whitham

(1965). Bretherton and Garrett (1968) developed the concept of wave action conservation to study short waves riding on long waves. Zhang and Melville (1990) studied the steady modulation of the nonlinear short waves riding on a finite-amplitude long wave using conformal mapping. As Phillips (1981), Longuet-Higgins (1987) and Zhang and Melville (1990) concluded, in deep water as the short waves interact on the crest of long waves, their wavelengths become shorter and the amplitudes become larger. Conversely, the short waves become longer and smaller in the trough of the long waves. Zhang and Melville (1992) and Naciri and Mei (1992) discussed the instabilities of short waves riding on long waves. Both papers developed their own nonlinear Schrödinger equations. Furthermore from observations, short waves travelling along internal solitary waves are modulated by the internal solitary waves (Osborne and Burch 1980). Therefore similar results are expected for free surface solitary waves. Under specific circumstances the short waves tend to break on the crest of the solitary waves, not on the trough. By breaking, the energy of the short waves transfers to the solitary waves. But in shallow water the factors of wave interaction which cause wave breaking are still not clear. Through the work presented in this chapter the author wishes to provide some evidence for the mechanism of local wave breaking as in the case of short waves on regular long waves (Longuet-Higgins 1987). It is, therefore, of importance to study the modulation of short wavetrains riding on solitary waves.

In this chapter the focus is on two waves travelling in the same direction and the methodology is based on that of Zhang and Melville (1990). By applying the theories of conservation and considering the conservations with respect to solitary waves, the discussion of the modulation of short wavenumber, frequency and amplitude will provide a further understanding of wave interaction in shallow water.

3.2 The Modulation Theory

3.2.1 Governing Equations for Short Waves Riding on a Solitary Wave

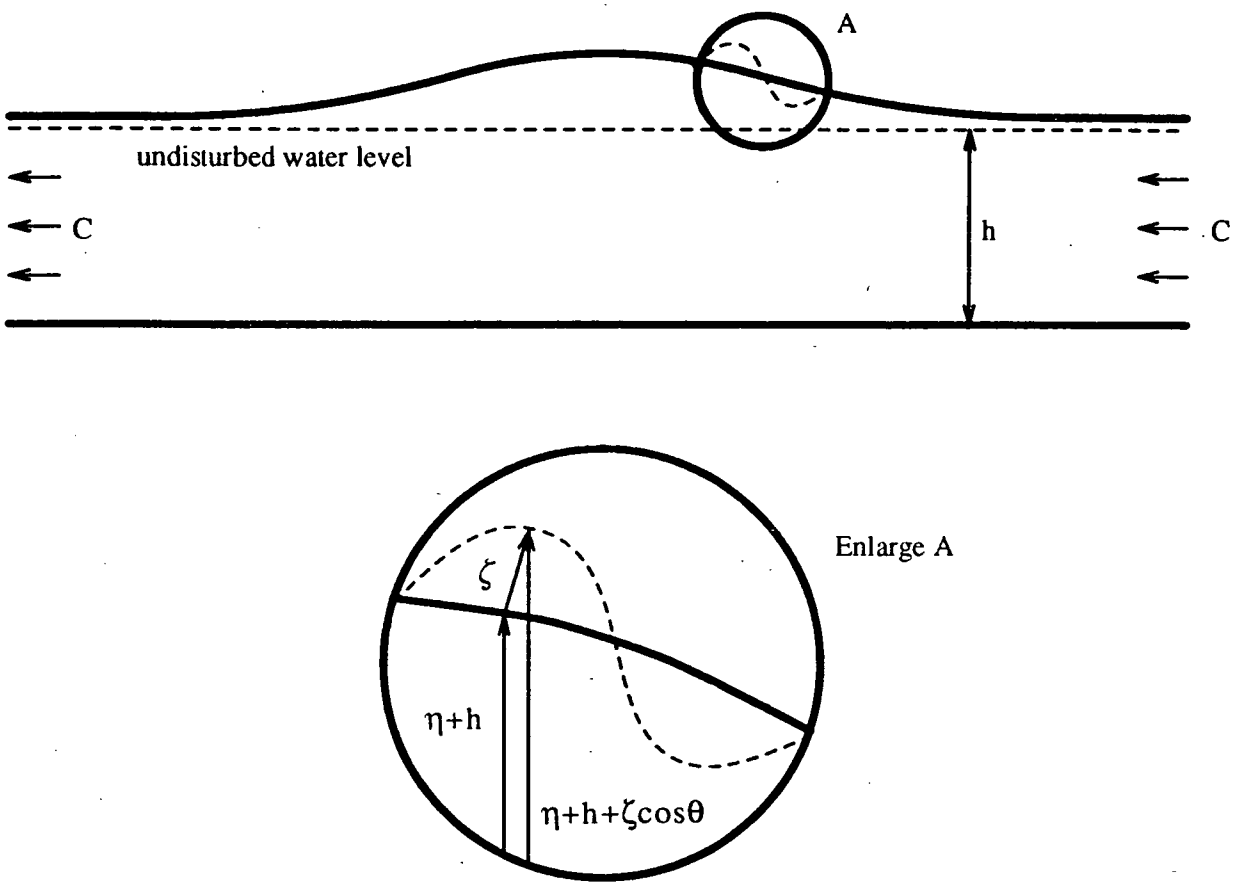

Fig. 3.1 Sketch of short waves riding on a solitary wave.

The first task is to introduce the governing equations for a two-dimensional short gravity wave riding on a collinear two-dimensional solitary wave. Both are travelling in the same direction. The flow is assumed to be incompressible and irrotational and the pressure on the free surface is constant. The governing equations (3.1)-(3.4) for short waves riding on the solitary wave in the fixed rectilinear co-ordinates (OX, OZ). (3.5)-(3.8) are for the rectilinear co-ordinates (x, z) which are moving at the phase velocity of the solitary wave C.

$$\Phi_{XX} + \Phi_{ZZ} + \phi_{XX} + \phi_{ZZ} = 0, \qquad 0 < Z \leq \eta + \zeta + h \tag{EQ 3.1}$$

$$\eta_t + \zeta_t + (\eta_X + \zeta_X)(\Phi_X + \phi_X) - \Phi_Z - \phi_Z = 0 \qquad \text{at } Z = \eta + \zeta + h \tag{EQ 3.2}$$

$$\Phi_t + \phi_t + g(\eta + \zeta) + \frac{1}{2}[(\Phi_X + \phi_X)^2 + (\Phi_Z + \phi_Z)^2] = 0 \qquad \text{at } Z = \eta + \zeta + h \tag{EQ 3.3}$$

$$|\nabla \phi| \to 0, \text{at } Z \to 0 \tag{EQ 3.4}$$

where Φ and η+h represent the velocity potential and the profile of the solitary wave, ϕ and ζ represent the potential and profile of the short wave, and g is the gravitational acceleration. The coordinates are fixed in space with the z-axis being positive upwards and with z=h defined at the level of the calm water with the depth h.

$$\Phi_{xx} + \Phi_{zz} + \phi_{xx} + \phi_{zz} = 0, \qquad 0 < z \leq \eta + \zeta\cos\theta + h \tag{EQ 3.5}$$

$$\cos\theta\zeta_t + [\eta_x + (\cos\theta\zeta)_x](C + \Phi_x + \phi_x) = \Phi_z + \phi_z \qquad \text{at } z = \eta + \zeta\cos\theta + h \tag{EQ 3.6}$$

$$\phi_t + \frac{1}{2}[(C + \Phi_x + \phi_x)^2 + (\Phi_z + \phi_z)^2] + g(\eta + \zeta\cos\theta) = C_0, \text{at } z = \eta + \zeta\cos\theta + h \tag{EQ 3.7}$$

$$\phi_z \to 0 \qquad \text{at } z \to 0 \tag{EQ 3.8}$$

where C_0 is the Bernoulli constant, and θ is the angle between the horizontal axis and the profile of the solitary wave.

3.2.2 Governing Equations in Orthogonal Curvilinear Co-ordinates

Using the conformal mapping technique, a transformation of the governing equations (3.5)-(3.8) from rectilinear coordinates into orthogonal curvilinear coordinates (s,n) is based on the velocity potential and the stream function Ψ of the solitary wave. So let

$$s = \frac{\Phi}{C}, \; n = \frac{\Psi}{C} \tag{EQ 3.9}$$

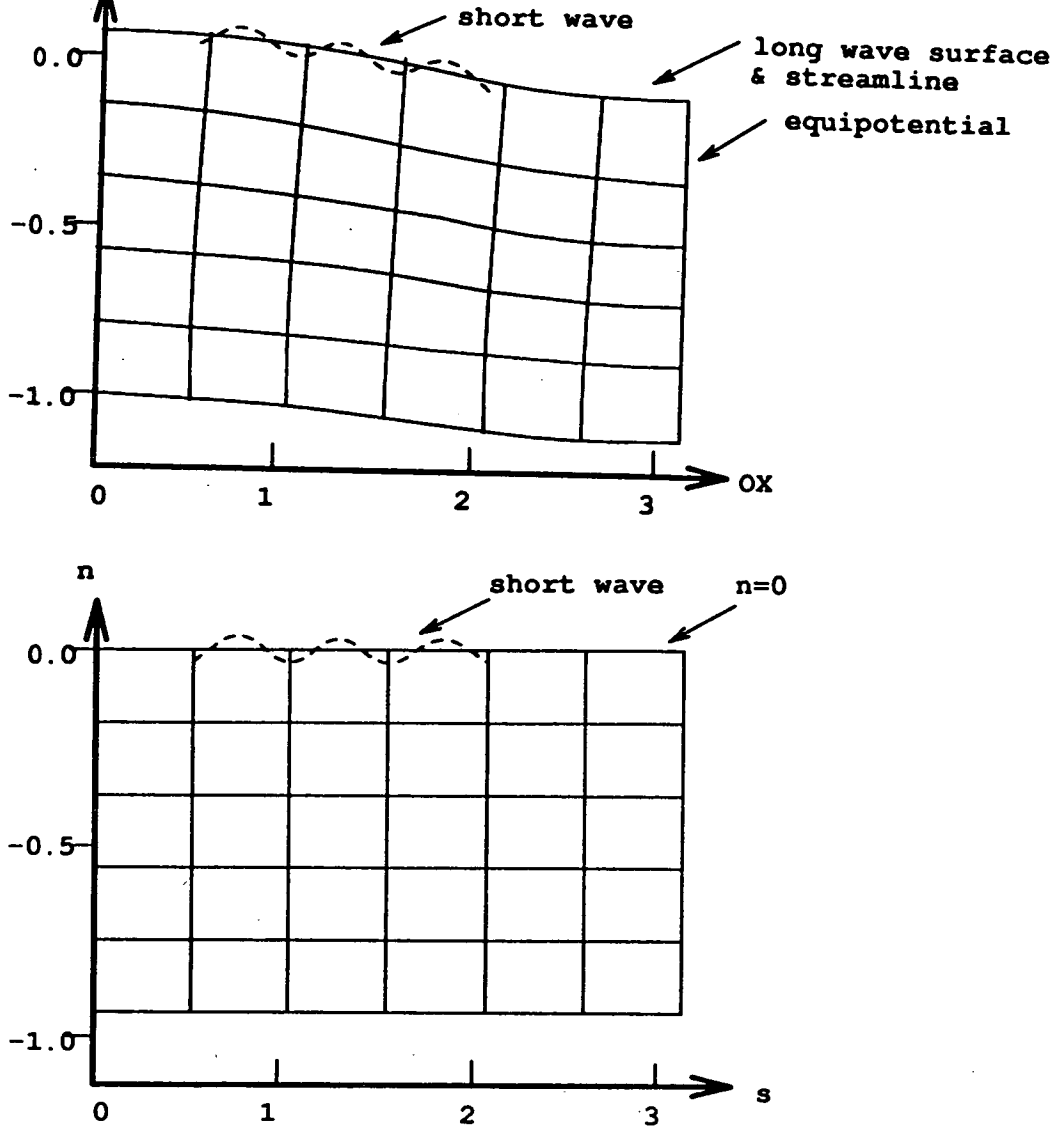

Fig. 3.2: Sketch of conformal mapping.

$$\frac{\partial}{\partial s}[hU_0(s,n)+\phi_s]+\frac{\partial \phi_n}{\partial n}=0, \qquad -\infty < n \le \zeta \tag{EQ 3.10}$$

$$\phi_t+\frac{1}{2}\left[(U_0(s,n)+\frac{1}{h}\phi_s)^2+\frac{1}{h^2}\phi_n^2\right]+g\eta(s)+gh\cos\theta\zeta=C_0 \qquad \text{at } n=\zeta \tag{EQ 3.11}$$

$$\zeta_t+\frac{1}{h}(U_0(s,n)+\frac{1}{h}\phi_s)\zeta_s=\frac{1}{h^2}\phi_n \qquad \text{at } n=\zeta \tag{EQ 3.12}$$

$$\phi_n \to 0 \qquad \text{at } n \to -\infty \tag{EQ 3.13}$$

where h is the scale factor in the coordinate transformation.

$$h = h(s,n) = \frac{C}{U_0(s,n)} \qquad \text{(EQ 3.14)}$$

The subscripts s, n and t denote the partial derivatives. Here there are three assumptions to be explained before applying Taylor expansions for expanding the free boundary conditions, Eqns. (3.11) and (3.12), at the solitary wave surface. First, the steady profile and velocity field of the solitary waves will not be changed by the riding of the short waves. Secondly, it is necessary to assume the velocity field $U_0(s,n)$ of the solitary wave can be analytically extended to the region between $n = 0$ and $n = \zeta$, even it is weak, Eqn. (3.15).

$$U_0(s,n) = U_0(s,0) + \zeta \frac{\partial}{\partial n} U_0(s,n)\Big|_{n=0} + O(\zeta^2) \qquad \text{(EQ 3.15)}$$

Last, since the wavelength ratio of the short waves to the solitary waves is near zero (the solitary wavelength is infinite) and assuming the slope of the short waves is small, then Eqns. (3.11) and (3.12) can be expanded at the free surface of solitary waves. Subtracting the steady solution of the solitary wave, the governing equations become:

$$\phi_{ss} + \phi_{nn} = 0, \qquad -\infty < n \le 0 \qquad \text{(EQ 3.16)}$$

$$\begin{aligned}&\phi_t + H_0 U_0(s,0)\,\phi_s + \zeta g_1 + \zeta \phi_{tn} + H_0 U_0(s,0)\,\phi_{sn}\zeta + 2H_0\beta\phi_s\zeta \\ &+\frac{1}{2}H_0^2(\phi_s^2 + \phi_n^2) + \frac{1}{2}\phi_{tnn}\zeta^2 + \frac{1}{2}H_0 U_0 \phi_{snn}(s,0)\,\zeta^2 + 2H_0\beta\phi_{sn}\zeta^2 \\ &+\frac{1}{2}H_0(\phi_s^2 + \phi_n^2)_n\zeta = 0 \qquad \text{at } n = 0\end{aligned} \qquad \text{(EQ 3.17)}$$

$$\begin{aligned}&\zeta_t + \zeta_s H_0 U_0(s,0) - H_0^2\phi_n + 2\beta H_0\zeta\zeta_s - 2\frac{\beta}{C}H_0\zeta\phi_n + H_0^2(\phi_s\zeta)_s \\ &+\frac{1}{2}H_0^2(\phi_{sn}\zeta^2) = 0 \qquad \text{at } n = 0\end{aligned} \qquad \text{(EQ 3.18)}$$

$$\phi_n \to 0 \qquad \text{at } n \to -\infty \qquad \text{(EQ 3.19)}$$

$$\beta = \frac{\partial}{\partial n} U_0(s,n)\Big|_{n=0} \qquad \text{(EQ 3.20)}$$

$$g_1 = \frac{g\cos\theta}{H_0} + U_0(s,0)\beta \qquad \text{(EQ 3.21)}$$

g is the acceleration of gravity and g_1 is the effective acceleration of gravity.

$$H_0(s) = \frac{U_0(s,0)}{C} \qquad \text{(EQ 3.22)}$$

H_0 is the scale factor.

3.2.3 Multiple-Scale Perturbation Method

Stokes' expansions for $\phi(s, n, t)$ and $\zeta(s, t)$ of short waves are given by:

$$\phi = \phi^{(0)} + \phi^{(1)} e^{i\hat{\theta}} + * + \phi^{(2)} e^{i2\hat{\theta}} + * \qquad \text{(EQ 3.23)}$$

$$\zeta = \zeta^{(0)} + \zeta^{(1)} e^{i\hat{\theta}} + * + \zeta^{(2)} e^{i2\hat{\theta}} + * \qquad \text{(EQ 3.24)}$$

$$\frac{\partial\hat{\theta}}{\partial s} = k \text{ and } \frac{\partial\hat{\theta}}{\partial t} = -\omega' \qquad \text{(EQ 3.25)}$$

where * denotes the complex conjugate and $\hat{\theta}$, k and ω' are the phase function, wavenumber and frequency of the short wave respectively. $\phi^{(0)}$ and $\zeta^{(0)}$ are the velocity potential and amplitude of the solitary wave caused from the interaction of two waves. $\phi^{(1)}$, $\zeta^{(1)}$, $\phi^{(2)}$ and $\zeta^{(2)}$ are the short wave velocity potential and amplitude plus higher harmonics. They can be further expanded with respect to ε_1, see Eqns. (3.26)-(3.29). The physical meaning of ε_1 is defined according to the steepnesses of the short waves.

$$\phi^{(1)} = \phi^{(11)} + \varepsilon_1\phi^{(12)} + \varepsilon_1^2\phi^{(13)} + \ldots \qquad \text{(EQ 3.26)}$$

$$\phi^{(2)} = \varepsilon_1\phi^{(22)} + \varepsilon_1^2\phi^{(23)} + \ldots \qquad \text{(EQ 3.27)}$$

$$\zeta^{(1)} = \zeta^{(11)} + \varepsilon_1\zeta^{(12)} + \varepsilon_1^2\zeta^{(13)} + \ldots \qquad \text{(EQ 3.28)}$$

$$\zeta^{(2)} = \varepsilon_1\zeta^{(22)} + \varepsilon_1^2\zeta^{(23)} + \ldots \qquad \text{(EQ 3.29)}$$

$$\phi^{(11)} = -ibe^{kn} \qquad \text{(EQ 3.30)}$$

$$\zeta^{(11)} = a \qquad \text{(EQ 3.31)}$$

$$b = \frac{ag_1}{\sigma} \qquad \text{(EQ 3.32)}$$

$$\sigma^2 = H_0^2 g_1 k \qquad \text{(EQ 3.33)}$$

where $\sigma = \omega' - kH_0U_0(s,0)$. Equation (3.33) is the dispersion relation of the short waves riding on a solitary wave.

3.2.4 The Nonlinear Schrödinger Equation and Wave Action Conservation

Here it is necessary to recall the equations of Zhang and Melville (1990). The above equations are similar to those, because either the flow of solitary waves or that of long waves is based on potential theory. So the following nonlinear Schrödinger equation has been derived (see Eqn. (3.5) of Zhang and Melville (1990), from $\phi^{(12)}$, $\zeta^{(12)}$, $\phi^{(13)}$ and $\zeta^{(13)}$) to describe the evolution of short waves riding on a long solitary wave.

$$\frac{1}{g_1}\frac{\partial b}{\partial t} + \left[\frac{H_0^2 C}{g_1} + \frac{H_0^2}{2\sigma}\right]\frac{\partial b}{\partial s} + \frac{H_0^2 C b}{2\sigma}\frac{\partial}{\partial s}\left[\frac{\sigma}{g_1}\right]$$

$$= -i\left\{\frac{1}{2\sigma}\left[\frac{\partial}{\partial t} + H_0^2 C\frac{\partial}{\partial s}\right]\left[\frac{1}{g_1}\frac{\partial b}{\partial t} + \frac{H_0^2 C}{g_1}\frac{\partial b}{\partial s}\right] + \frac{2k^4 H_0^4 D|b|^2 b}{g_1\sigma}\right\} \qquad \text{(EQ 3.34)}$$

where $D = 1 + \dfrac{4\beta H_0}{\sigma}$.

Ignore all the terms, which are higher-order, on the right-hand side of Eqn. (3.34), and then multiply Eqn. (3.35) with the complex conjugate of b.

$$\frac{1}{g_1}\frac{\partial b}{\partial t} + \left[\frac{H_0^2 C}{g_1} + \frac{H_0^2}{2\sigma}\right]\frac{\partial b}{\partial s} + \frac{H_0^2 C b}{2\sigma}\frac{\partial}{\partial s}\left[\frac{\sigma}{g_1}\right] = 0 \qquad \text{(EQ 3.35)}$$

Then Eqn. (3.36), which is originally derived by Zhang and Melville (1990), describes the wave action conservation for linear short waves riding on a long solitary wave.

$$\frac{\partial}{\partial t}\left(\frac{|a_d|^2\bar{g}}{2\sigma}\right)+\frac{\partial}{\partial s_d}\left((U_0(s,0)+\frac{\bar{g}}{2\sigma})\frac{|a_d|^2\bar{g}}{2\sigma}\right)=0 \qquad \text{(EQ 3.36)}$$

$$\bar{g} = H_0 g_1$$

$|a_d|$ is the modulated short wave amplitude normalized by its own value at the 'outskirts' of the solitary wave. The subscript d denotes that the parameters $|a_d|$ and s_d are in the original physical lengthscale.

3.2.5 The Numerical Scheme for Solitary Waves

In this scheme, the solitary wave is considered from the co-ordinates (x,z) moving with this wave. The function z(x) describes the solitary wave profile as measured from the canal bed. Clearly the water in the 'outskirts' of the solitary wave moves with velocity $-C\hat{i}$ and the dimensionless Froude number F is given by $C/(gh)^{1/2}$. As conventional, $\eta(x)$ represents the wave amplitude as measured from the still water level h; that is $z(x) = \eta(x) + h$.

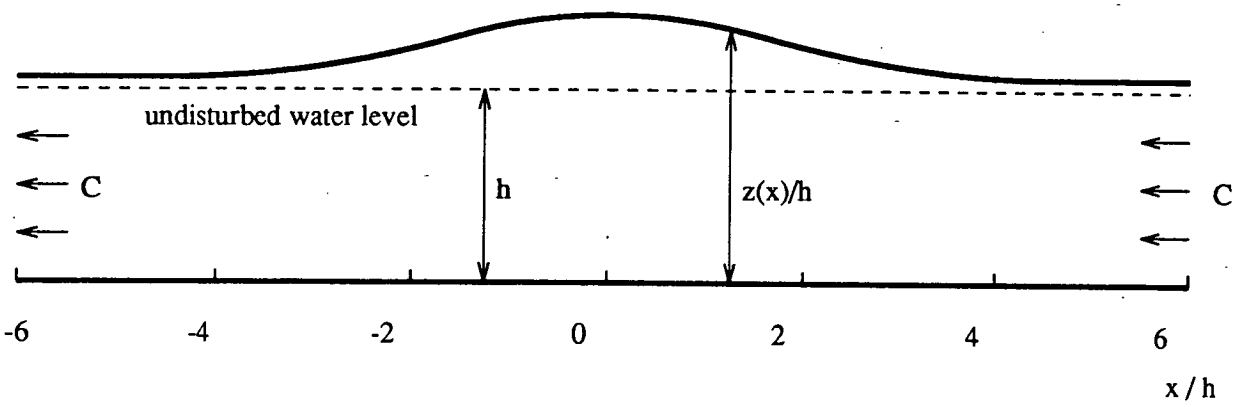

Fig. 3.3: Sketch of solitary wave as viewed from a co-ordinate system moving with the wave.

As the solitary wave is considered as a phenomenon of potential flow, velocity potential Φ and stream function Ψ obey the 2-D Laplace's equation. As described in Evans and Ford (1994), Green's theory is applied to the domain

$$\Psi(r_0) = \oint_c (\Psi(r) \nabla (G(r, r_0)) - G(r, r_0) \nabla \Psi) \bullet dA \qquad \text{(EQ 3.37)}$$

with a choice of Green's function

$$G(r, r_0) = \frac{1}{2\pi} ln \left(\frac{|r - r_0|}{|r - \bar{r}_0|} \right) \qquad \text{(EQ 3.38)}$$

where $\bar{r}_0 \equiv (x_0, -z_0)$ is the image of r_0 in the canal bed (line **ED** in fig. 3.4), $\hat{i}$ and $\hat{k}$ are the unit vectors in the moving co-ordinates (x,z). This form of the Green's function evidently vanishes at all points along the canal bed.

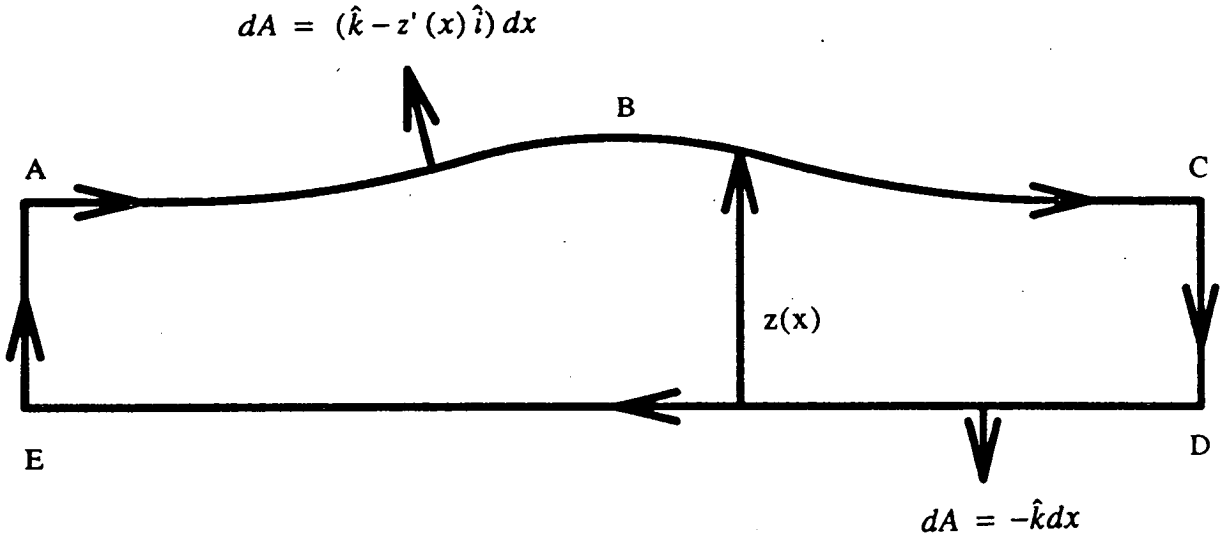

Fig. 3.4 Sketch for Green's theorem.

Utilizing Bernoulli's equation

$$P + \frac{1}{2}\rho U^2(x) + \rho g z(x) = \text{constant} \qquad \text{(EQ 3.39)}$$

along the surface streamline, the relation is given

$$U^2(x) = C^2 - 2g(z(x) - h) = C^2 - 2g\eta(x) \qquad \text{(EQ 3.40)}$$

where ρ=1, the fluid density; P is constant along the free surface.

U(x) is the local velocity on the free surface of the solitary wave.

Then, for any point, $r_0 \equiv (x_0, z_0)$, within **ABCDE**, adopting the convention that Ψ vanishes along the surface streamline, it is shown that (in units where h=1)

$$\frac{\Psi(x_0, z_0)}{F} =$$

$$1 + \int_{-\infty}^{\infty} \left((1+\eta'(x)^2)\left(1 - \frac{2\eta(x)}{F^2}\right)\right)^{1/2} ln\left(\frac{(x-x_0)^2 - (1+\eta(x)-z_0)^2}{(x-x_0)^2 + (1+\eta(x)+z_0)^2}\right)\frac{dx}{4\pi} \qquad \text{(EQ 3.41)}$$

whence, if Ψ is evaluated at the surface, i.e. $\Psi(x_0, 1+\eta(x_0))$, a self-consistent integral equation (3.42) is given through Eqn. (3.41).

$$1 + \int_{-\infty}^{\infty} \left((1+\eta'(x)^2)\left(1 - \frac{2\eta(x)}{F^2}\right)\right)^{1/2} ln\left(\frac{(x-x_0)^2 - (\eta(x)-\eta(x_0))^2}{(x-x_0)^2 + (2+\eta(x)+\eta(x_0))^2}\right)\frac{dx}{4\pi} = 0 \qquad \text{(EQ 3.42)}$$

for the surface profile function $\eta(x)$. Equation (3.42), of course, applies at all values of x_0. To solve the above, Evans' numerical scheme is employed for the integral equation (3.42) with tailored quadrature weights and abscissas and parametrise the form of $\eta(x)$ by a polynomial in $e^{-\mu x}$ viz.

$$\eta(x) = \sum_{m=1}^{NL} b_m e^{-m\mu x} \qquad \text{(EQ 3.43)}$$

where μ is Stokes' decay coefficient given by

$$F^2 = \frac{\tan\mu}{\mu} \qquad \text{(EQ 3.44)}$$

The parametric form (3.43) will have the correct asymptotic decay in the outskirts and is capable of representing both a flat-topped wave and one with a cusp at x=0. In an early paper, Longuet-Higgins (1974) used a similar form with just three terms to obtain a very good parametrization of the maximum wave profile. The cases discussed here typically have ten or more terms in the polynomial which affords an excellent parametrization. The integral equation (3.42) has a logarithmic singularity at $x=x_0$, which was handled in the computation using a 'tailored quadrature' extension of Gaussian quadrature (see Harris and Evans, 1977) to accurately cater for this type of integrable end-point singularity. The solitary wave profiles obtained in this manner were highly accurate even at large amplitudes. The various types of solitary waves are best characterised by Longuet-Higgins and Fenton's ω (1974) parameter defined by

$$\omega = 2 \sum_{m=1}^{NL} b_m + 1 - \frac{\tan(\mu)}{\mu} \qquad \text{(EQ 3.45)}$$

which ranges from 0 for the lowest amplitude solitary wave to 1 for the maximum wave. It is in $1 \leftrightarrow 1$ correspondence with the various solitary wave solutions in contrast to, say, the Froude number F. As Longuet-Higgins and Fenton (1974) discovered, where more than one large amplitude solitary wave can have the same F value (velocity maximum as the height tends towards the maximum).

3.2.6 The Modulation of Short Waves Riding on a Long Solitary Wave

Longuet-Higgins & Stewart (1961,1962) introduced a radiation stress tensor to determine the evolution of water waves in non-uniform velocity fields with variable depth or horizontal current. After that Whitham (1965) first introduced a conservation law of wave action Eqn. (3.47).

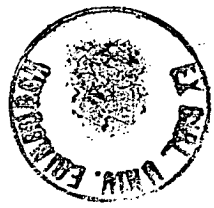

$$A_1 = \frac{E}{\sigma} \qquad \text{(EQ 3.46)}$$

$$\frac{\partial A_1}{\partial t} + \nabla \bullet [(\vec{U} + C_g) A_1] = 0 \qquad \text{(EQ 3.47)}$$

$$C_g = \frac{\partial \sigma}{\partial \vec{k}} \qquad \text{(EQ 3.48)}$$

A_1: the wave action; E: the energy of short waves.

C_g: the group velocity observed in a frame moving with the local mean flow $\vec{U}$.

σ: the local frequency (intrinsic frequency) as seen by an observer moving with the local velocity $\vec{U}$.

The short wavetrain is assumed to remain coherent: that is, it can be described, locally, in terms of a single wave-mode of wavenumber $\vec{k}$.

$$\frac{\partial \vec{k}}{\partial t} + \nabla (\sigma + \vec{U} \cdot \vec{k}) = 0 \qquad \text{(EQ 3.49)}$$

Equations (3.47) and (3.49) are called the equation of conservation of action and the equation of conservation of 'wave crest' or of 'phase'.

In this chapter the main purpose is to consider the steady modulation of a linear short wavetrain riding on a long solitary wave. From the mathematical point of view it is reasonable to interpret short waves riding on the free surface streamline ($\Psi = 0$) of the solitary wave. So applying conformal mapping, the co-ordinates (s,n) are equivalent to (Φ, Ψ). The notations follow those in the paper given by Zhang and Melville (1990). In Eqns. (3.47) and (3.49) the Laplace operator ∇ can be $\partial / (\partial s)$. Furthermore under the steady assumption, from the phase conservation and the wave action conservation, the modulated short wave riding on the solitary wave in shallow water is described by Eqns. (3.50), (3.51) and (3.54). More details for the conservations are given in Appendix A.

$$\frac{1}{k}\frac{\partial k}{\partial s} = -\frac{2}{H_0}\frac{\partial H_0}{\partial s} - \frac{1}{2g_1(R_c+\frac{1}{2})}\frac{\partial g_1}{\partial s} \qquad \text{(EQ 3.50)}$$

$$\frac{1}{\sigma}\frac{\partial \sigma}{\partial s} = \frac{1}{2g_1}\frac{\partial g_1}{\partial s}\left[1 - \frac{1}{2(R_c+\frac{1}{2})}\right] \qquad \text{(EQ 3.51)}$$

k: the modulated short wavenumber normalized by its own value at the 'outskirts' of solitary wave.

σ: the modulated short wave frequency (intrinsic frequency) normalized by its own value at the 'outskirts' of solitary wave.

Recall Eqn. (3.21) and let $\beta = 0$. Then

$$g_1(s) = \frac{g(s)\cos\theta}{H_0(s)} \qquad \text{(EQ 3.52)}$$

g: the gravity acceleration; g_1: the effective gravity acceleration.

θ: the angle between the surface profile of the solitary wave and the horizontal axis. Where

$$R_c = C\frac{\sigma}{g_1}$$

R_c: the phase velocity ratio of the long wave to the short wave.

$$H_0(s) = \frac{U_0(s)}{C} \qquad \text{(EQ 3.53)}$$

H_0: the scale factor.

$$\frac{\partial}{\partial s_d}\left[(U_0(s) + \frac{\bar{g}}{2\sigma})\frac{|a_d|^2\bar{g}}{2\sigma}\right] = C \qquad \text{(EQ 3.54)}$$

3.2.7 Numerical Results

The following cases have been considered, the solitary wave profiles shown in fig. 3.5; the effective gravity acceleration g_1 shown in fig. 3.6; the scale factor H_0 shown in fig. 3.7; the modulated short wavenumber (fig. 3.8), intrinsic frequency (fig. 3.9), and amplitude (fig. 3.10), along the free surface of a long solitary wave (note: along X-axis) for each value of the parameter ω. Let $\omega = 0.20, 0.40, 0.60$. The derivatives of the modulated short wavenumber, frequency and amplitude with respect to X are shown in figs. 3.11, 3.12 and 3.13.

Furthermore it is worth looking at the steady modulated short wavenumber (fig. 3.14), frequency (fig. 3.15) and amplitude (fig. 3.16) at the solitary wave crest as against the parameter ω. Here let $R_c = 10$ at the 'outskirts' of solitary wave.

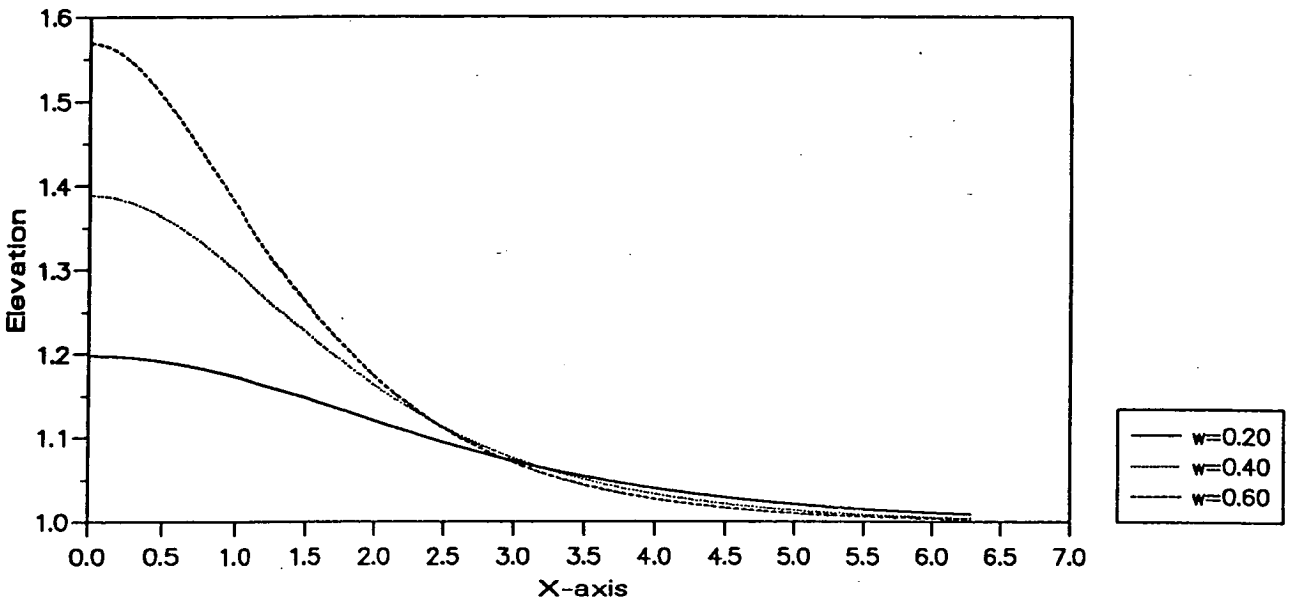

Fig. 3.5: The solitary wave profiles.

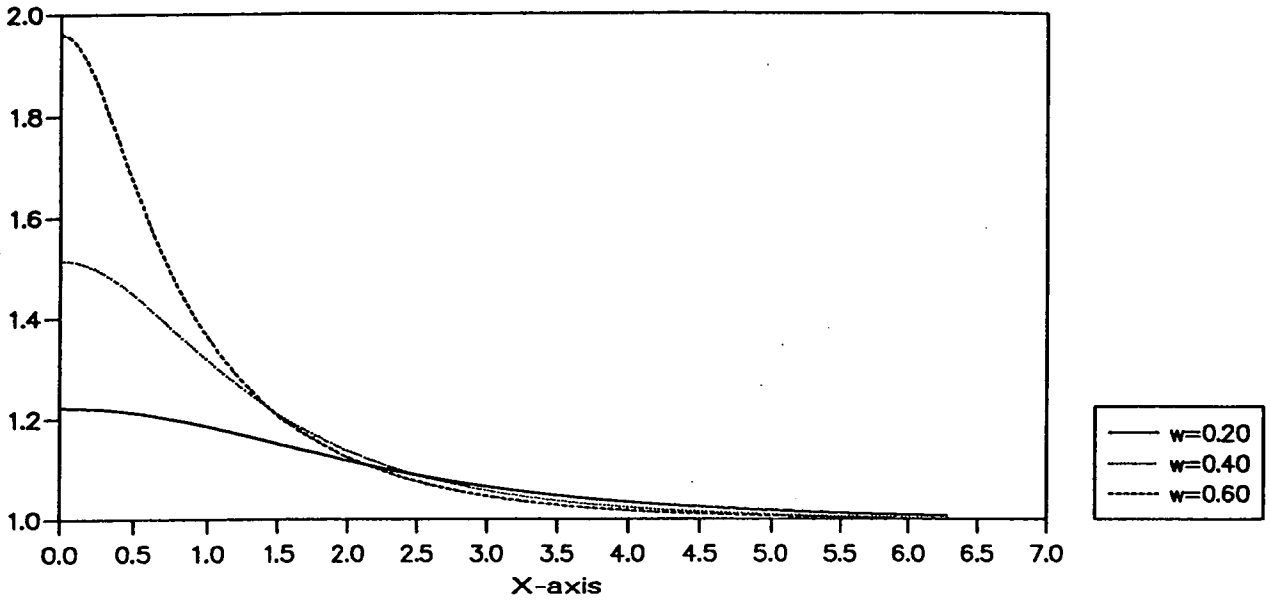

Fig. 3.6: The effective gravity acceleration g_1.

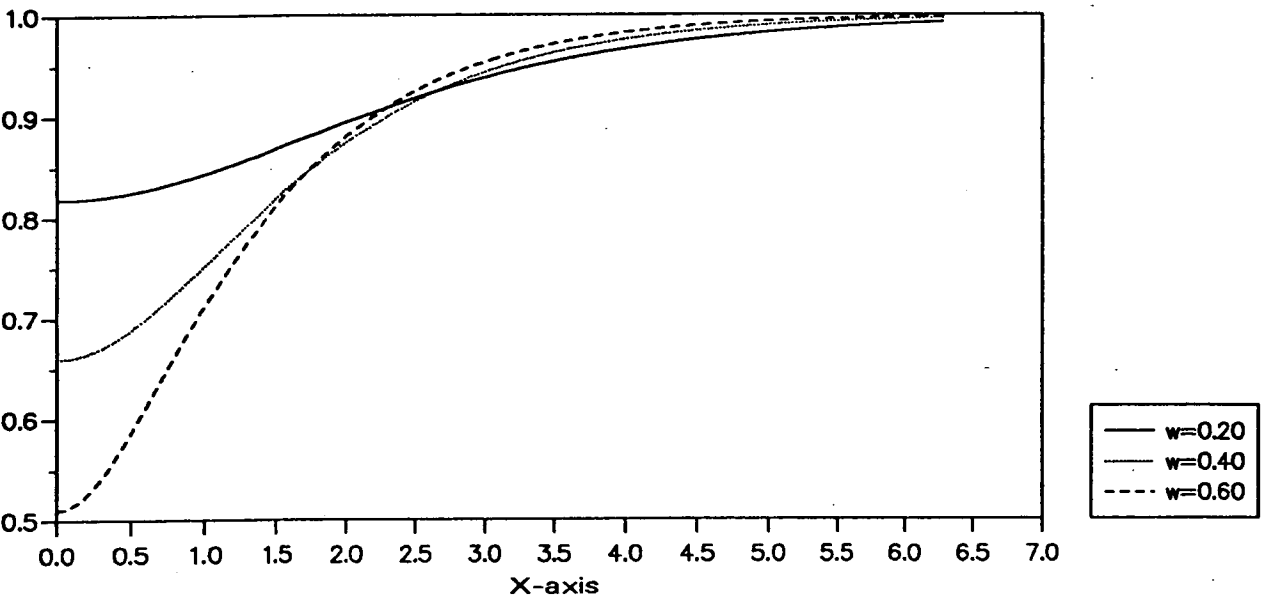

Fig. 3.7: The scale factor H_0.

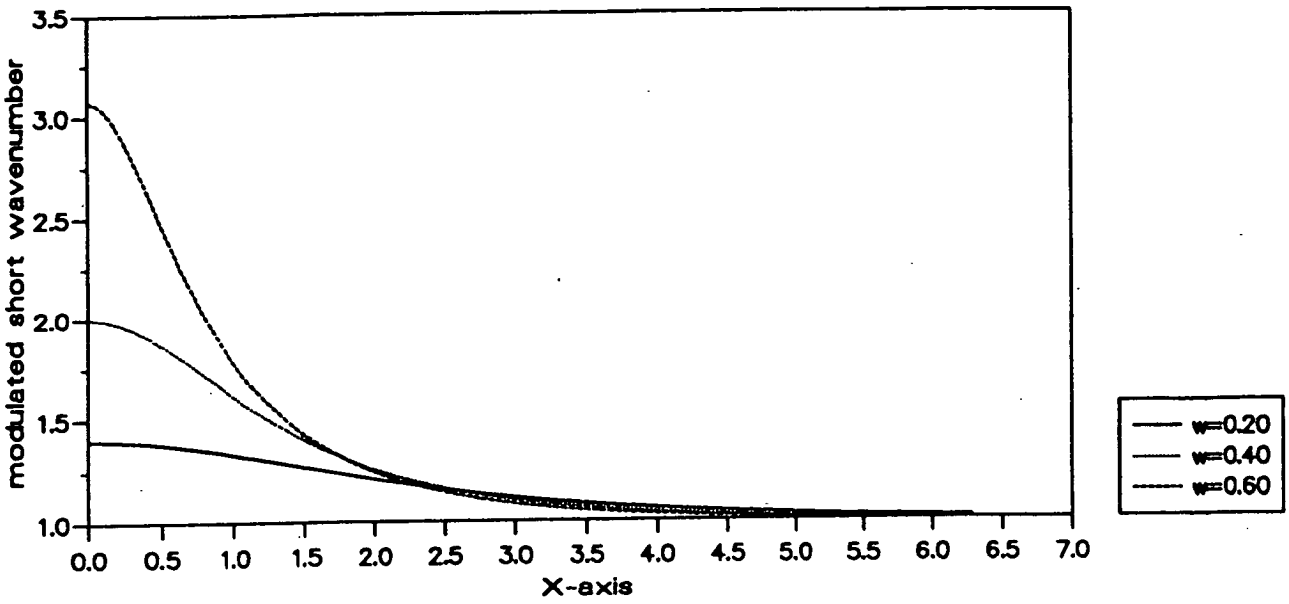

Fig. 3.8: The modulated short wavenumber along the solitary wave.

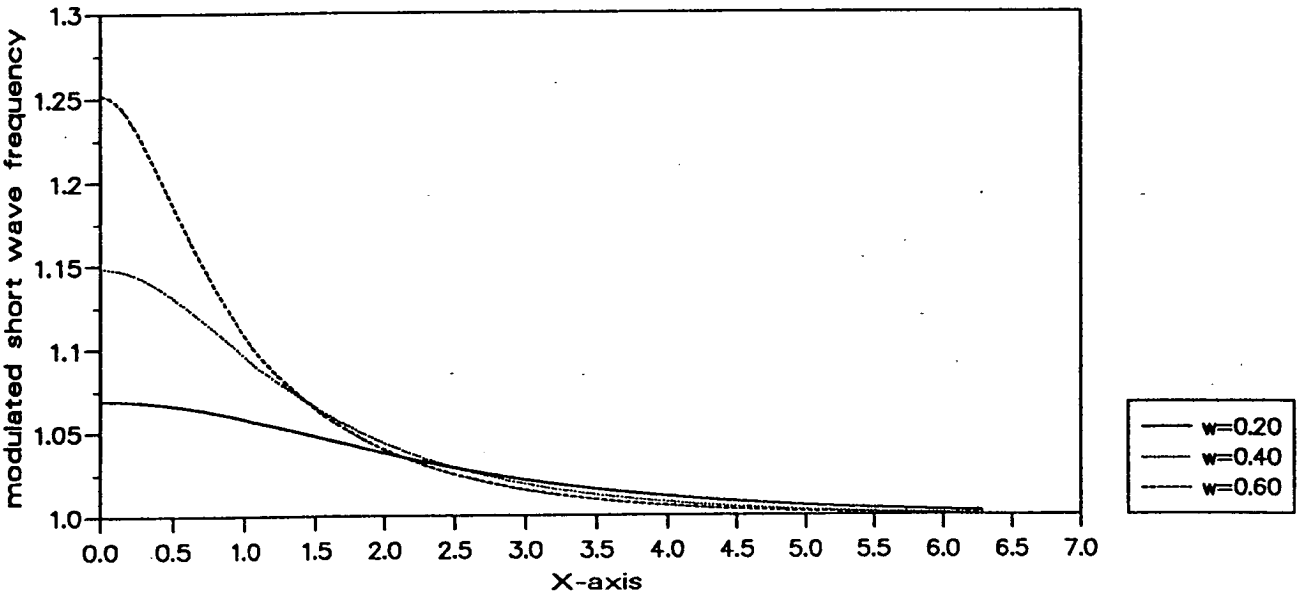

Fig. 3.9: The modulated short wave frequency along the solitary wave.

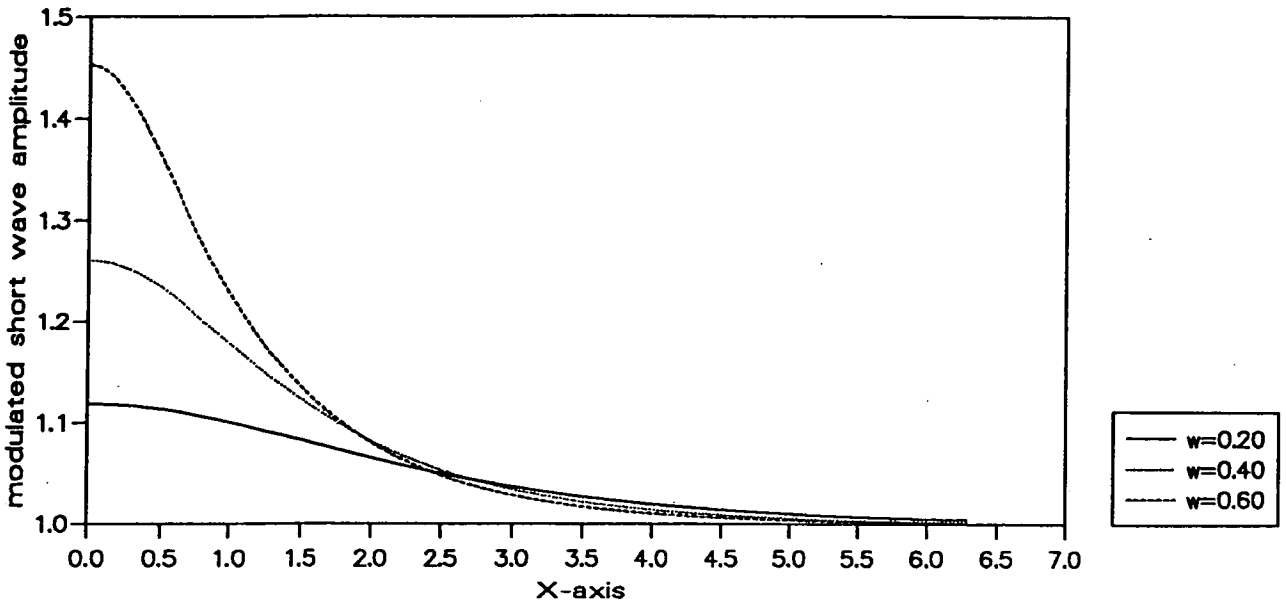

Fig. 3.10: The modulated short wave amplitude along the solitary wave.

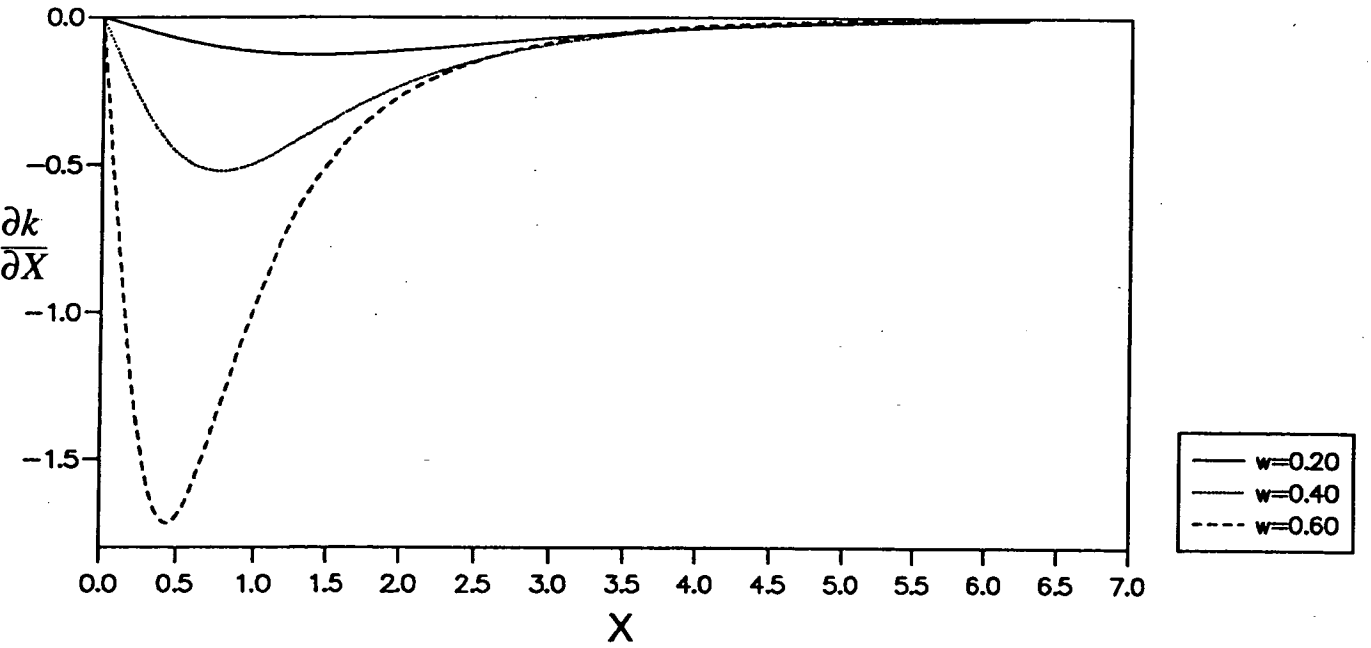

Fig. 3.11: The derivative of the modulated wavenumber with respect to X along the solitary wave.

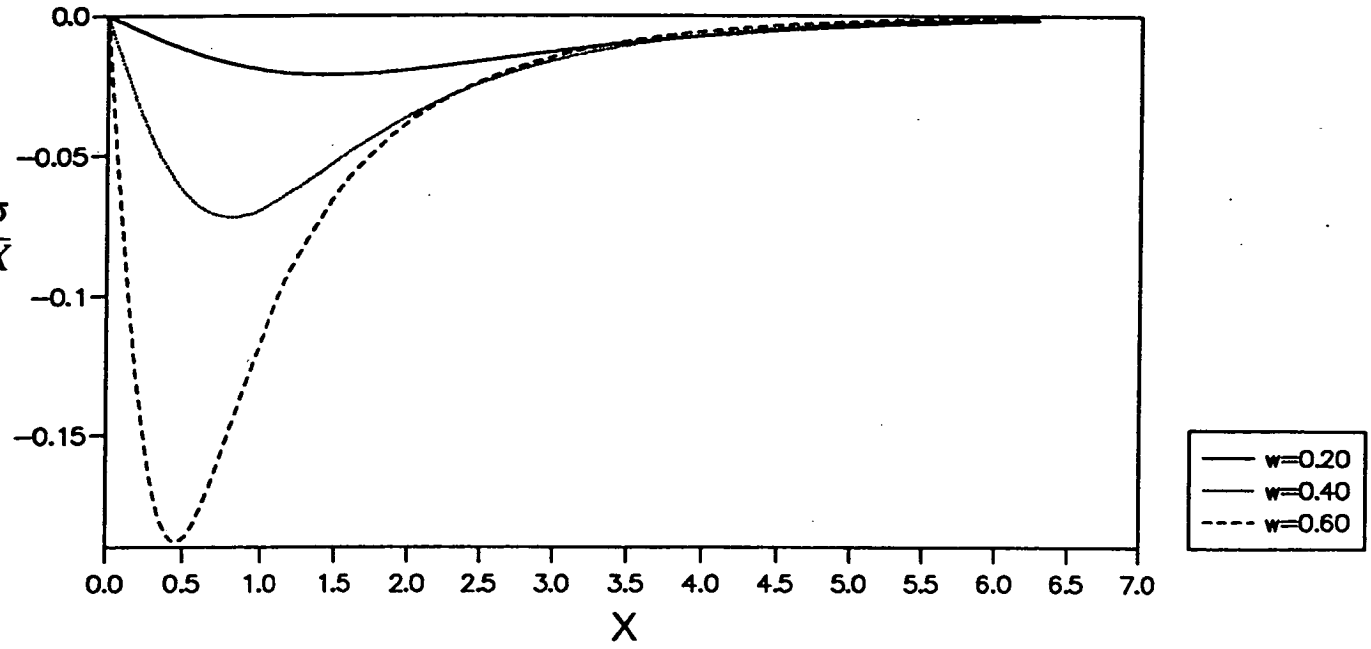

Fig. 3.12: The derivative of the modulated frequency with respect to X along the solitary wave.

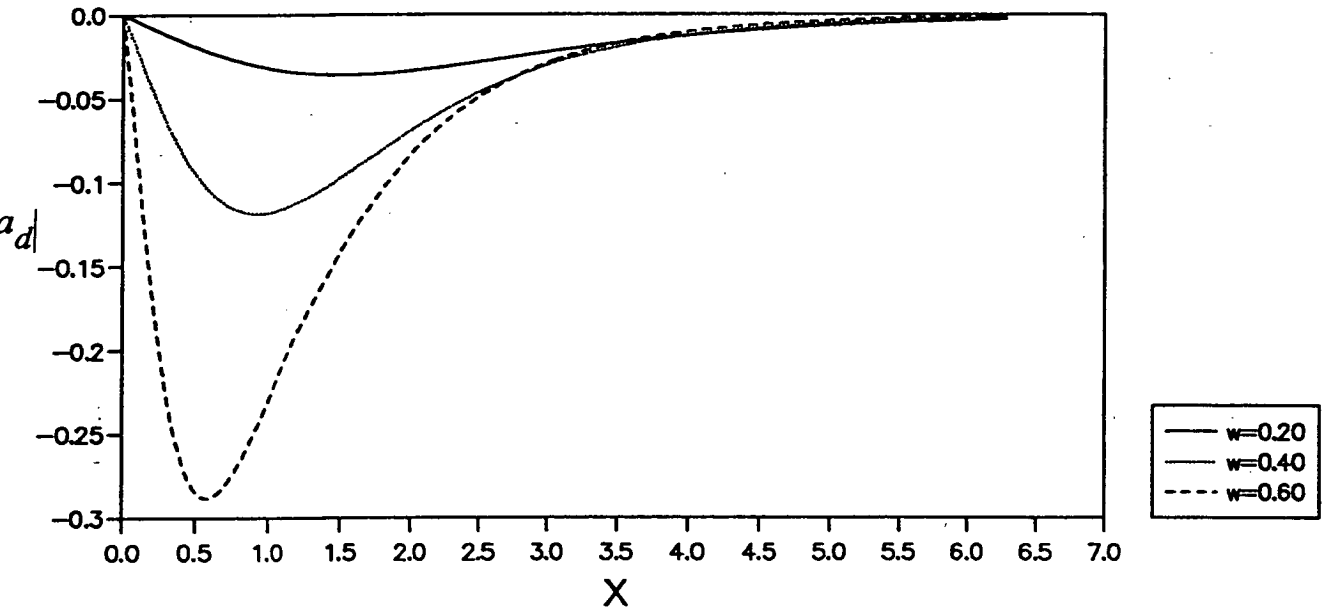

Fig. 3.13: The derivative of the modulated amplitude with respect to X along the solitary wave.

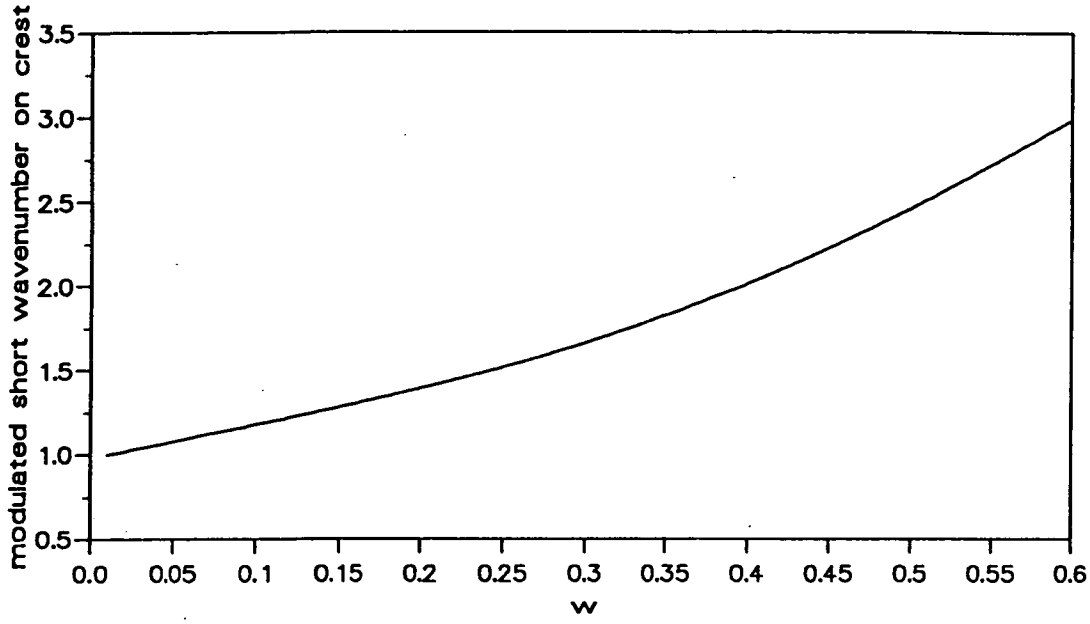

Fig. 3.14: The modulated short wavenumber at the solitary wave crest.

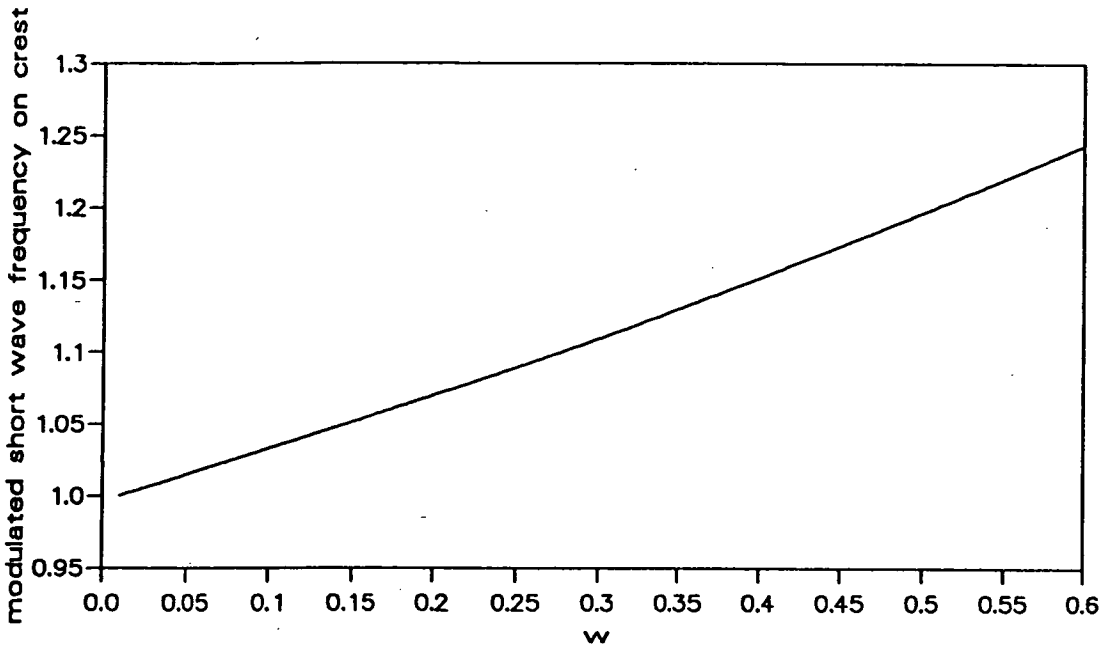

Fig. 3.15: The modulated short wave frequency at the solitary wave crest.

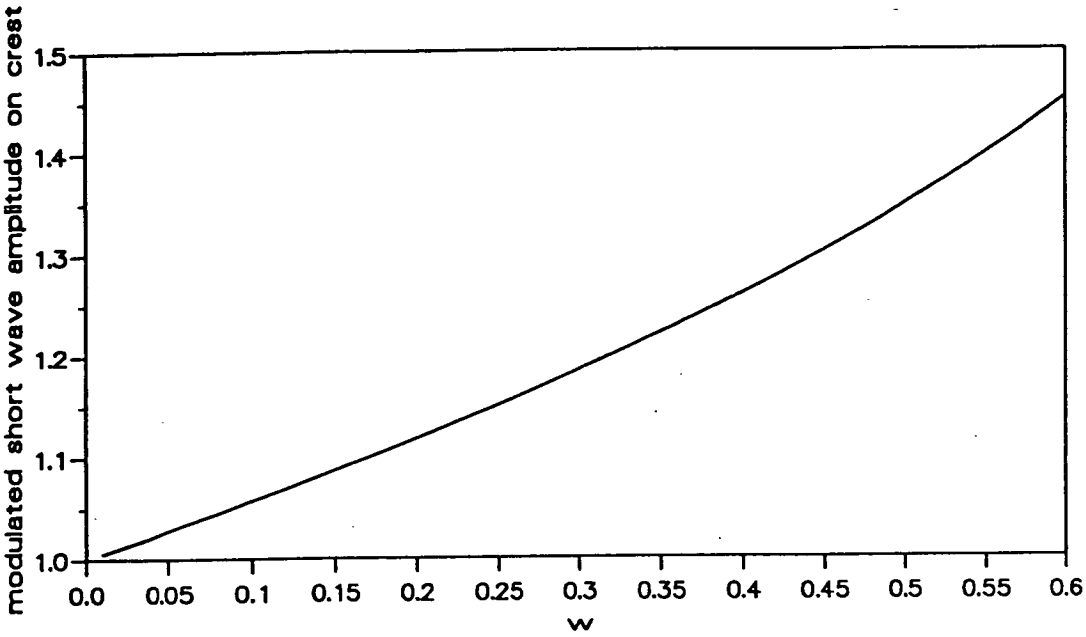

Fig. 3.16: The modulated short wave amplitude at the solitary wave crest.

3.3 Discussions

In this chapter, which is principally based on the linear theory of wave conservation, the steady modulation of linear short waves riding on long solitary waves has been discussed. Along the free surface of the solitary wave, from the 'outskirts' to the crest, the short wavelength is shortening, and the short wave amplitude and frequency are increasing. Another main physical conclusion for the modulation is that the short wavelength becomes shorter, and the amplitude and frequency become larger on the crest of the solitary wave as the amplitudes of the solitary waves increase. It is found that the 'outskirts' of the solitary wave provide a natural position for normalization of the modulation because of their asymptotic decay. Figures 3.8, 3.9, and 3.10 demonstrate that the maximum modulated wavenumber, frequency, and amplitude of short waves always occur

at the crest of the solitary waves. In figs. 3.14, 3.15, and 3.16 it is shown that the modulated short wavenumber, frequency, and amplitude increase on the crest of solitary waves by increasing the amplitude of solitary waves. In comparing figs. 3.14, 3.15, and 3.16, when ω is from 0 to 0.6, the modulated short wavenumber grows 206.96%, the modulated short wave frequency grows 25.15% and the modulated short wave amplitude grows 45.24%. The growth rate of the modulated short wavenumber on the solitary wave crest is the largest among the three. From the curve in fig. 3.14 the relationship between the modulated short wavenumber and parameter ω is fully nonlinear; i.e., the short wavenumber is strongly modulated by the long solitary waves. It is therefore reasonably concluded that the modulated short wavenumber is most sensitive within the interaction of short waves and solitary waves. That means the significant shortening of the short wavelength on the crest of the solitary waves is related to local breaking and caustics.

It is shown that the modulated short wavenumber, frequency and amplitude have asymptotic decay. Their derivatives with respect to the horizontal co-ordinate are shown in figs. 3.11, 3.12 and 3.13 which are symmetric about the z axis. These results for the modulation by solitary waves are different from those of the modulation by long waves.

Unlike the regular wave case where Zhang and Melville (1990) suggested an upper limit of the steepness of long waves as 0.3 for the modulation, there is no limitation for solitary waves on the value of ω because of the asymptotic decay of solitary waves. However, it is to be expected that for large values of ω the short waves may well break. The limit for the parameter ω in the numerical modulation is not clear. So it should be noted that in the large amplitude solitary

waves the local disturbance and the instability will appear, i.e. $\omega > 0.88$, with a large growth rate of instability (Tanaka 1986). Furthermore the problem of the evolution of short waves and the problem of weakly nonlinear short waves riding on a long solitary wave based on the nonlinear Schrödinger equation (3.34) remain open.

Chapter 4

EXPERIMENTAL FACILITIES FOR WATER WAVES

4.1 The Wave Tank and the Wave Generator

4.1.1 Wave Tank

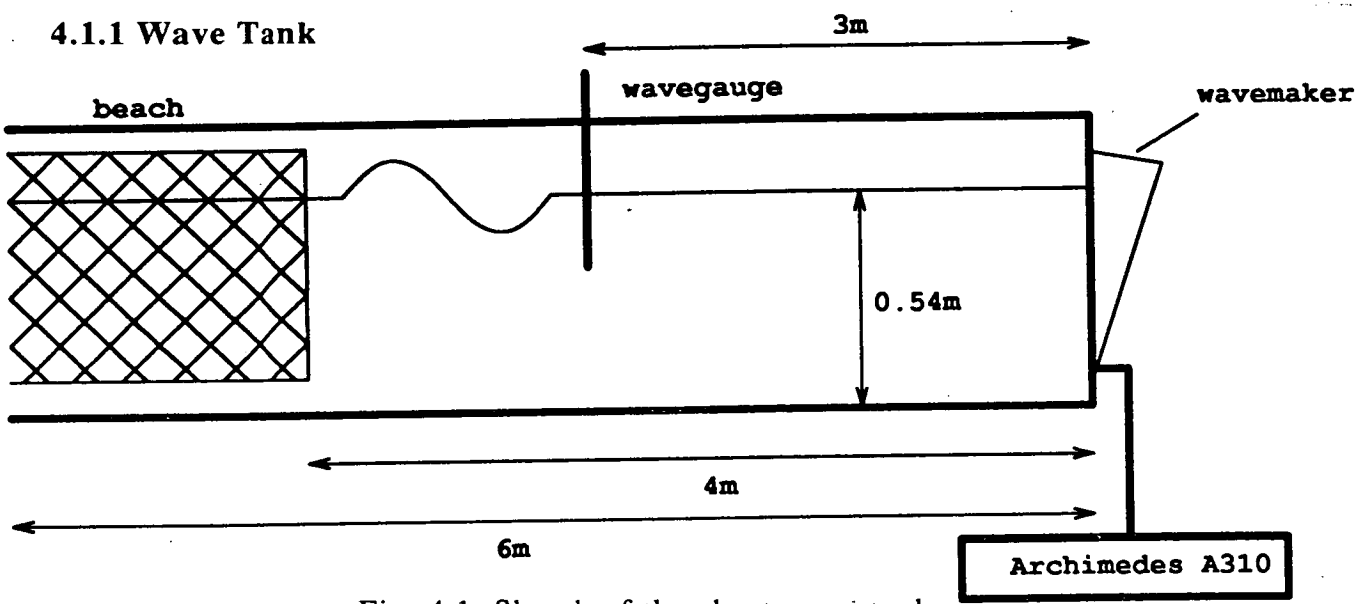

Fig. 4.1: Sketch of the short wave tank.

All the experimental work was undertaken in the short wave flume at Edinburgh University. The flat-bedded tank, which has a still water depth of 0.54m, has a width of 0.3m and a length of 6m (4m long for waves freely travelling and 2m long with a wave absorber, which is an expanded aluminium beach). The walls and the bed in the 2m long central section are made out of 19mm thick glass to allow optical access. The waves, two dimensional, are generated by a single hinged paddle which serves as a wavemaker. The wavemaker employed in this tank is of the single flap type produced by Edinburgh Designs (Salter 1982). The paddle pivots on a fabric hinge fixed to the bottom edge of the wavemaker box. Figure 4.1 shows the structure of the short wave tank.

4.1.2 Wavemaker

The paddle is driven by a servo-motor via a drive belt and springs. The servo-motor is a torque driver to offset the hydro-dynamic force. In addition there is a tachometre in line with the motor for measuring the angular velocity of the paddle. The offset torque is calculated through two high-gain feedback loops. The first loop is to calculate the torque between the motor and a piezo-electric torque transducer. The second loop is to calculate the externally required torque which equates the angular velocity and the angular position. The piezo-electric torque transducer is located between the drive belt and the paddle, and filters the velocity of the paddle. Also the position of the paddle is calculated from the tachometre, velocity encoder, on the servo-motor. These are used to optimise the process of absorbing reflected waves. The paddle therefore acts as an absorber of reflected waves as well as a wave generator. This is because the paddle incorporates a force feedback mechanism which balances the hydro-dynamic force, the sum of the drive signal and the filtered velocity signal, and it therefore

simultaneously generates waves and absorbs reflected waves. The drive signal to the paddle is given by an Arcon Archimedes A310 micro-computer which can also sample wave resistance gauges and trigger one camera. All the processes can be programmed and operated synchronously. Figure 4.2 shows the mechanism of the Edinburgh-design wavemaker.

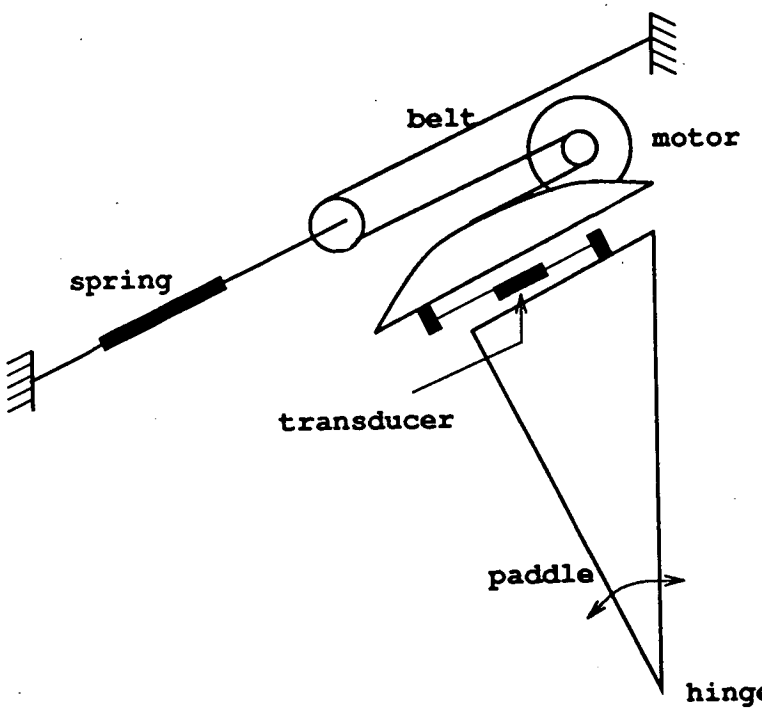

Fig. 4.2: Sketch of the mechanism of the wavemaker of Edinburgh Designs.

4.1.3 Wave Generation Software

A simple C programme includes several intrinsic functions and the inputs of the programme are the numbers of waves, wave amplitude, frequency and initial phase for wave generation. To drive the wavemaker it is necessary to have a calibration between drive voltage signals and desired waves. A transfer function is found by driving the wavemaker with small sinusoidal voltage signals of known amplitude at a series of frequencies. This is an intrinsic calibration for wave generation programmes. Skyner (1992) found that the required sinusoidal

voltage to drive the wavemaker and produce a wave of given height in the flume depends strongly on the frequency. The transfer function, which is the relation for signal voltage, wave amplitude and initial phase, could be predicted by linear theory or experiments. The transfer function applied in the short tank has been experimentally measured by Dave Skyner.

The calibration contributing to its own value can be given in a straightforward spectrum experiment. The spectrum experiment is an algorithm for wave spectrum generation represented by continuous spectra with a list of linear wave fronts, each with an amplitude, frequency, and phase. Therefore a desired wave field is generated by a specific continuous spectrum. The desired wave elevation record is then measured by a wave gauge in the tank so that the transfer function is calculated from the wave elevation for spectral analysis and shifted back to the wavemaker using linear theory.

Because of the strongly non-linearity of steep waves, in extreme cases the transfer function is not ready-made, therefore Skyner (1992) suggested that the empirical transfer function for such particular waves can be achieved by iteration of the above procedures. However, for all experiments in this thesis the required wave fields are generated in the flume and then chosen as desired.

4.1.4 Reflection and Resonance

The absorbing beach is made from wedge-shaped, expanded aluminium meshwork. The main function of the absorbing beach is to reduce wave reflection. The reflection coefficient is defined by two spectra that split from two gauges into incident and reflected components for determining the reflection coefficient. For example, the calculated wave reflection coefficient is 5.1% for the wave of 0.94 Hz and 20 mm, 3.3% for the wave of 0.94 Hz and 30 mm, and

2.8% for the wave of 0.94 Hz and 40 mm. Therefore, the reflection of long waves is also playing a minor role in the empirical modulation of short waves riding on long waves. This spectra analysis under the assumption of linear wave superposition breaks down in both the most extreme cases as well as those of high frequencies. Therefore, this analysis is used only to calculate a reflection coefficient at the wave generation frequencies (frequency range is between 0.75 and 1.5 Hz). The reflection coefficient of this beach decreases as wave amplitudes increase. So the effect of wave reflection decreases as wave amplitudes increase.

The resonant effect is produced by waves of an integer multiple of wavelengths equal to the length of the flume, 6 metres. These resonant frequencies and wavenumbers are calculated from the linear theory of dispersion. The spectra have then been checked to see if the wave amplitude increases more than 0.3 mm on specific frequencies from the resonant effect.

4.2 Surface Measurement Techniques: Wave Gauges

Surface elevations are measured in the short wave flume using resistance-type wave gauges. These gauges are used to sample the resistance at a specific frequency between two parallel metal conductors, and the elevation measurements depend on the different resistivities between water and air. As changes occur to the part of the length of immersed-in-water conductors, so the voltage across the conductors changes and this is sampled by a micro-computer (Archimedes A310) which also controls the wave generation. The change in voltage is taken to vary linearly with surface elevation so wave surface elevation is determined by

subtracting the voltage given at the mean water line and multiplying by a calibration constant. A diagram of a wave gauge is shown in fig. 4.3 (a). Figure 4.3(b) gives the relationship of output voltages from the wave gauges against the length of wave gauges immersed in water.

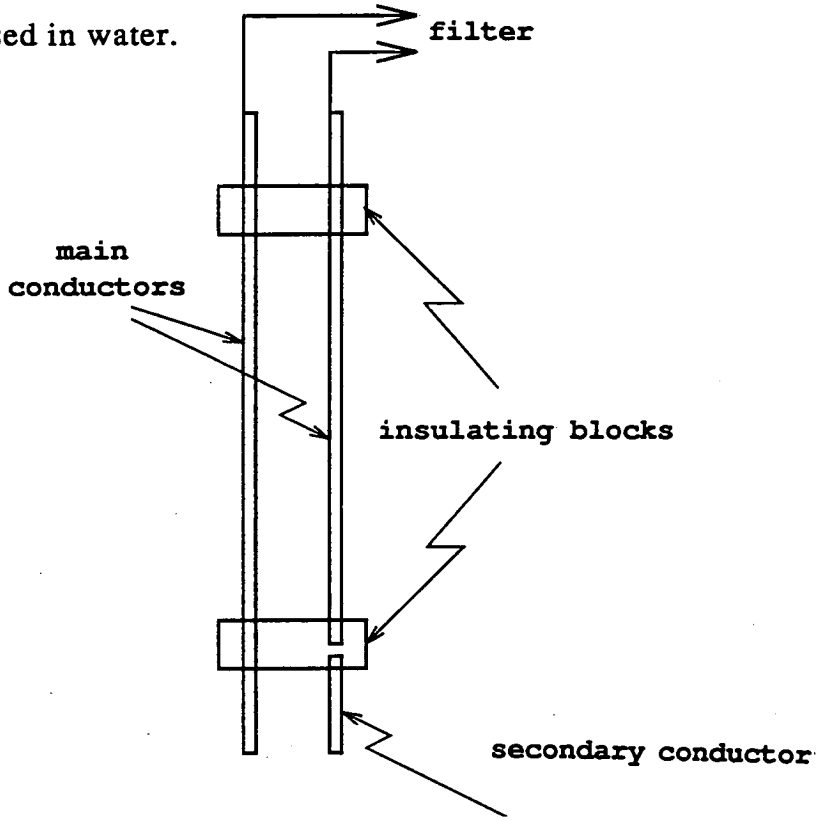

Fig. 4.3 (a): Sketch for a resistance-type wave gauge.

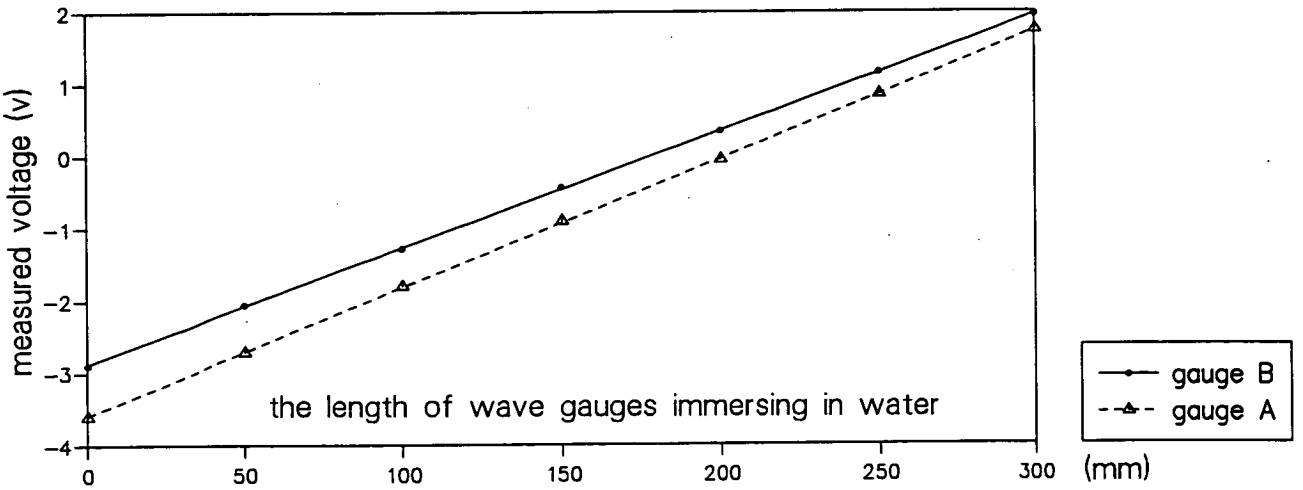

Fig. 4.3 (b): The graph for reading voltage against the length of wave gauges immersed in water (mm).

For a reading to be made, the wave surface must be between the two insulating blocks. The secondary conductor is used to determine the conductivity of the water. The calibration factor and the voltage at mean water level are determined experimentally each time the gauges are used.

4.3 Internal Kinematics Measurement

In this thesis the Particle Image Velocimetry technique (PIV) is the only experimental technique used for wave internal kinematics. In PIV, small seeding particles illuminated by high-power laser are introduced into fluids and photographed onto negative films. The seeding images on the negative have been studied for flow kinematics.

The development of Laser Doppler Anemometry (LDA) resulted in the first non-intrusive point flow measurement technique. The advantage of LDA is that it is non-intrusive. But its disadvantage is that each time it only measures at one point. The desire to achieve a greater degree of accuracy from flow field measurements is the driving force behind the development of what becomes known as Particle Image Velocimetry (PIV).

4.3.1 The Particle Image Velocimetry Acquisition

The PIV apparatus is sketched in fig. 4.4. The short tank can be seen with the measurement area (actually a volume due to the finite width of the laser beam) illuminated by the high-power laser. The parabolic mirror of the scanning system is located below the tank and the camera is facing and located 1.7 metres away from the

side wall of the flume. An Acorn Archimedes micro-computer (A310) controls the wave paddle, samples the signals from wave gauges and triggers the camera with specific time delay. The laser beam path can be traced back under the flume (seen in fig. 4.4).

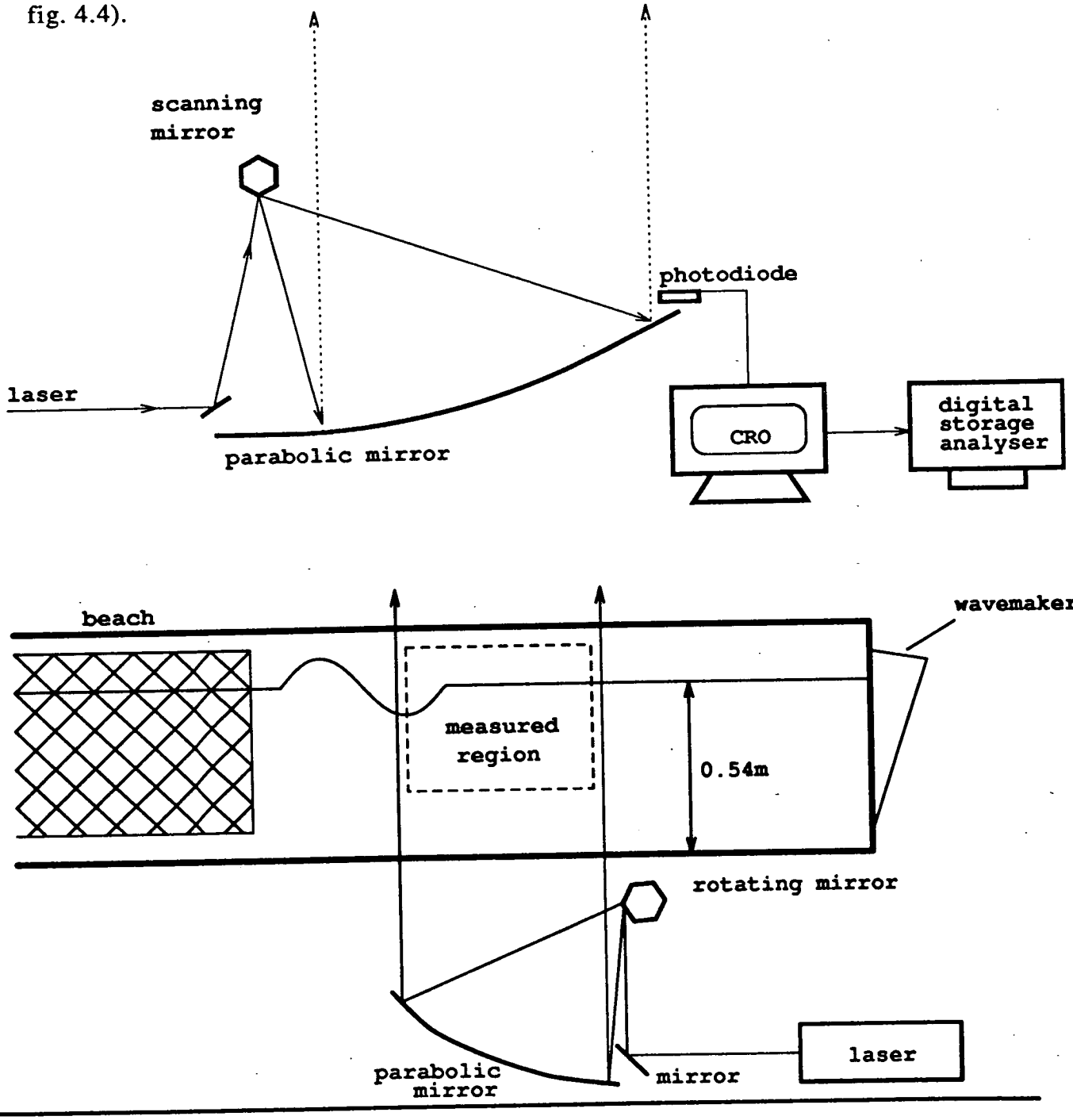

Fig. 4.4: Sketches of the scanning beam system and the PIV apparatus.

4.3.1.1 Camera, Lens and Film

The choice of photographic equipment is of importance in PIV. The camera should be equipped with a flat-field lens if image plane distortions are not to be a problem. The choice of the focal length of the lens can reduce the effect of out-of-illuminated-plane motions and improve the imaged region of the flow.

The lens employed here is of focal length 80mm or 150mm, depending on experimental considerations. Lens distortion was measured by Gray (1989), who mentioned 1.5% distortion will be at the edge of the photographed film.

The two timing aspects of the camera's operation rely on mechanical devices which are checked. An accurate knowledge of the delay between triggering the camera and its shutter opening is essential, and an idea of the actual shutter timing is important if the number of particle exposures is to be reasonably well predicted.

parameter setting	
film rate	100 ASA
apperture	f4
shutter speed	1/30 sec
laser power	12W
scanning period	7.4 ms

Tab. 4.1: The parameters for the PIV acquisition.

The trigger and shutter times are measured by detecting the signal from a photodiode placed on the path of a low-powered laser beam passing through the lens. From the duration of the signal the actual shutter times are determined from 80mm lens, which houses the timing mechanism, and these are given in tab. 4.1.

These are some large departures from the nominal speeds, but the consequence of this is only a small change in the number of particle images recorded.

The PIV photographs are taken with a Hasselblad 500EL/M camera with a Zeiss Planar CF 80mm f/2.8 flat focus lens, which is positioned about 1.7 m away from the illuminated plane, with the camera's view centred 0.2 m below the still water surface. The choice of lens is to minimize distortion. The film used is T MAX 100 which is 120 format (i.e. negative size = 56.5 x 56.5 mm^2). This film is rated 100 ASA and has a high resolution of 200 lines/mm over 5000 dpi. The shutter is triggered (via a relay switch) by the Acorn Archimedes micro-computer which also controls the wave generation and samples the wave gauge signals.

The above factors make the combination of lens, camera and film ideally suited to the full-field measurement of an area as it can then be analyzed accurately, using a relatively small interrogation spot area, over a large grid of points.

The optical axis of the camera is lined up on a small reference cross-marker on the side of the flume at the calm water level. The kinematics near the long wave crests is of most interest here. As image distortions are the smallest near the optical axis and velocities near the crest are difficult to measure due to reflections off the underside of the wave free surface. These considerations are reduced by having the camera close to the surface.

The shutter speed is set so that multiple exposures (3 to 5 preferred) can be taken. The effect of sharpening the Young's fringes is related to the particle image pair density and the correlation between pairs separated by the flow. The choice of shutter speed balances the desire for multiple images and the separations between two consequent images with the proper scan period and the need to 'freeze' the wave motion (to limit velocity gradients in the analysis region). According to the

maximum speed of waves, a shutter speed of 1/60 second is set with a typical scan period of 4 - 5 ms to ensure 3 or 5 images to each particle.

The photographic magnification is determined by placing a ruler in the location of the illuminated region. This is then photographed and the magnification determined from the image of the ruler. The camera must not be moved during calibrating the magnification and the PIV photos. The distortion, due to the lenses and air-glass-water interface, will be ignored.

4.3.1.2 Laser and Scanning Beam System

The laser used in the experiments is a Spectra Physics 15W continuous wave Argon-Ion laser, model 171. The produced wavelengths range from 454 to 515 nm. This is reflected off special high-power laser mirrors onto the scanning beam system.

The purpose of the illumination is to produce multiple well-exposed, sharp images of the seeding particles. The illumination must therefore occur for a short period of time (relative to the period during one exposure and the movement of particles) so that the motion of the particles is frozen and the image displacement of particles is large compared to the size of particles. The only purpose in using a high-power laser is to illuminate the seeding particles. The optical coherent property is not important.

The scanning beam system at Edinburgh was originally designed by Gray (1989), as shown in fig. 4.4. The laser beam in the system is reflected off, an octagonal rotating mirror onto a parabolic mirror and up into the flow. As the octagonal mirror rotates, the beam is swept along the parabolic mirror. As the octagonal mirror is at the focus of the parabolic mirror, the expanding beam is recollimated.

Here the direction of the beam off the parabolic mirror is vertically up through the glass base of the flume. This provides a non-divergent scan through the measurement region. One of the advantages of the scanning-beam system over the expanded sheet is an increase in the percentage of available light used.

In this system, the rotating mirror is controlled by an adjustable control circuit. A photodiode is placed at the end of parabolic mirror to detect the scan rate, which is stored and analyzed by a Thurlby Digital Storage Analyser and a 20 MHz CRO.

Scanning rate is sensitive in production high-quality PIV negatives, at the dynamic range that can be limited by the analysis system. The scanning rate must be adjusted to try to make the maximum velocities which produce the maximum separation measurable on the negative (about 0.25 mm). Adjusting the scanning rate also depends on the photographic magnification. The scanning rate may be altered depending on the results of the first run of the experiment.

The seeding used is conifer pollen. Conifer pollen is able to reflect the laser light reasonably well and provides sharp and clear images on the film. Moreover, if the photographic magnification is 0.08, then 5 μm in diameter is a minimum resolvable size of the image on the film. So the size of conifer pollen with a diameter of 70 μm is approximately the optimal value for the acquisition of PIV. According to experience, it is also almost neutrally buoyant and small enough to drift with the flow. This suggests that it will follow the fluid motions accurately and so is suitable for use as PIV seeding. The seeding density is adjusted to yield about ten particle pairs in each interrogation zone of one negative.

A sketch of a negative photographed by the PIV technique is shown in fig. 4.5.

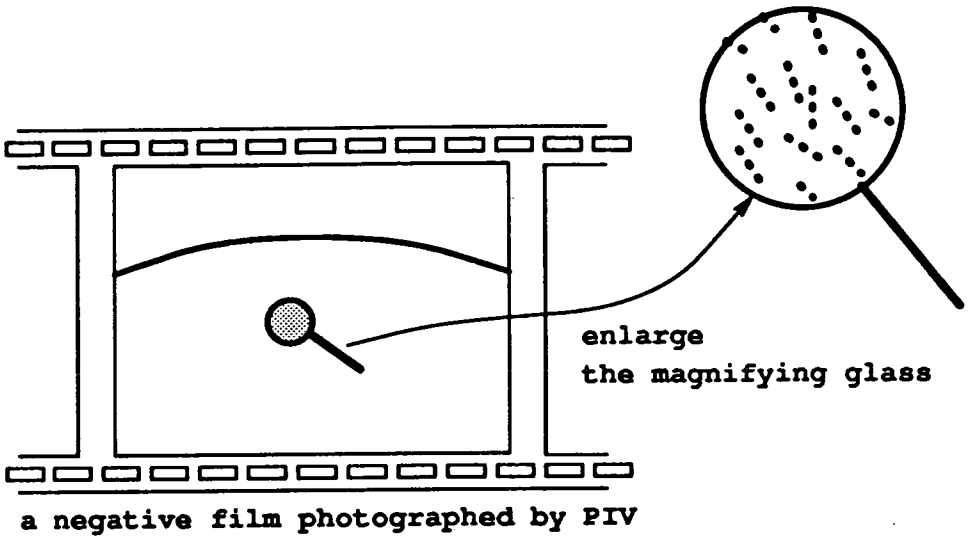

Fig. 4.5: Sketch of a negative photographed by the PIV technique.

4.3.2 PIV Acquisition Errors and Limitations

4.3.2.1 System Error in the Scanning Beam System

The system error includes several aspects which can affect the accuracy of the final velocity measurements in the acquisition of PIV photographs due to inadequacies in the apparatus and experimental uncertainties. The error aspects of PIV acquisition here were first considered by Gray (1989). Geometric distortions are due to the imperfection of camera lens and refractive index changes between the camera and the measurement zone can be thought of as introducing a small modification onto the magnification dependent on the position within the negative. The region of greatest interest of the flow field will be photographed in the area of minimum distortions of lenses. A similar type of error is introduced by the deviations of the light sheet due to flatness and thickness. The consequences of the 3 mm variation of flatness and random thickness are to give systematic and random errors of up to 0.3% and 0.2% when the camera is positioned 1.7 m from the measured zone. There are two particular concerns about how well the seeding follows the flow as well as the seeding's

ability to drift with unsteady flows. Typical systematic and random errors in the acquisition of PIV photographs are summarised in tab. 4.2. However, the errors are small, in practice they are conveniently ignored.

Error Factor	Random Error	Systematic Error
Illumination Interval	0.2%	
Photographic Magification	0.3%	
Illumination Plane Thickness	0.1%	
Illumination Plane Flatness		0 ~ 0.3%
Photographic Distortion		0 ~ 0.3%
Scanning-Beam Time Effect		0 ~ 0.2%
Seeding not Following Flow		0.1%

Tab. 4.2: The errors involved for the PIV acquisition.

Besides the errors introduced in the above paragraph, one disadvantage of the scanning beam system results from a small systematic error due to the movement of the seeding and the variation of pulse duration with position.

4.3.2.2 Systematic Error in Time Between Pulses

Equation (4.1) was derived in the paper of Gray et al. (1987) for the systematic error introduced in the scanning beam system by the movement of the seeding and

the non-uniform scan velocity through the measured area. The error caused by the movement of the particles is calculated, assuming an average scanning velocity of the beam through the measurement region. Moreover, the same paper gave an expression for the scanning velocity which is dependent on horizontal position within the measuring volume and geometrical factors of the system.

The horizontal and vertical co-ordinates are x and z which the origin being on the horizontal and vertical axes of symmetry of the parabola, which is of length L and height L/2. The laser beam is incident onto, and reflected from, the rotating mirror at the point (0, L/2). The systematic error ξ in the calculation of horizontal velocities can now be given:

$$\xi = \frac{\Delta x L N}{2\pi (L^2 + x^2)} \qquad \text{(EQ 4.1)}$$

where Δx is the measured horizontal particle displacement, L is the scan length, N is the number of faces in the rotating mirror and x is the horizontal position along the scan length (measured from x=0 below the rotating mirror, hence $0 \le x \le L$). It can be seen that the measured velocity should be multiplied by the correction factor $(1-\xi)^{-1}$ in Eqn. (4.2). The systematic error of vertical velocities have a similar expression as Eqn. (4.1). The formula for calculating PIV velocities is

$$v_{x,z} = \frac{CM}{(1-\xi)\tau} s_{x,z} \qquad \text{(EQ 4.2)}$$

where v_x and v_z is the x (horizontal) and z (vertical) velocity components respectively in the illumination plane. C is a scale factor of the system, M is the photographic magnification, ξ is a correction given by Eqn. (4.1), τ is the scan period and $s_{x,z}$ is the measured displacement peak location of the seeding.

It should be noted that the systematic and random errors could in principle be measured or estimated, and a correction made to the data.

4.3.3 The PIV Analysis System

The aim of the PIV analysis method is to measure the accurate separation of two consecutive images from localised regions or interrogation areas on the developed negative photographed by the PIV technique, and hence to determine the local velocity by knowing the time duration between the separation.

4.3.3.1 Young's Fringe and Autocorrelation Calculation

The analysis system used at Edinburgh is a two-dimensional Fourier transform technique first developed by Gray (1989) by applying Huntley's method (Huntley 1986) which gave more accurate results than other methods used. Huntley's method involves a fully automated fringe analysis based on the two-dimensional Fourier transformation of the fringe intensity distribution. So the photographic negatives containing velocity information are analysed using Young's fringe technique (Huntley 1986). The previous description of this is merely pointed out how to produce Young's fringes and stated that the flow velocities could be determined from the separation and orientation of two consecutive images. The schematic diagram of the analysis system is illustrated in fig. 4.6.

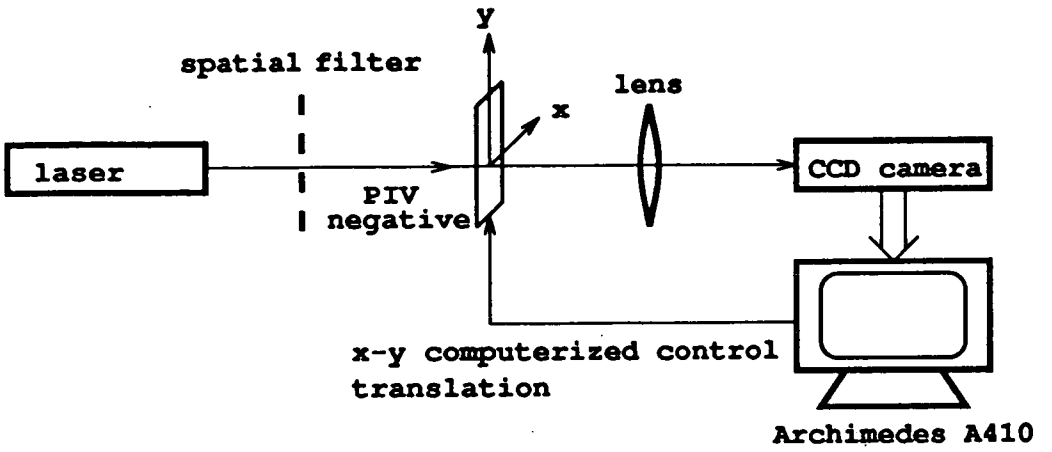

Fig. 4.6: Sketch of the PIV analysis system.

In the implementation of Young's fringe analysis method at the Edinburgh-design PIV analysis system- i.e. the Fourier method- is adopted. The fringe pattern, which are the first optical transform, is captured and digitised via the CCD (Charge-Coupled Device) camera and averaged into 64x64 arrays. Then the arrays are processed in Arcon Archimedes micro-computer A440 in order to determine local velocities. The optical Fourier transform is achieved by illuminating with a low-power laser beam. A two-component precision micro-translation stage is used to physically transport the negative between the fixed optics.

The negative photographed by the PIV technique is framed on two orthogonal micro-translational stages, which are used for the horizontal and vertical movements of the framed negative and are controlled by the analysis computer, an Acorn Archimedes micro-computer A440. The PIV negative is analysed in small regions, about 1 mm^2 (defined by the size of the laser beam interrogation spot). Each spot has been analysed and then the stages move the negative so that a new area is interrogated by the beam. The process is repeated over a grid of points until the area of the desired flow field is covered.

The interrogation spot on the PIV negative is from a He-Ne laser with power 0.5mW and wavelength 633 nm. The laser power is controlled by a pair of polarisers, and the spatial noise of the beam is limited by a spatial filter. This is one focal length from the converging lens centred on the beam path and a further focal length from a CCD video camera, also on the beam path. There is a small optical stop in the centre of the video lens to remove the DC (un-deviated) component of the beam.

The Fourier transform of the fringe intensity equals the convolution of the amplitude of the interrogation-spot image field. This results in an autocorrelation plane with self-correlation peak, symmetrical and opposite displacement peaks and noise peaks. The self-correlation peak can be reduced by subtracting the average diffraction halo. An average diffraction halo is determined from an average of 40 sets of fringe patterns is sampled from random positions and angles throughout the flow. The diffraction halo is caused by singular particle images. This aids the resolution and detection of small particle separation. The self-correlation peak is not usually completely removed so the central area of the self-correlation plane is set to zero.

The dominant separation is then found by locating the displacement peaks and measuring their distance from the centre (the function is symmetrical about its centre). This is done by locating the position of the highest correlation value and then calculating the centroid of the surrounding displacement peak.

Young's fringe diagram shows that the lens is used to perform a two-dimensional Fourier transform from the interrogation spot of the PIV negative. Each seeding particle image acts as a point-light source and hence each pair of images acts as a pair of coherent light sources and produces a set of Young's fringes in the Fourier

plane (the back focal plane of the lens where the video camera is situated).

The random distribution of the seeding particles in the flow produces a random set of fringes which forms speckle-type background noise. Each pair of successive images of the same seeding particle also produces a set of fringes related to the flow characteristics. If there are no great velocity gradients across the analyzed region then the flow will superimpose a similar separation between successive images of all the particles and each set of images will form similar fringes. This leads to the reinforcement of that fringe pattern and the formation of a dominant set of fringes caused by the flow. These fringes are perpendicular to the flow direction and their separation is inversely proportional to the magnitude of the seeding displacement.

The results, in arbitrary displacement units, are converted into velocities by the analysis programme using the photographic magnification, the scan period and a scale of the analysis system. PIV has a limited dynamic range. If the particle images are too close on negatives, they cannot be resolved. On the other hand, if they are too for apart, they are outside the measurement zone of the analysis rig.

The film photographed by the PIV technique is a multi-exposure negative of a large flow area (here approximate 500mm x 500 mm). The raw output of the analysis of the negative is a set of results in a grid of points covering the negative. Each result comprises a pair of co-ordinates, horizontal and vertical velocity components and a measure of the displacement peak visibility at that point (a measurement of the signal-to-noise ratio). The output then undergoes post-processing to remove spurious results. The processed output can then be used in comparisons with theories or to look at flow structures and turbulence etc.

The analysis system provides a result for every point on the analysis grid. Obviously this extends above the surface elevation at certain points on the grid and a spurious result is produced there when noise is measured. These results are removed by post-processing of the data. The velocity map is displayed on the screen of the analysis computer. Data points from above the surface are deleted by selecting them with the mouse. Other spurious points may be deleted in this way, too. These unsuccessful data points may result from a lack of seeding or illumination or a lack of correlation due to out-of-illuminated-plane motion. They tend to have a very low signal-to noise ratio and show no continuity in magnitude or direction with their immediate neighbours.

The second major element of the post-processing is the scaling of positions and velocities back to full scale. This is done using the measured photographic magnification, measured scan period and a scaling factor of the analysis rig. Errors in these values are discussed in the previous section.

All the quantitative velocity measurements are completed by the PIV analysis technique. A copy of the full field data is edited down to a few columns of data under the crest. The choice of which columns to retain was made by selecting the block at the centre of the negative where the horizontal crest velocities were highest and the vertical velocities lowest. The wave crests are at the centre of the negative due to the wave gauges iteration procedure. The measured wave phases are close to zero, but are not exactly zero. Therefore a block of results could be presented together. The block is typically 2 to 4 columns wide, which corresponds to about 2 to 4% of a wavelength.

There are a few points at each elevation as results from 2 to 4% of a wavelength are shown to cover any error in fitting PIV measurements to theoretical results.

Errors are ignored to the PIV results as the magnitude of the errors was so small at the crest. The spread in velocities due to using a block of results provided a suitable measure of the uncertainty in fitting theoretical profiles to the measurements, as the wave phases measured are not always exactly zero.

4.3.4 PIV Analysis Errors and Limitations

A PIV negative contains information from which the underlying flow can be deduced. The accuracy of the analysis process depends on the optimisation of the PIV acquisition parameters, and, even if these were ideally set, is fundamentally limited.

Random and systematic errors are two major types of error inherent in the analysis process. They vary with the velocity gradients present in the flow. General speaking, the systematic errors are more dangerous than the random errors, as the random errors manifest themselves clearly when the acquired data is of low quality. In fact, the random errors range between 0.3% to 0.5%. Actually these errors were obtained and estimated from artificially generated PIV negatives, made by plotting random patterns of dots, with known separations, followed by photographic reduction. Gray (1989) has investigated systematic errors and random errors using a Monte Carlo simulation for the measurement of waves in the flume and for the analysis rig used here.

There is always uncertainty with regard to the location of the centre of the correlation peak, due to the random sampling of the particles in the interrogation area, and this uncertainty increases as the range of particle displacements increases and the correlation peak broadens. The systematic error associated with the displacement gradient tend to bias the average displacement measurement towards the lower displacement, since the larger particle image separations tend to locate outside the interrogation area. In algebraic and numerical studies it has

been found that there is a systematic bias introduced which varies linearly with the displacement gradient.

Here it is necessary to recall Eqn. (4.2) for further discussion on the relative errors of the parameters. The scale factor C, which is estimated from the analysis of known measurements, has a relative error of 0.1% (Sutherland 1992). The magnification M is obtained from measurements of a photograph of a known reading. Its value varies systematically with position due to lens distortion and randomly due to measurement errors. A typical relative error of the magnification is estimated 0.5%. The scan period τ is determined using a digital storage analyser which is as reliable as possible. For the PIV system used here in Eqn. (4.1) $\Delta x \ll L$ so ξ is negligible. Normally, as Sutherland (1992) suggested, $\xi \leq 0.006$. Therefore the relative error of ξ was considered to be too small to be worth calculating explicitly. In fact the errors in ξ depend on geometrical factors and $s_{x,z}$ and are taken to be small in comparison to ξ. As the term (1-ξ) is itself treated as one, ξ can be treated as an uncertainty, with relative error $\xi/(1-\xi) \leq 0.006/0.994$.

There is a random error and a systematic error in determining s_x and s_z and they both depend on the displacement gradients present on the film which relates the velocity gradient.

The relative uncertainty in v_x can be given by

$$\left(\frac{\sigma_{v_x}}{v_x}\right)^2 = \left(\frac{\sigma_C}{C}\right)^2 + \left(\frac{\sigma_M}{M}\right)^2 + \left(\frac{\sigma_\tau}{\tau}\right)^2 + \left(\frac{\sigma_{s_s}}{s}\right)^2 + \left(\frac{\sigma_{s_r}}{s}\right)^2 + \left(\frac{\xi}{1-\xi}\right)^2 \qquad \text{(EQ 4.3)}$$

There is a similar equation for v_z. The error is taken to comprise a relative component of approximately 1% and an absolute error of about 1.1% of the maximum measurable velocity. The scan period is adjusted so that the anticipated

crest velocity equals the maximum measurable and the experiment is repeated if the measured velocity is too high, so the maximum measured velocity is close to the upper limit. Therefore the absolute error may increase slightly but should be lower than about 1.3% of the highest measured velocity.

The total relative error increases as the velocities decrease, due to the increasing relative importance of the absolute error. The total error, however, decreases as velocities decrease and should always be less than 2% of the maximum measured velocity.

The papers of Keane and Adrian (1991) and Quinn et al. (1992) obtained values for the systematic error σ_{s_s} and the random error σ_{s_r}, when the maximum measurable velocity was estimated. The errors determined will be the maximum for any of the waves measured. The values of random and systematic errors are 0.3% and 1.1% respectively.

However, these errors can be kept small (i.e. within 1%), by careful control. Another error in the PIV analysis is in the calibration of the analysis rig which was obtained by an artificially generated PIV film. In this way, the calibration values have been found with an accuracy of about 0.1%. The vertical and horizontal values found from the artificial PIV film were different because the pixels on the CCD array are not square (Skyner 1992).

Chapter 5

SHORT WAVE MODULATION BY LONG WAVES

5.1 Introduction

The main purpose of this chapter is to present the modulation and kinematics of short waves modulated by long waves by comparing the experimental work with theoretical approaches. Section 5.2.1 discusses the experimental frequency modulation of short waves riding on long waves according to wave elevation measurements and a function fitting scheme. Section 5.2.2 gives the theoretical modulation of short waves riding on Stokes' waves which will be useful for further experimental survey in studying the interaction between short waves and long waves. The theoretical modulation of short waves riding on long waves will be shown in Section 5.2.2. Here conservations only under steady state are applicable because the evolution solution for the modulated short wave frequency is almost intractable. Besides, a theoretical long wave field is desired for the conservations.

Stokes' wave has been chosen as a mathematical model of the long waves as the major non-uniform velocity field, though so many mathematical models have been well established for monochromatic long waves. There are many further discussions based on Stokes' expansions, such as the instability problems (subharmonic and superharmonic instabilities). Also Stokes' waves are popular in engineering applications for monochromatic long waves. Therefore Stokes' wave is a reasonable and good model to represent the long waves in the theoretical approach of modulation. Section 5.3 presents kinematics comparisons between experimental measurements and linear theory, the Wheeler stretching, Chakrabarti stretching and superposition stretching methods. In addition, the comparisons between measurements and the time-stepping method for monochromatic long waves will be performed in Section 5.3.4.

To empirically explore the modulation of short waves riding on monochromatic long waves, mechanically-generated short waves and long waves are produced in the same direction of propagation by a hinged wavemaker. In the theoretical work both waves are also travelling in the same direction. All waves are generated at frequencies given by $f = j/25.6$ Hz, where j is an integral input (for example, j=30 then $f = f_{30} = 30/25.6 = 1.17$Hz). In the past the relative steepness H/gT^2 and the relative depth d/gT^2 are used to represent design waves. Nevertheless, either the relative steepness and depth or wave steepness ak can be chosen as representation of various wave environments. But in fact and traditionally, the theoretical modulation of short waves riding on long waves is a function along long wave phases as increasing long wave steepnesses ak. So for comparisons between the experimental and theoretical modulation by increasing long wave steepnesses, it will be convenient to use the steepness ak in representation rather than the relative steepness and the relative depth.

5.2 The Modulation: Frequency

In this section, a theoretical approach is compared with experiments for frequency modulation of short waves riding on monochromatic long waves. The theoretical methodology employed here was first presented by Zhang and Melville (1990). First of all, it is necessary to choose the frequency ranges for both short and long waves, to be used in the following experiments. Then the sectionized net records of short waves, which are deducted the cases of long waves from the cases of short waves riding on long waves with respect to long wave phases, will show amplitude modulation in quality. That means the local short wave heights are functions of the long wave phase. Long wave phases will be given by the long wave periods where are determined by down zero-crossing of long wave records. The spectra of wave records are also required, either the cases of regular waves or the cases of two-component waves, from FFT and will aid in understanding amplitude distribution against frequency ranges for amplitude and frequency modulation from other points of view.

Choosing suitable frequency ranges for both short waves and long waves is a crucial task. Short wave frequency shall be much larger than long wave frequency. An assumption can then be made: short waves are strongly modulated by long waves and long waves are not affected by short waves. Since short wave frequency cannot be too large because of the physical limitation of the wavemaker and long wave steepnesses will be as high as possible if linear and weakly nonlinear long waves are qualified. This implies that the strongly nonlinear long waves will increase the difficulty for getting the empirical modulation. In this thesis, the frequency ratio of short waves and long waves is

close to 3, but not exactly 3. This is a purpose for offsetting the modulation of short waves riding on long waves from the third harmonic effect of long waves. The ratio 3 gives three periods of short waves almost riding on one period of long waves; that means almost ten short wavelengths are involved in one long wavelength. Therefore, short waves are strongly modulated by long waves in a high wavelength ratio. However, any higher frequency ratio than 3 is not applicable because long wave frequency reduces as the ratio increases. The reduced long wave frequency is of the same reduced long wave steepness. Furthermore, if any smaller ratio - such as 2 - is chosen, then the second harmonics of long waves will play an important role in the interaction. Somehow, this will result in confusion between short waves and the second harmonics because the second harmonic amplitude of long waves will be of the same order as short wave amplitude. Both are involved in the modulation, and this involvement will lead to further complication. According to the above consideration, there are three frequencies used as long wave frequencies, 0.63 Hz, 0.78 Hz and 0.94 Hz. Also by increasing either long wave amplitude or frequency, long wave steepness increases. Table 5.1 gives the parameters of the design waves used in this chapter.

experiment reference	e1t2	e1t4	e3t2	e3t4
long wave amplitude (mm)	10	20	10	20
short wave amplitude (mm)	0	0	0	0
long wave frequency no.	16	16	20	20
short wave frequency no.	49	49	59	59
long wave steepness ak	0.02	0.04	0.027	0.054
short wave steepness ak	0	0	0	0

experiment reference	e2t1	e2t2	e4t1	e4t2
long wave amplitude (mm)	10	20	10	20
short wave amplitude (mm)	10	10	10	10
long wave frequency no.	16	16	20	20
short wave frequency no.	49	49	59	59
long wave steepness ak	0.02	0.04	0.027	0.054
short wave steepness ak	0.147	0.147	0.214	0.214

experiment reference	e5t2	e5t4	e5t6	e5t8
long wave amplitude (mm)	10	20	30	40
short wave amplitude (mm)	0	0	0	0
long wave frequency no.	24	24	24	24
short wave frequency no.	73	73	73	73
long wave steepness ak	0.037	0.074	0.110	0.147
short wave steepness ak	0	0	0	0

experiment reference	e6t1	e6t2	e6t3	e6t4
long wave amplitude (mm)	10	20	30	40
short wave amplitude (mm)	10	10	10	10
long wave frequency no.	24	24	24	24
short wave frequency no.	73	73	73	73
long wave steepness ak	0.037	0.074	0.110	0.147
short wave steepness ak	0.327	0.327	0.327	0.327

Tab. 5.1: Notations of the cases of regular and two-component waves in this chapter.

The acquisition of experimental modulation is derived from the following procedures. Once the wave maker starts functioning, wave records in both cases: regular waves and two-component waves, are taken from the beginning of the 16th second for 25.575 seconds at a sampling frequency of 40 Hz. These experiments are repeatable owing to the use of a computer-controlled digital time series for wave generation and sampling. For the cases of two-component waves, during the interaction between short waves and long waves, long waves are not perturbed by short waves as assumed. This means that if, since both records start and end at the same time during the measurements, a net record of short waves can be obtained by subtracting a record of long waves from a record of two-component waves, this net record will show elevation difference modulation of short waves. The three sets shown in figs. 5.1 for both cases of long waves and short waves riding on long waves, (**e5t2** and **e6t1**), (**e5t6** and **e6t3**) and (**e5t8** and **e6t4**) are detailed in tab. 5.1. The time series for the cases of regular waves (solid curves) and two-component waves (dashed curves) are shown in figs. 5.1(a), (d) and (g). The net records of short waves, which are obtained by deducting the records of regular wave from the records of two-component waves, are shown in figs. 5.1(b), (e) and (h). The trace of the derived wave elevation difference clearly demonstrates the amplitude modulation, see figs. 5.1(b), (e) and (h).

Theoretically the modulation of short waves riding on long waves is a function of long wave phase. Therefore, it is more interesting to consider the elevation difference along long wave phase before approaching frequency modulation. To accomplish this stage one needs to recall the records of regular waves. The time series of regular wave elevation can be sectionized by down-zero crossing to determine a long wave period. Hence, a record of regular waves can be divided into many sections and each section is one long wave period. Therefore, any

specific time on the record can be identified into a phase of a long wave period according to the location of that specific time with respect to the long wave period. On the other hand, the records of short waves riding on long waves have the same long waves involved as in the records of long waves, the above-derived net records are transformed into the records of elevation difference against long wave phase in contrast to the sectionized records of long waves. The net records of elevation differences with respect to long wave phase over one long wave period are shown in figs. 5.1(c), (f) and (i). Here, as long wave phase is normalized by 2π. So the long wave trough and crest are near 0.25 and 0.75 of the long wave phase.

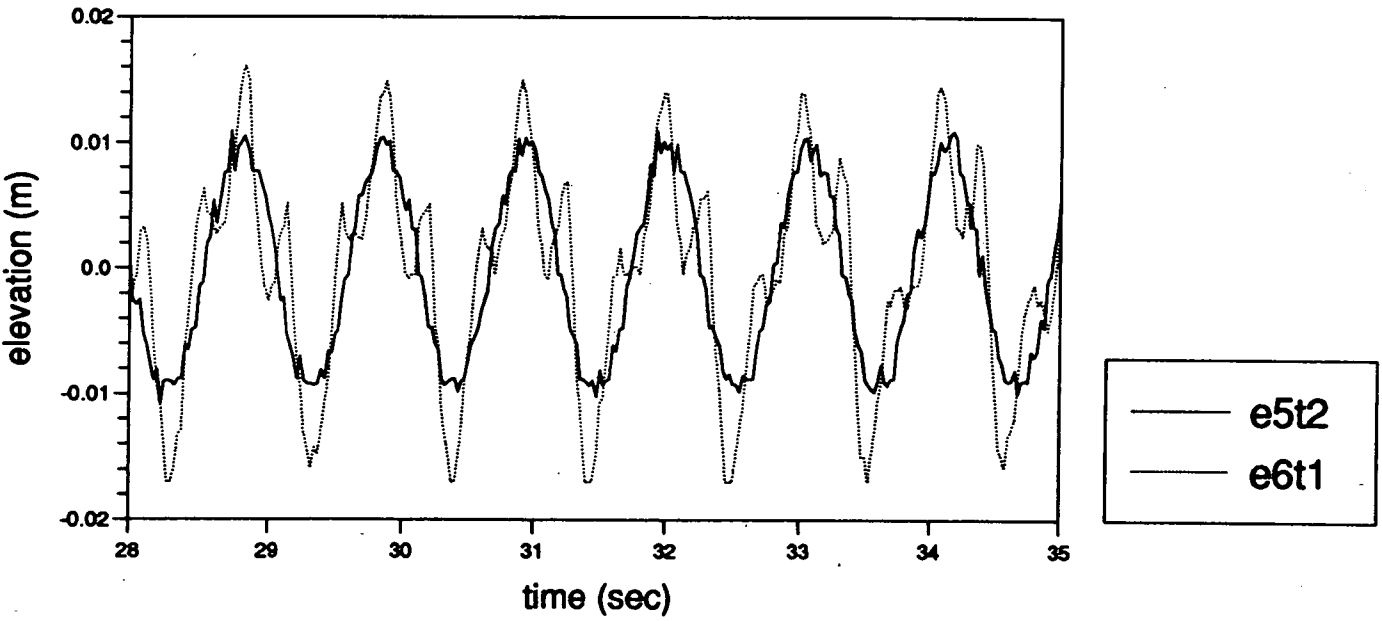

Fig. 5.1(a): The elevation records, **e5t2** (solid curve: regular waves) and **e6t1** (dashed curve: two-component waves).

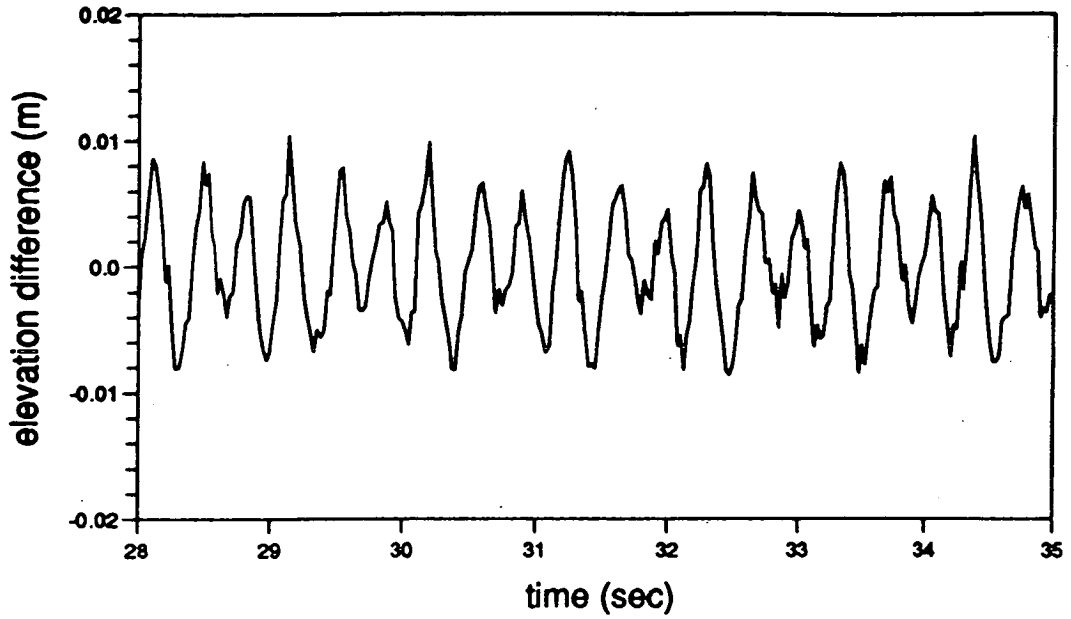

Fig. 5.1(b): The net difference record obtained by subtracting **e5t2** from **e6t1**.

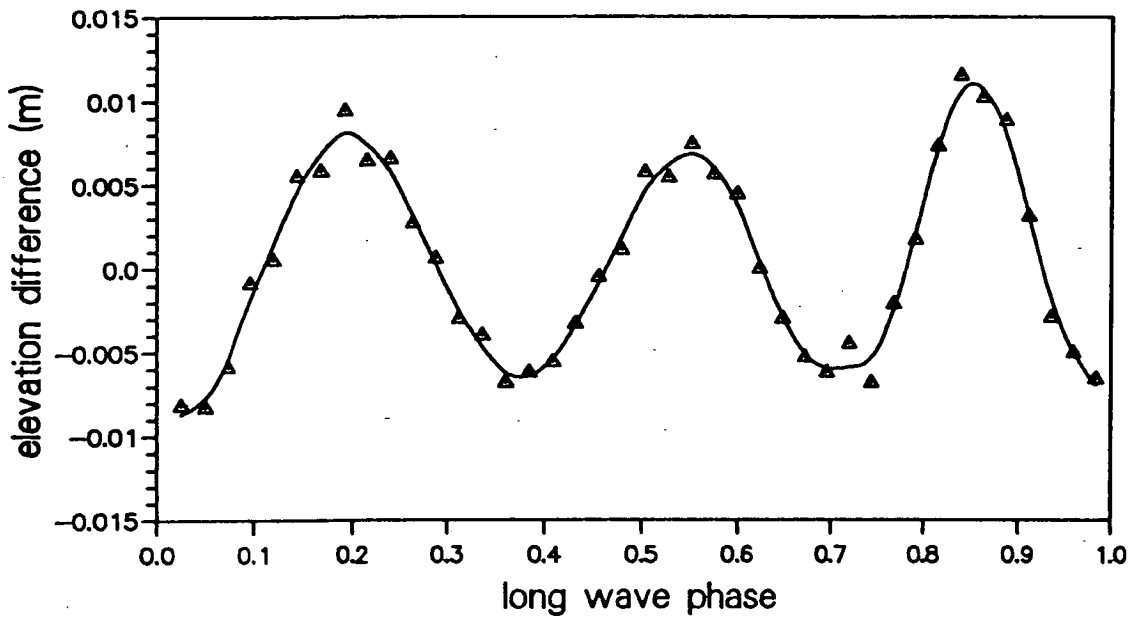

Fig. 5.1(c): A sectionized net record, obtained by subtracting **e5t2** from **e6t1**, riding on one long wave period (Δ: measured data, solid curve: best fitting).

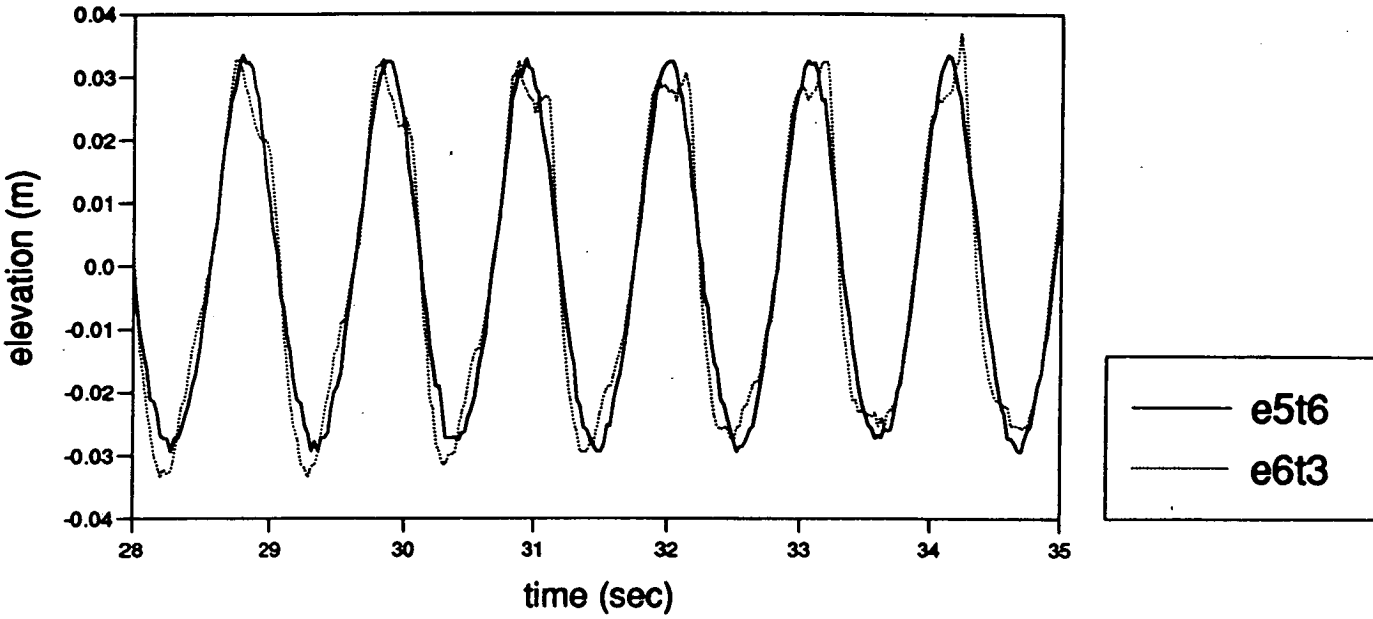

Fig. 5.1(d): The elevation records, **e5t6** (solid curve: regular waves) and **e6t3** (dashed curve: two-component waves).

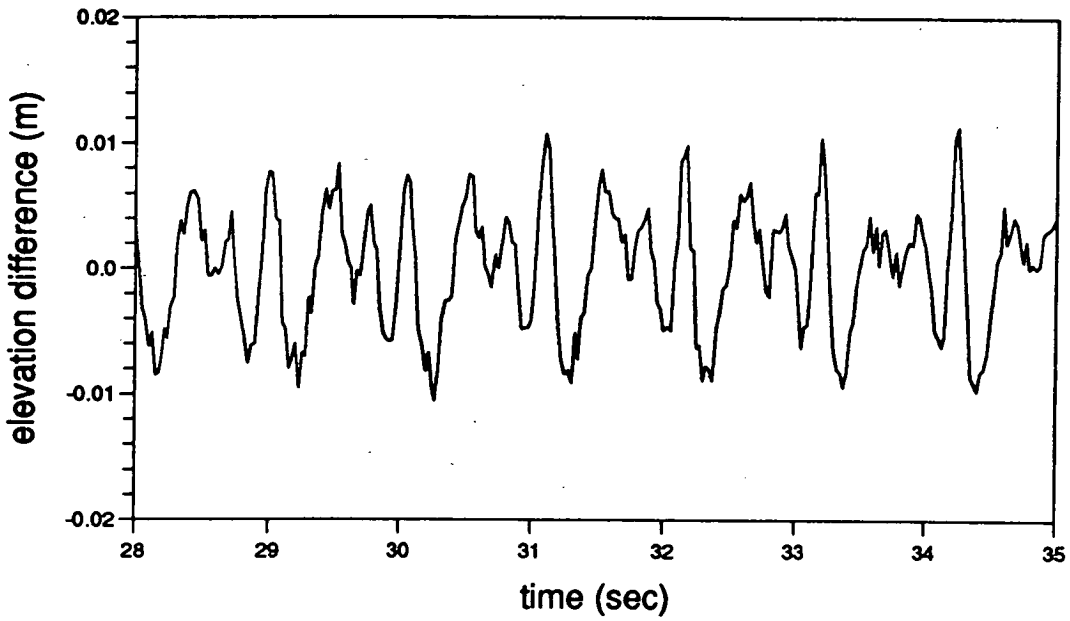

Fig. 5.1(e): The net difference record obtained by subtracting **e5t6** from **e6t3**.

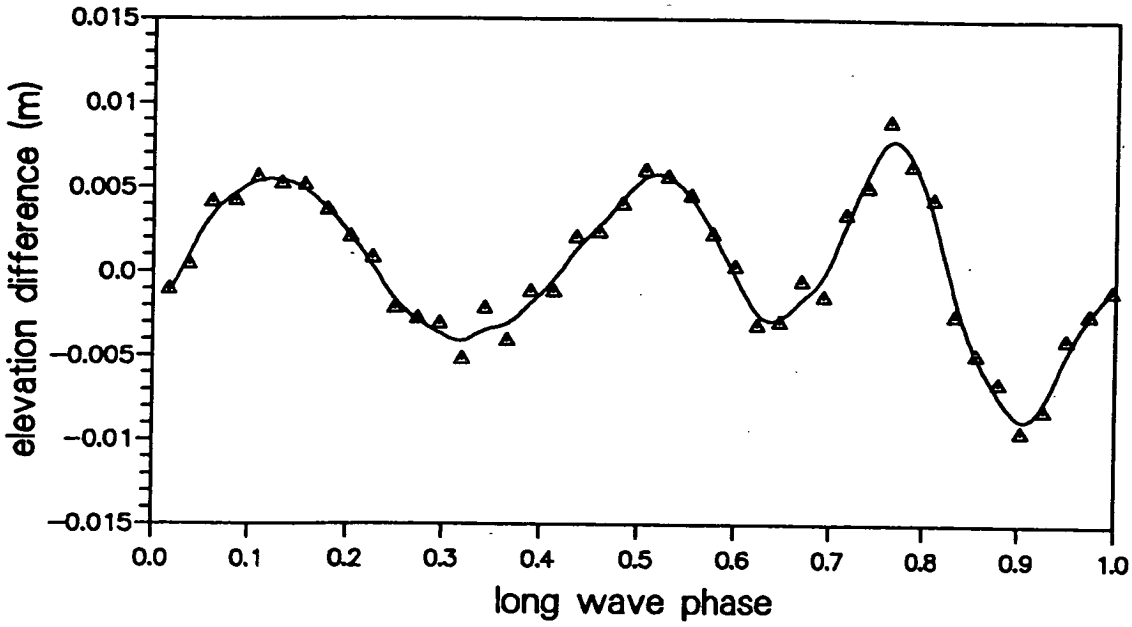

Fig. 5.1(f): A sectionized net record, obtained by subtracting **e5t6** from **e6t3**, riding on one long wave period (Δ: measured data, solid curve: best fitting).

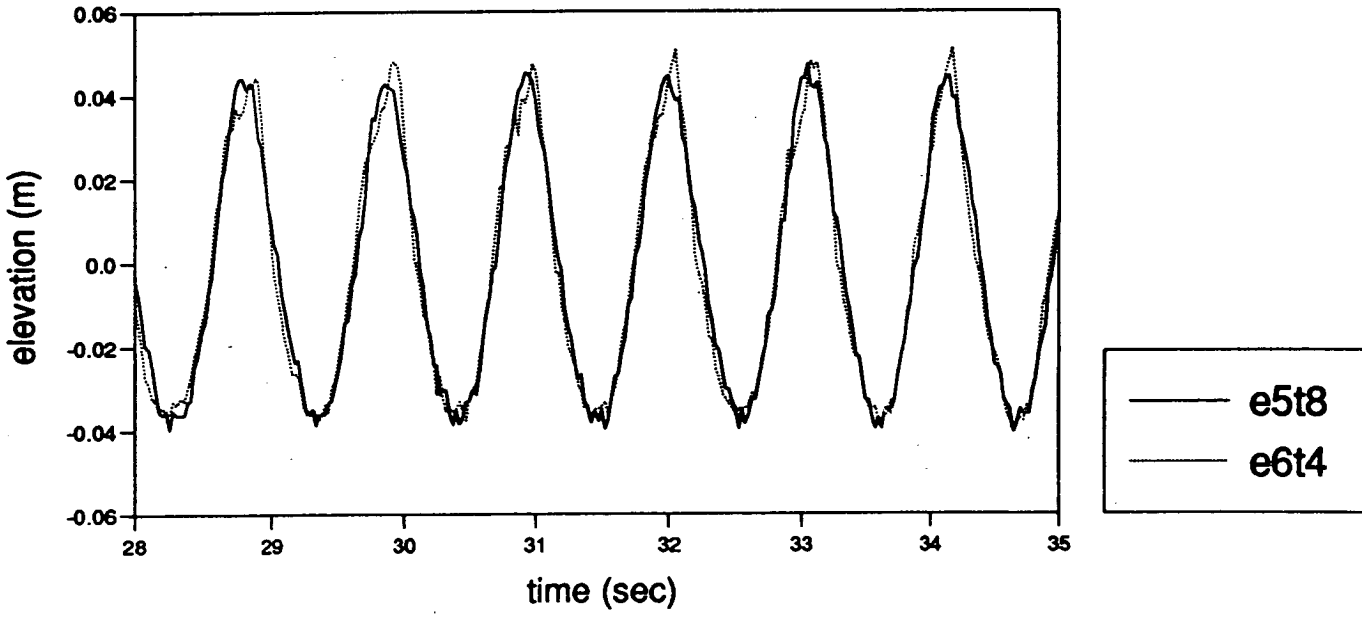

Fig. 5.1(g): The elevation records, **e5t8** (solid curve: regular waves) and **e6t4** (dashed curve: two-component waves).

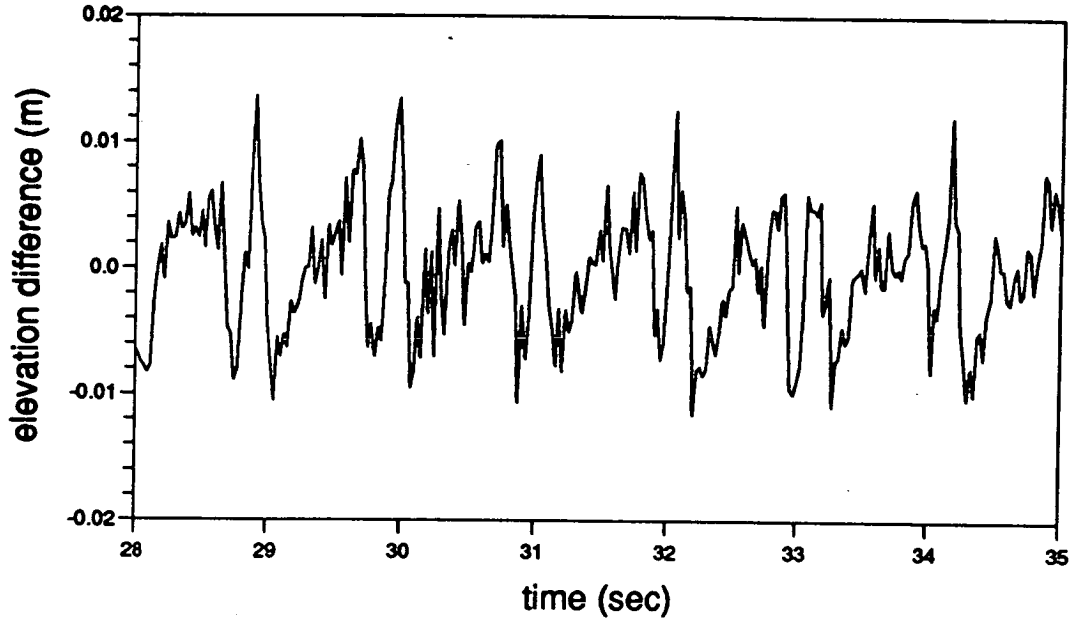

Fig. 5.1(h): The net difference record obtained by subtracting **e5t8** from **e6t4**.

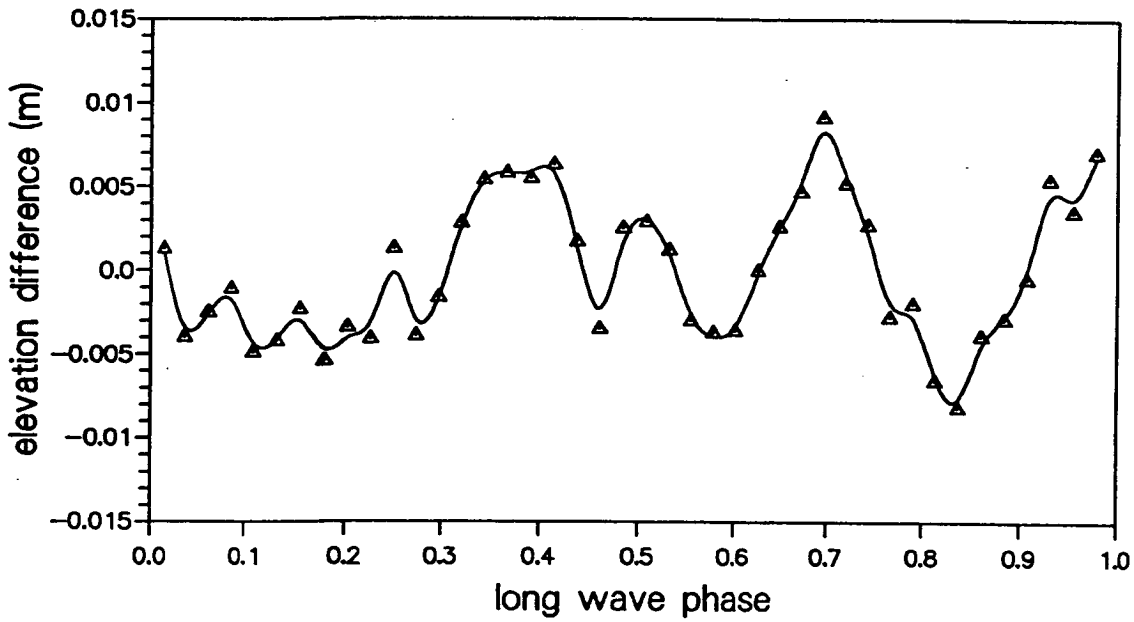

Fig. 5.1(i): The sectionized net record, obtained by subtracting **e5t8** from **e6t4**, riding on one long wave period (Δ: measured data, solid curve: best fitting).

Figs. 5.1: Wave records for the cases of regular waves and two-component waves, the net records of short waves (the records of regular waves deducted from those of two-component waves), and the sectionized net records riding on one long wave period.

Meanwhile, spectra analysis also provides an approach to investigate frequency modulation. The frequency of short waves is close to the third harmonic frequency of long waves. So there are four main amplitude peaks which will appear in a spectral map. It is found that the third harmonic amplitude of long waves in the cases of long waves is much smaller than the amplitude of the short waves riding on long waves in the spectral analysis, shown in figs. 5.2 (a), (b), (c) and (d). The four sets shown in figs. 5.2 for both cases of long waves and short waves riding on long waves, (fig. 5.2(a): **e5t2** and **e6t1**), (fig. 5.2(b): **e5t4** and **e6t2**), (fig. 5.2(c): **e5t6** and **e6t3**) and (fig. 5.2(d): **e5t8** and **e6t4**) are detailed in tab. 5.1.

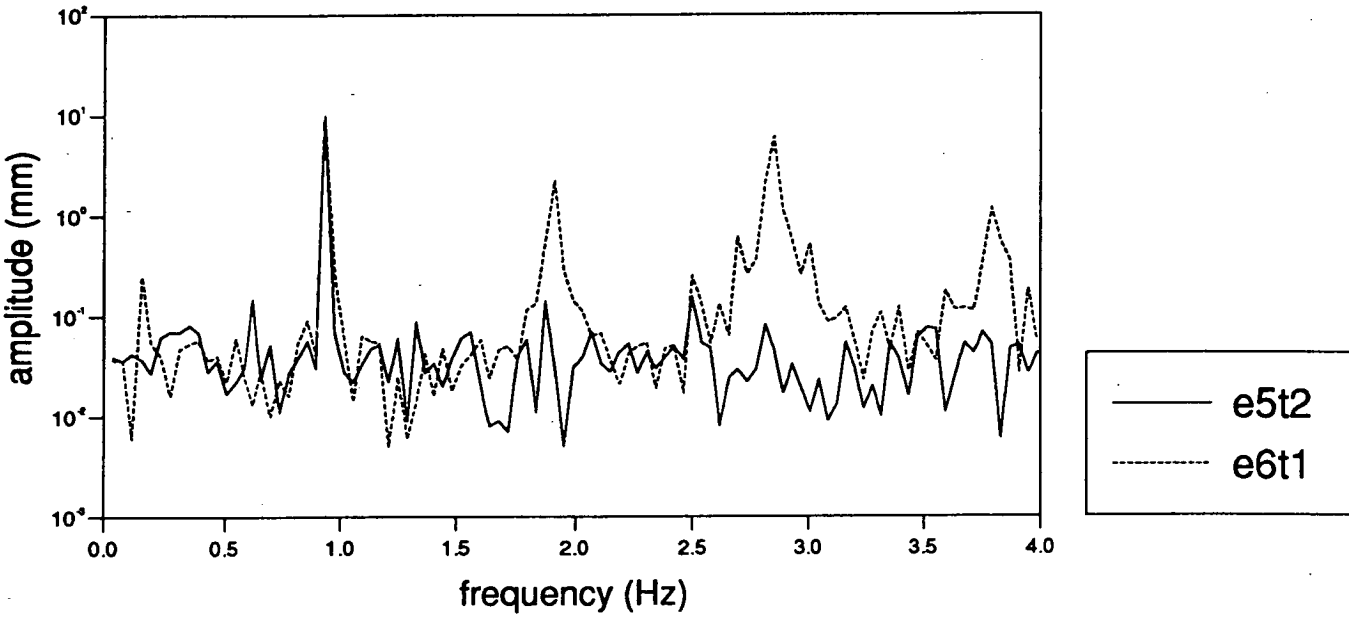

Fig. 5.2(a): The spectra of **e5t2** (solid curve: regular waves) and **e6t1** (dashed curve: two-component waves).

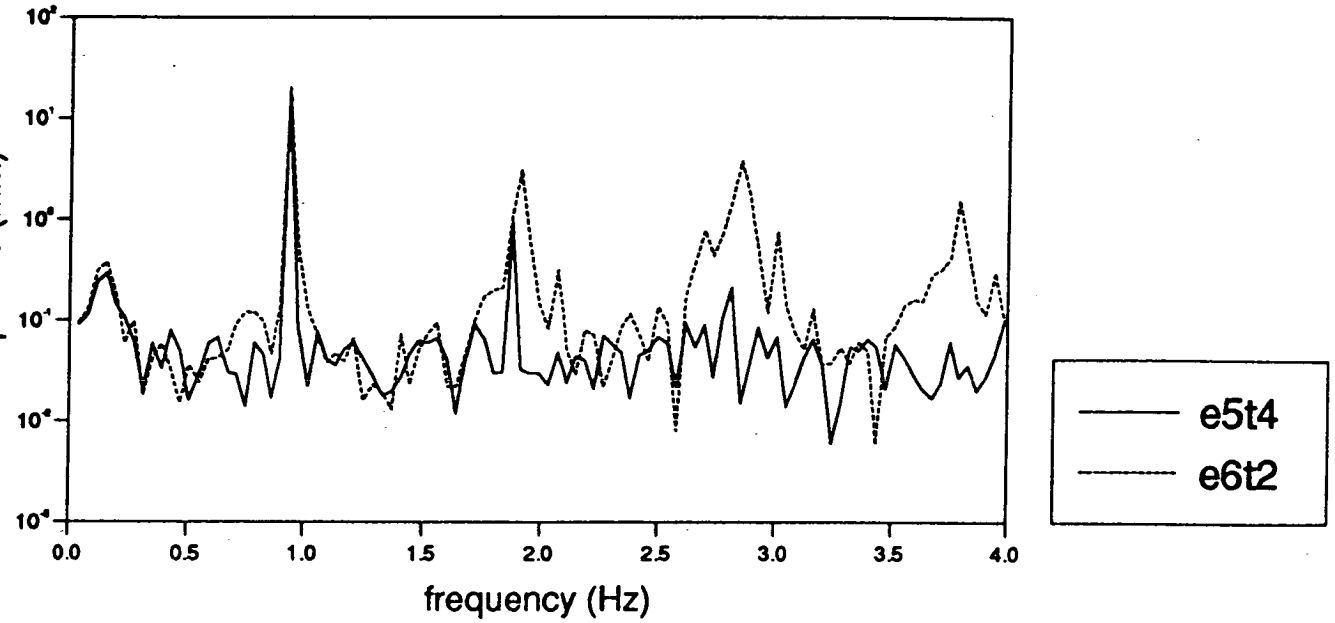

Fig. 5.2(b): The spectra of **e5t4** (solid curve: regular waves) and **e6t2** (dashed curve: two-component waves).

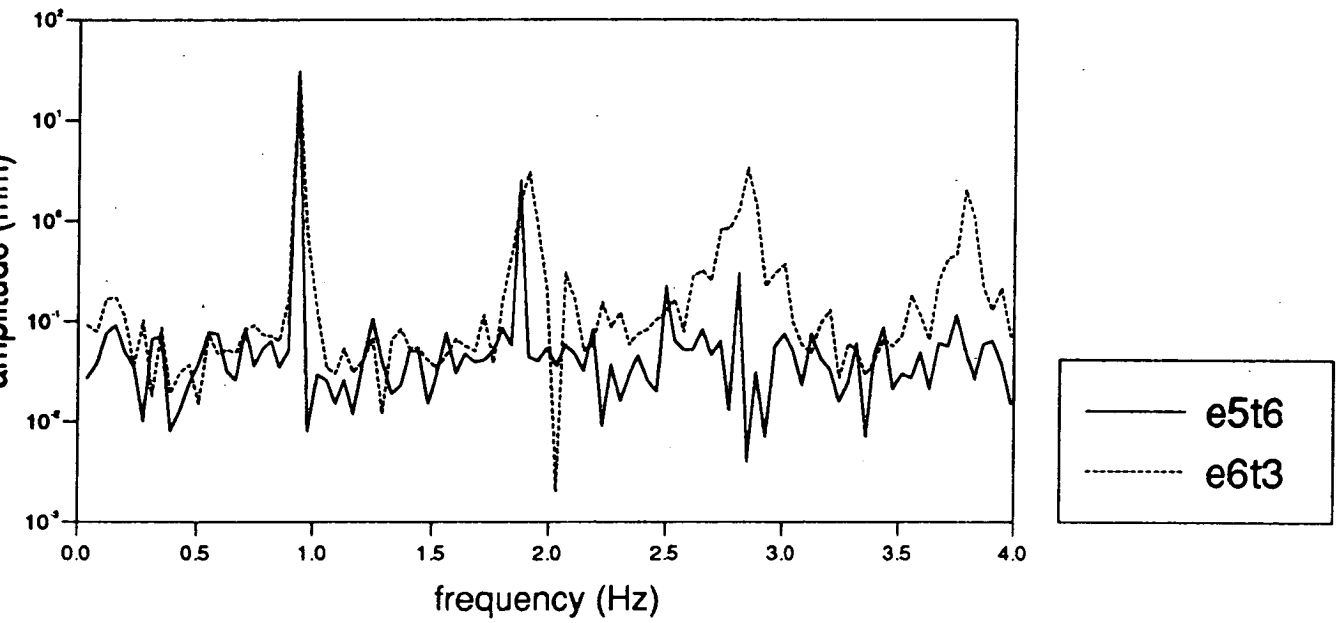

Fig. 5.2(c): The spectra of **e5t6** (solid curve: regular waves) and **e6t3** (dashed curve: two-component waves).

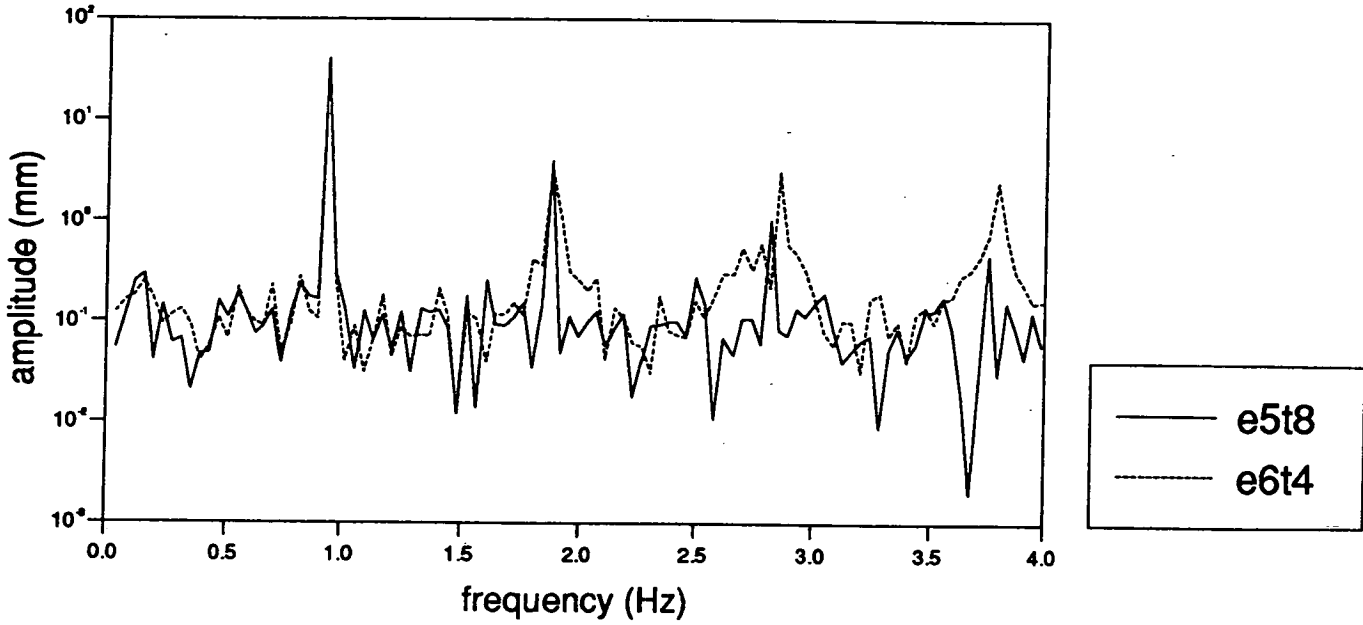

Fig. 5.2(d): The spectra of **e5t8** (solid curve: regular waves) and **e6t4** (dashed curve: two-component waves).

Figs. 5.2: Amplitude spectra for the cases of regular waves (solid curves) and two-component waves (dashed curves).

In figs. 5.2 the cut-off frequency is chosen as 4 Hz. This is because, when frequency is over 4 Hz, the amplitudes are small enough to be ignored. In these spectra of two-component waves (dashed lines in figs. 5.2), the short wave frequency is close to the third harmonic frequency of long waves, there are therefore four main amplitude peaks shown at specific frequencies. The first and largest peak is located at the frequency of long waves. The second peak appears at the frequencies of the second harmonics of long waves and (f_s-f_l), where f_s and f_l are the frequencies of short waves and long waves. The amplitude of short waves gives the third peak in these spectra of two-component waves. The fourth peak is given by the amplitude of frequency (f_s+f_l). Nevertheless, the third and the fourth harmonic effects are not particularly important in the third and the fourth peaks. Both are small and can be ignored in the spectra of regular waves.

If the spectra of long waves (solid lines in figs. 5.2) have been focused on, the second harmonic amplitude would be changing by changing the amplitude of long waves. That means, the second harmonics of long waves becomes more important in the cases of short waves riding on long waves. Furthermore, it is necessary to point out that the first peaks are almost the same in both the cases of regular waves and those of two-component waves. This is evidence which shows that long waves are quite steady when being involved in the two-component cases during the interaction. If the amplitude ratios of the third main peaks in the spectra for regular waves over two-component waves are taken, all ratios are found to be quite small. That means the net short wave amplitude is strongly modulated by long waves and the third harmonic effect of long waves does not play an important role in the modulation. Also if the third main peaks are focused in the cases of the two-component waves, these peaks show broad-banded short waves are expected because of the modulation of short waves riding on long waves.

5.2.1 Experimental Frequency Modulation

Generally speaking, the sectionized net records of short waves are used for deriving the frequency modulation. Each section in the sectionized net records is one long wave period, i.e. there are three periods of short waves along one period of long waves, see figs. 5.1(c), (f) and (i). Because of long wave modulation, these three periods of short waves are not identical. It is interesting and necessary to demonstrate and explain the difference within these three periods in details. Within a whole period of long waves, short waves are modulated in frequency and amplitude and the modulation is a function of long wave phases. A cosine function will be chosen for fitting the net records of short waves. In a sampling

rate of 40 Hz, there are almost 42 - 44 data for short waves (2.85 Hz) riding on one period of long waves (1/0.94 second). These 42-44 points represent three periods of short waves well. Therefore any consecutive 13-14 points in this case can be used to sort out a cosine function with amplitude, frequency and phase for a period of short waves (1/2.85 second) using a functional fitting scheme, where the amplitude is given by half of the local short wave height for this cosine function.

The routine **E04FDF** of the NAG library is applied for functional fitting. The consecutive points, which represent one short wave period within x_1 and x_2, where $[x_1, x_2]$ is the selected interval of the long wave phase, are used to fit the cosine function for the modulated short wave frequency σ_1. The modulated short wave frequency is normalized by the long wave frequency. Figure 5.3 shows the basic technique for function fitting. The modulated short wave frequency riding on long waves (the cases of **e1t2**, **e1t4**, **e3t2**, **e3t4**, **e5t2**, **e5t4** and **e5t6**: tabled in tab. 5.1) against the phase of the monochromatic long waves are shown in figs. 5.4, where the two-component waves are **e2t1**, **e2t2**, **e4t1**, **e4t2**, **e6t1**, **e6t2** and **e6t3** as set in tab. 5.1 with respect to the cases of long waves. Each Δ represents $((x_2-x_1)/2, \sigma_1)$. The error for each Δ in function fitting programme (E04FDF) is less than 0.005. It should be pointed out that the short wave period is normalized by the long wave period. Figure 5.5 demonstrates the modulated short wave frequency at the long wave crest against long wave steepnesses.

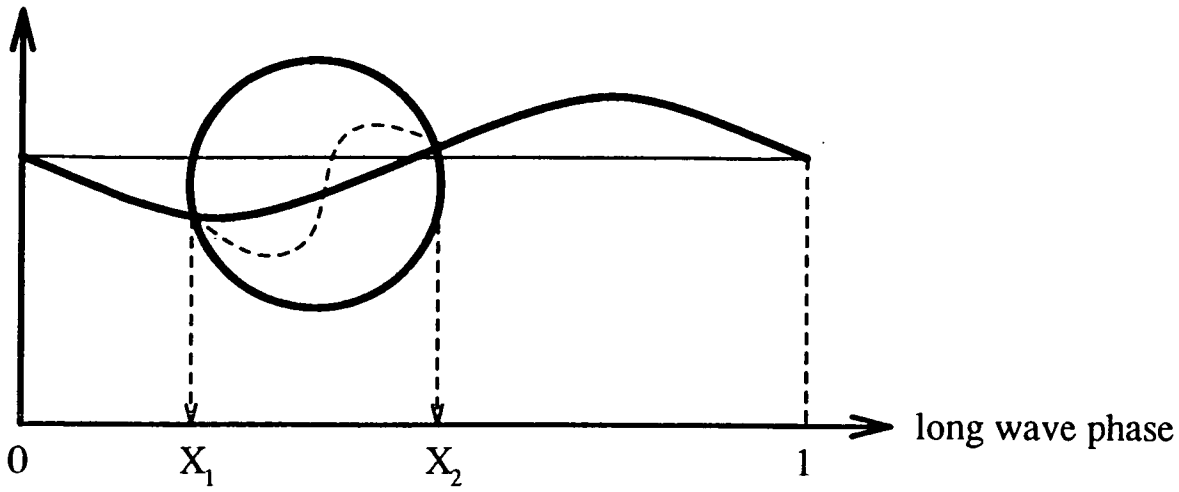

Fig. 5.3: Sketch of short waves riding on one long wave period in use of functional fitting.

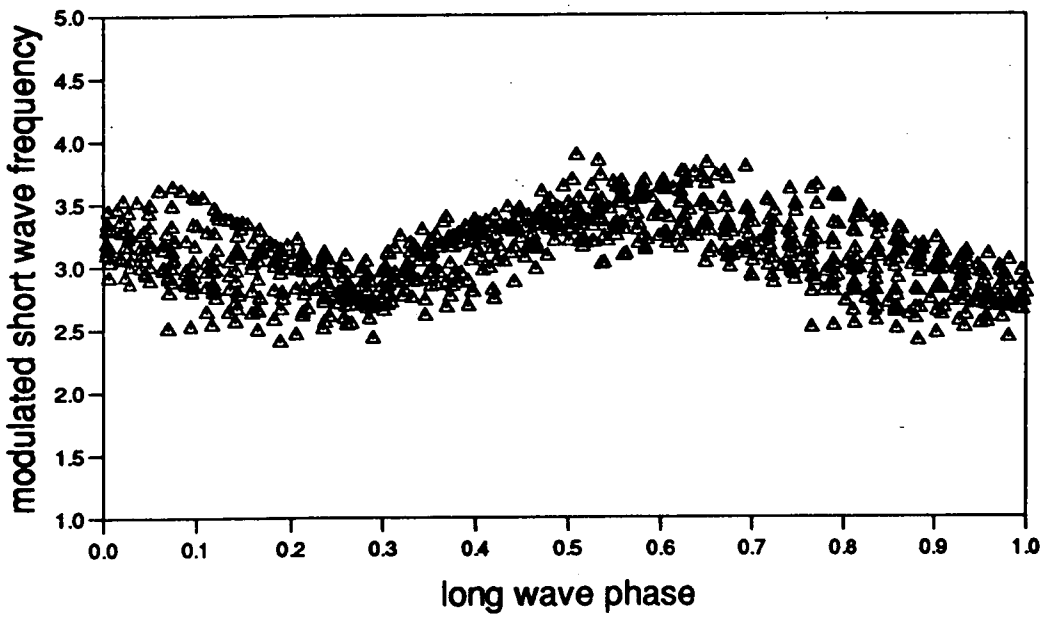

Fig. 5.4(a): The frequency modulation manipulated from **e1t2** (regular waves) and **e2t1** (two-component waves).

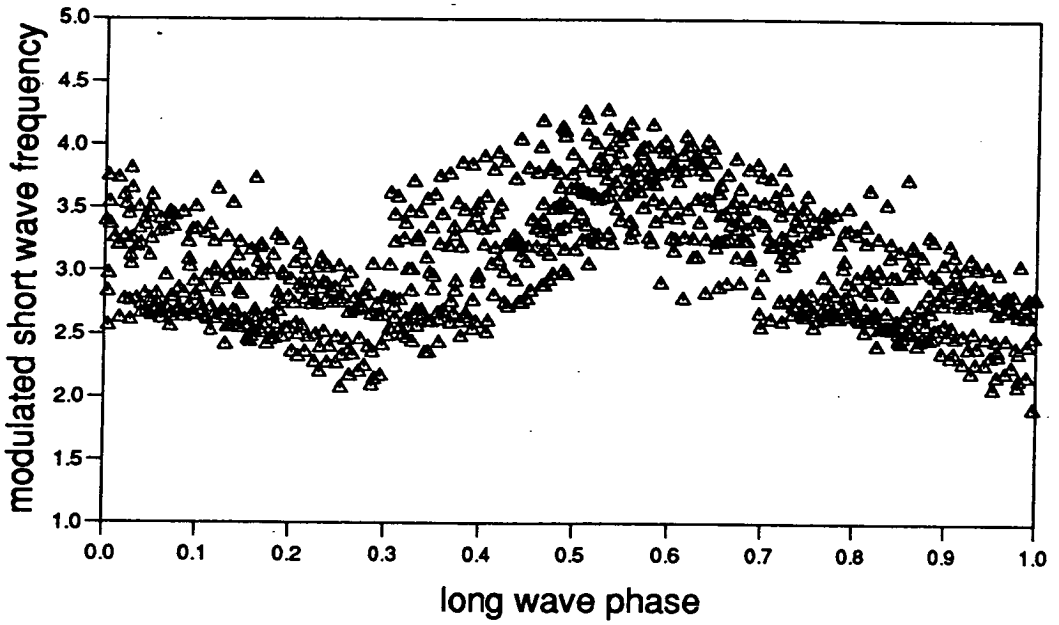

Fig. 5.4(b): The frequency modulation manipulated from **e1t4** (regular waves) and **e2t2** (two-component waves).

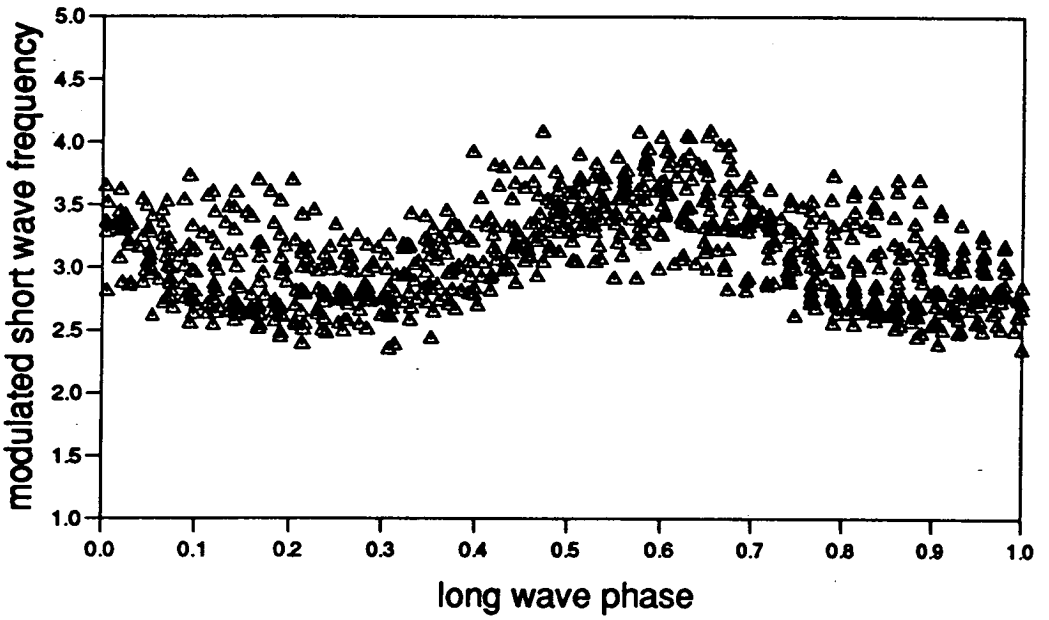

Fig. 5.4(c): The frequency modulation manipulated from **e3t2** (regular waves) and **e4t1** (two-component waves).

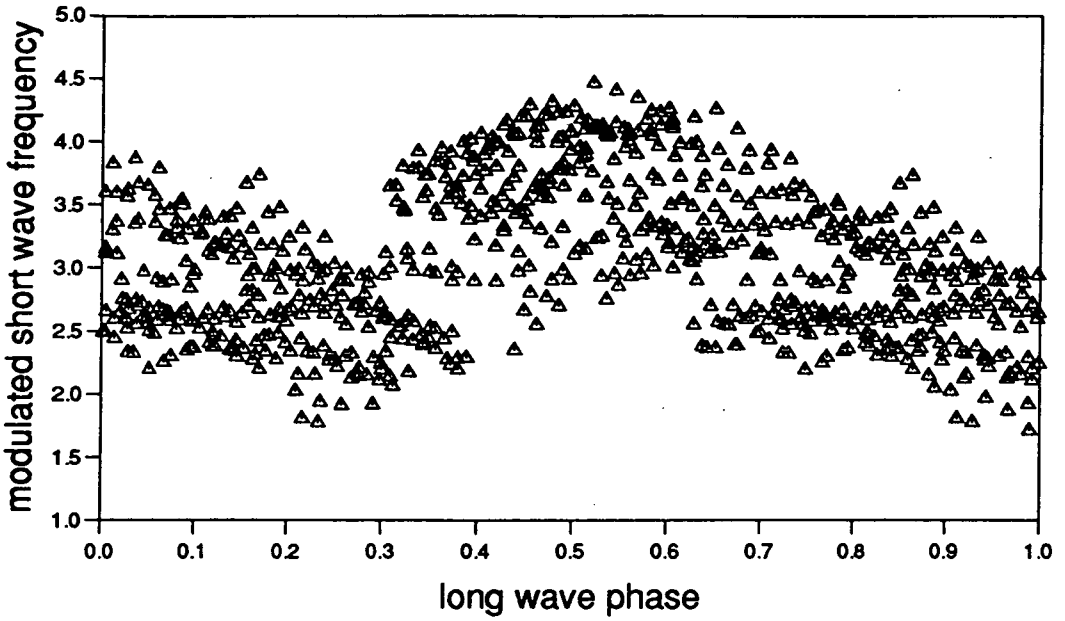

Fig. 5.4(d): The frequency modulation manipulated from **e3t4** (regular waves) and **e4t2** (two-component waves).

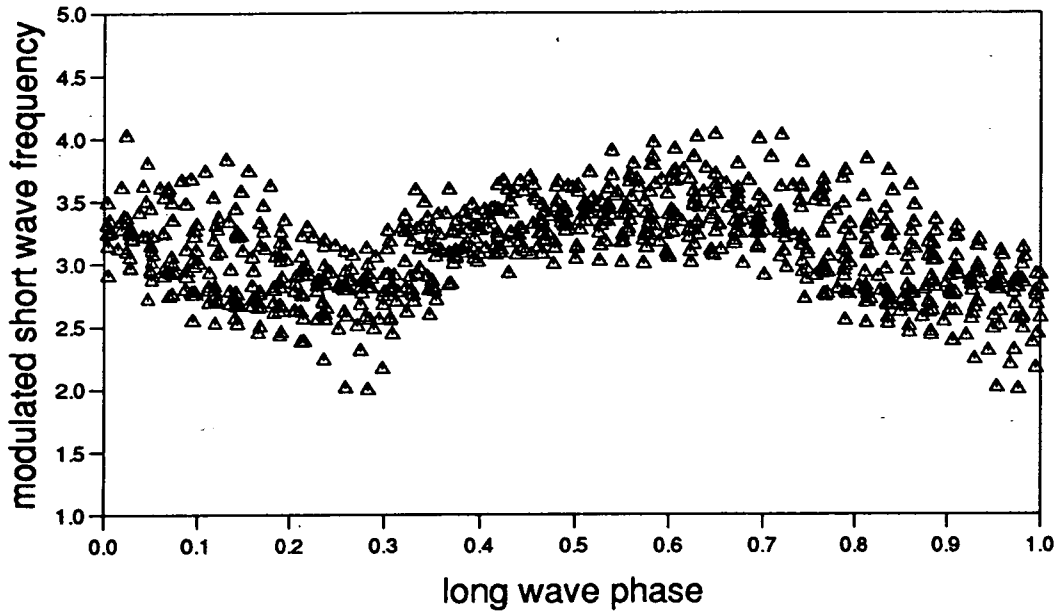

Fig. 5.4(e): The frequency modulation manipulated from **e5t2** (regular waves) and **e6t1** (two-component waves).

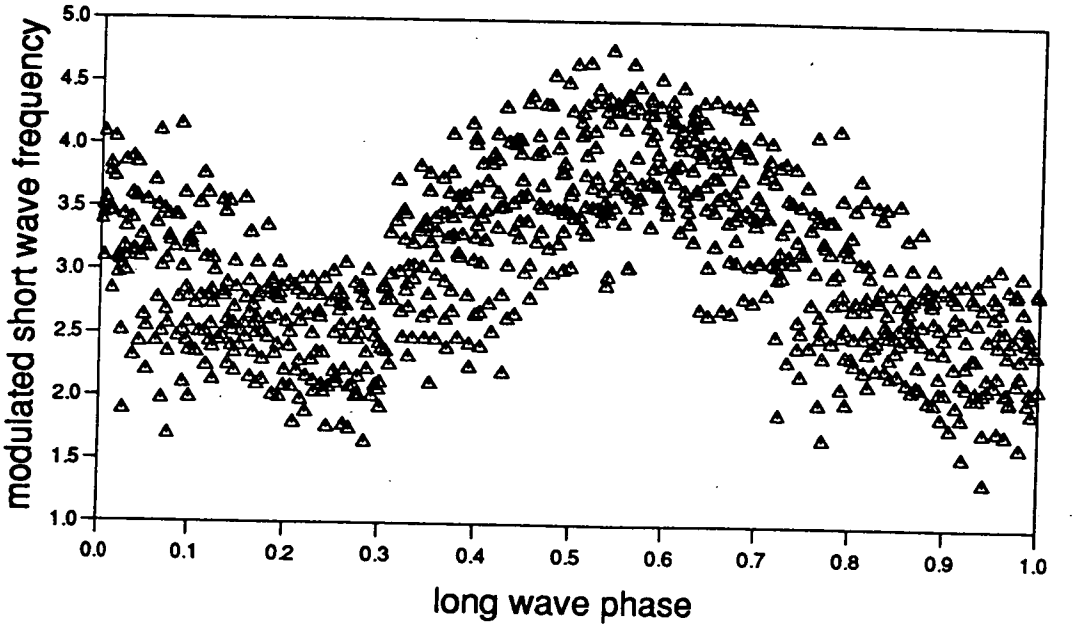

Fig. 5.4(f): The frequency modulation manipulated from **e5t4** (regular waves) and **e6t2** (two-component waves).

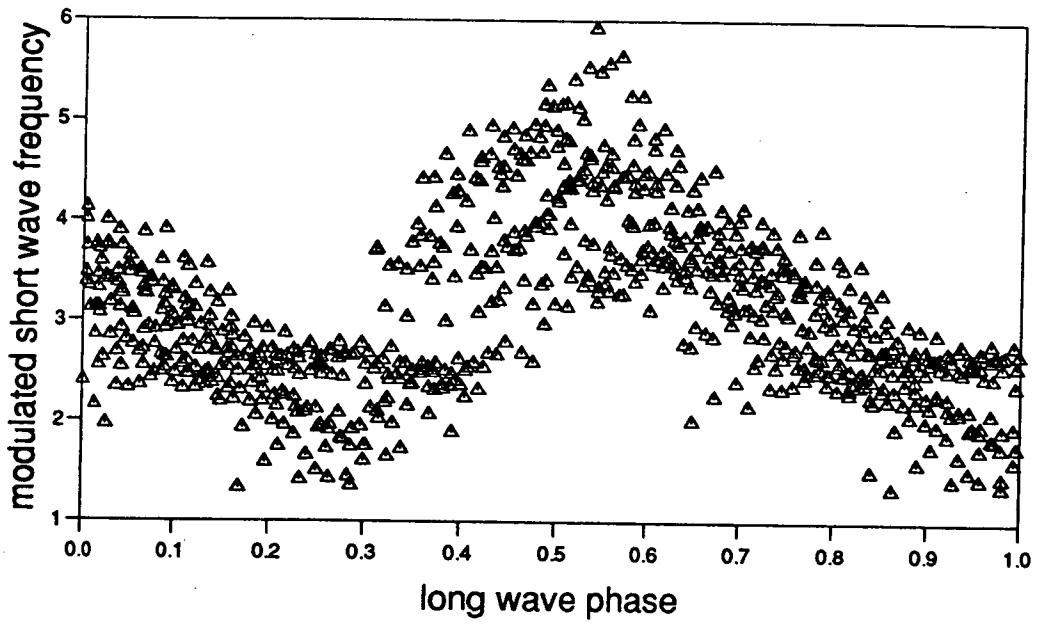

Fig. 5.4(g): The frequency modulation manipulated from **e5t6** (regular waves) and **e6t3** (two-component waves).

Figs. 5.4: Frequency modulation of short waves riding on long waves along the long wave phase.

Figures 5.4 show that modulated short wave frequency represents a narrow periodic strip along the long wave phase. Furthermore, it is interesting to look at the modulated frequency while short waves are riding on the crest and trough of long waves. The minimum modulated frequency always appears on the trough of long waves. Meanwhile the maximum modulated frequency shows up near the crest of long waves. Therefore, from the above seven cases in figs. 5.4 of different long wave steepnesses, fig. 5.5 shows the values of the maximum modulated frequency and the modulated frequency on the crest against long wave steepnesses. Both values of the maximum modulated frequency and the modulated frequency riding on the long wave crest are normalized by their own modulated frequency on the trough.

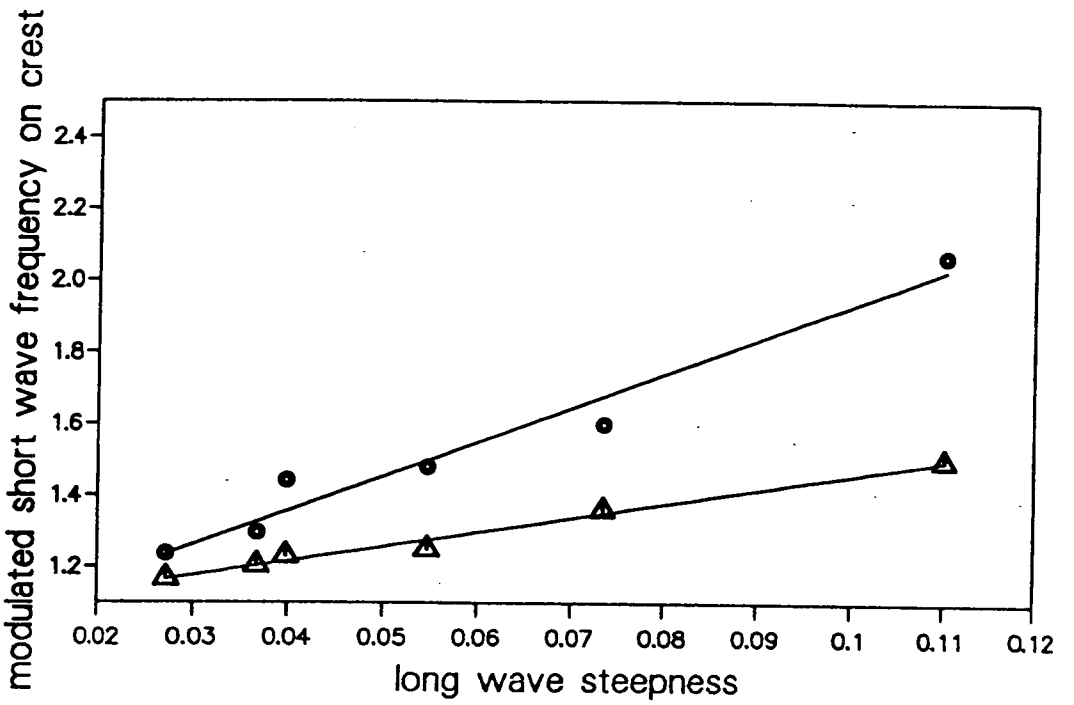

Fig. 5.5: The modulated frequency σ_1, of short waves riding on the crest of long waves (o: max modulated frequency, Δ: modulated frequency at the long wave crest).

Obviously, from fig. 5.5 the maximum modulated frequency and the modulated frequency riding on the long wave crest increase by increasing long wave steepnesses and the maximum modulated frequency grows faster than the modulated frequency riding on the long wave crest. In theory (this will be discussed in the next section 5.2.2) both would be of the same value. But from figs. 5.4 it is found that the maximum modulated frequency moves forward from the long wave crest to the long wave trough by increasing long wave steepnesses. So it implies that the phenomena of growth and movement are involved in the mechanism of local wave breaking.

5.2.2 Theoretical Approaches

It is well established that Stokes' waves provide a good representation of monochromatic long waves and are used to explore the parameters such as the effective gravity acceleration g_1 and the scale factor H_0. Since Stokes (1847) first discussed the irrotational theory of water waves in deep water or uniform finite depth, Stokes' waves have contributed a sound understanding of many periodic wave phenomena. However, viscosity did not play any role in this original paper. As a result, the numerical long waves are based on Stokes' expansions without considering viscosity or surface tension. The methodology of modulation employed here was first presented by Zhang and Melville (1990) who have discussed the theory of the weakly nonlinear short wave riding on a finite-amplitude long wave, which theory is limited to moderate long wave steepnesses, i.e. ak=0.30.

A monochromatic long wave is steady in the coordinates (OX-OZ) moving at its phase velocity C. According to the Cauchy theorem, its equipotential function (Φ=constant) and stream function (Ψ=constant) in the moving rectilinear

coordinates (OX-OZ) may be projected onto straight lines (s=Φ/C, n=Ψ/C) in the s-n coordinates through conformal mapping, with the curved long wave surface corresponding to the free surface(n=0). A similar figure is shown in fig. 3.6. The parameters g_1 and h_0 are given by Eqns. (3.52) and (3.53). The modulated frequency can be solved from Eqn. (3.50) by letting R_c=4 and $\Delta s = \pi/1024$ and by applying the central finite difference technique. Here $R_c \approx R^{1/2}$, if R is the wavelength ratio of long waves and short waves on the trough of long waves.

The following four cases of different long wave steepnesses (ak=0.05, 0.10, 0.15 and 0.20) have been considered. The elevations of Stokes' waves, the effective gravity acceleration g_1, the scale factor H_0, and modulated frequency and amplitude are shown in figs. 5.6, 5.7, 5.8, 5.9 and 5.10 along the free surface of a long wavetrain for each value of the parameter ak. The derivative of the modulated short wave frequency and amplitude with respect to the long wave phase is shown in figs. 5.11 and 5.12.

Moreover, it is worth representing the steady modulated short wave frequency and amplitude (figs. 5.13 and 5.14) at the long wave crest against the parameter, long wave steepnesses ak.

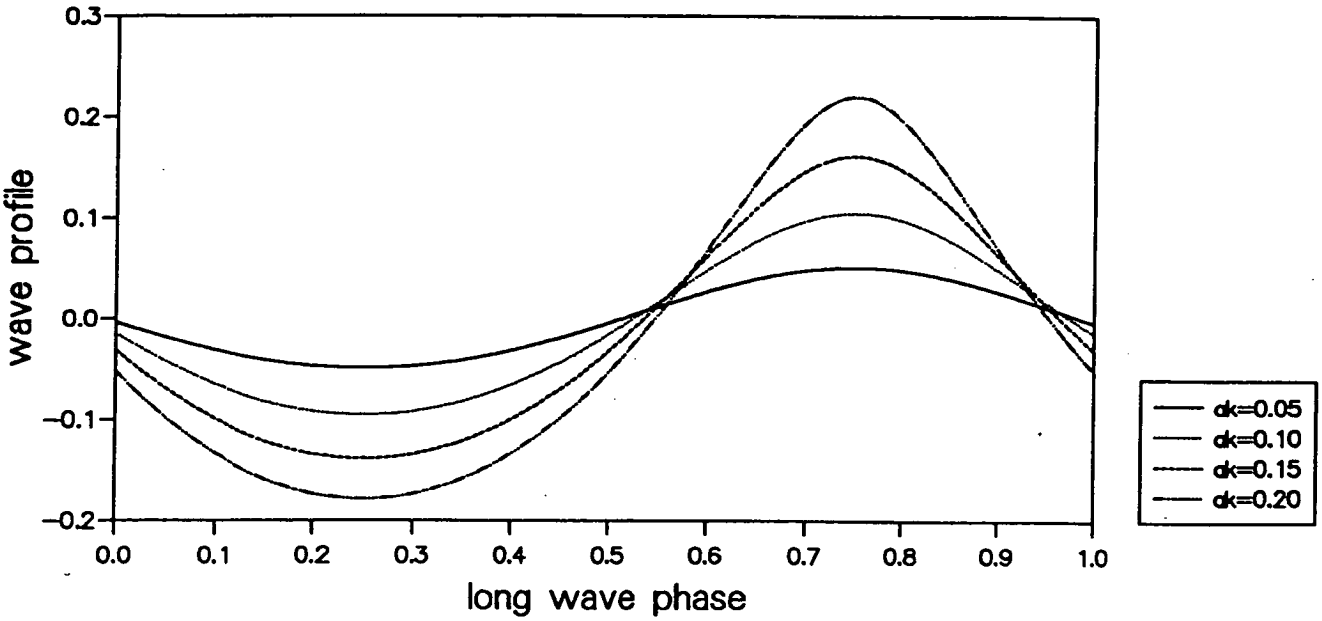

Fig. 5.6: Surface elevation of long Stokes' waves in deep water for different wave steepnesses, where the long phase is normalized by 2π.

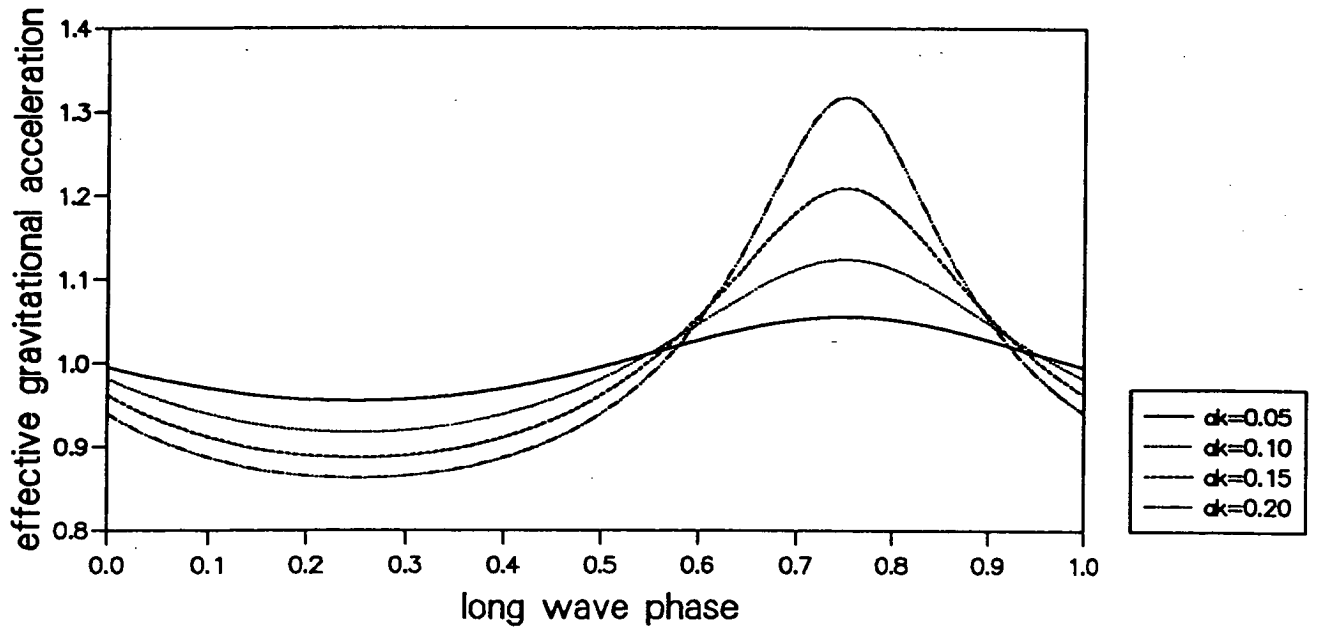

Fig. 5.7: The effective gravitational acceleration g_1, as a function of the long wave phase for different long wave steepnesses.

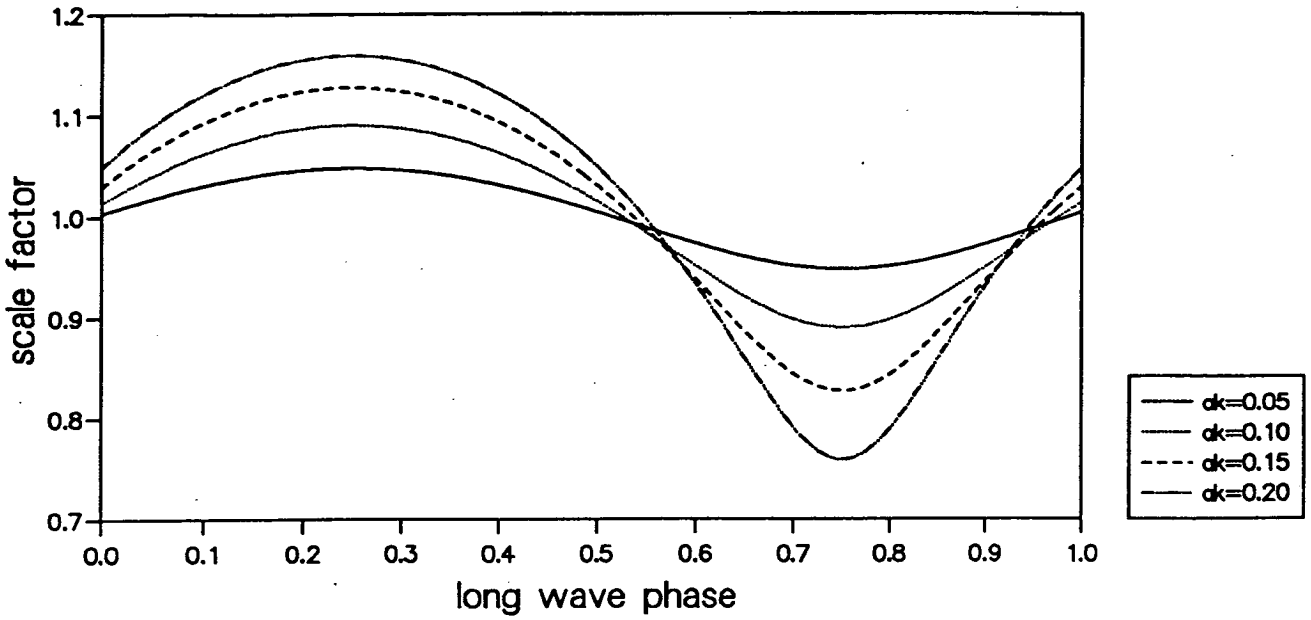

Fig. 5.8: The scale factor H_0, as a function of the long wave phase for different long wave steepnesses.

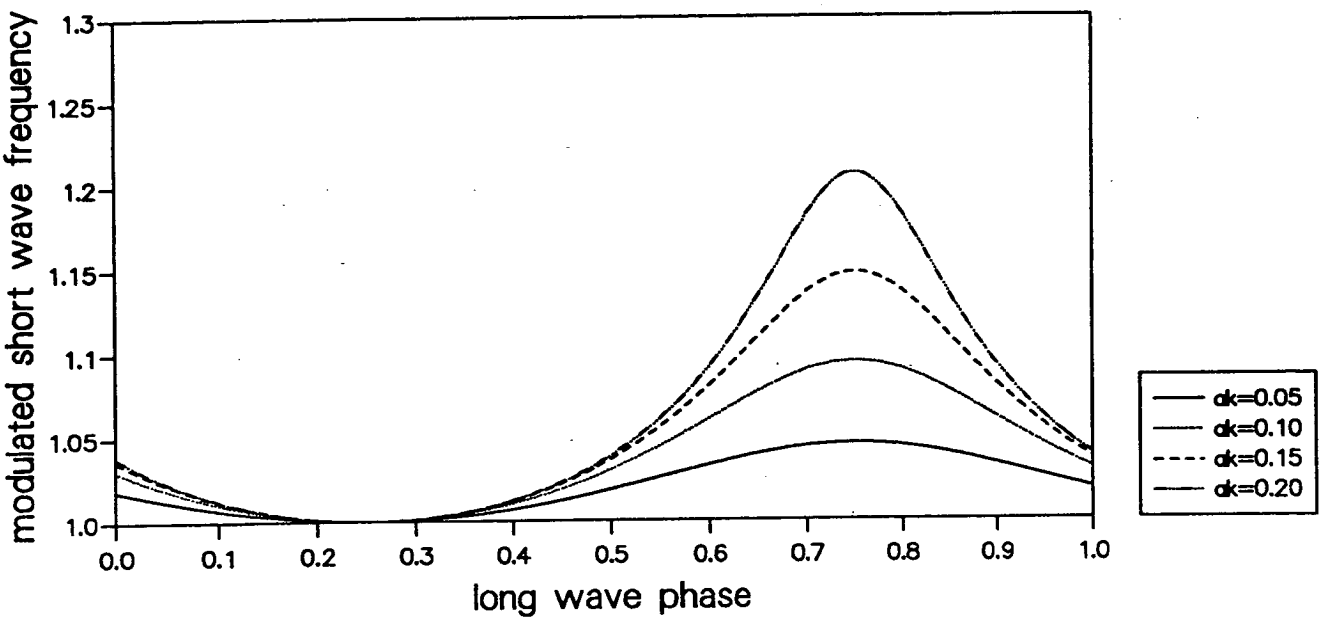

Fig. 5.9: The numerical modulated short wave frequency, as a function of the long wave phase, normalized by the value of at the trough, for different long wave steepnesses.

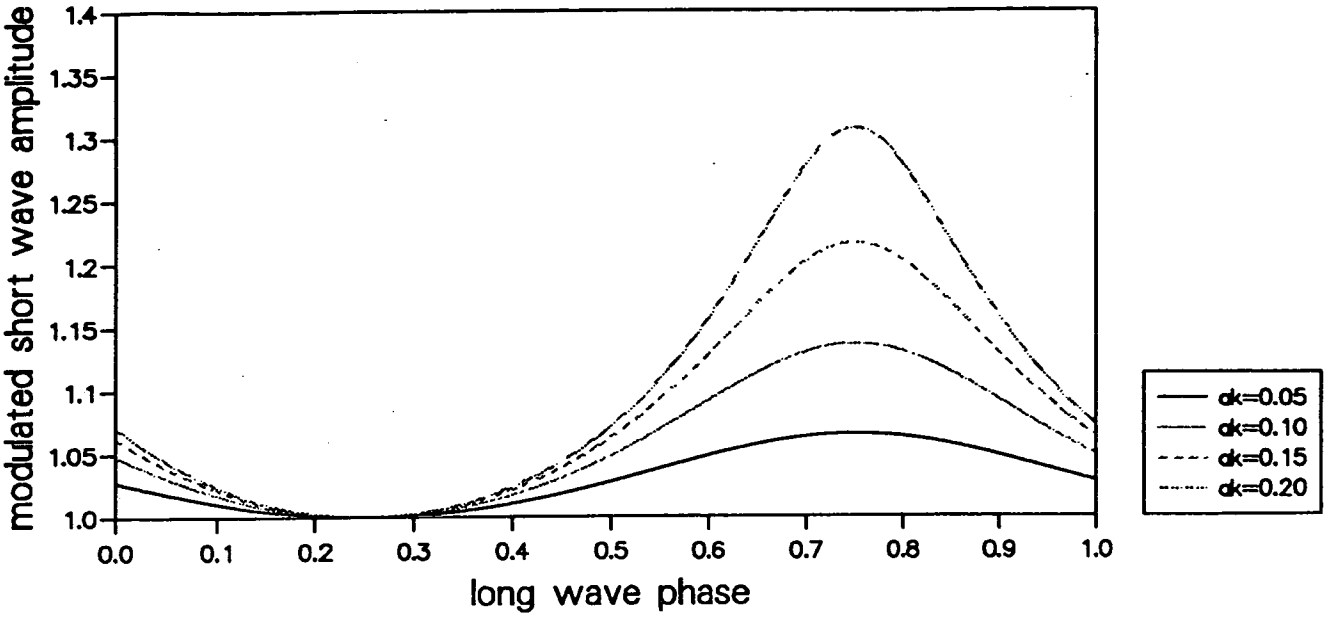

Fig. 5.10: The numerical modulated short wave amplitude, as a function of the long wave phase, normalized by the value of at the trough, for different long wave steepnesses.

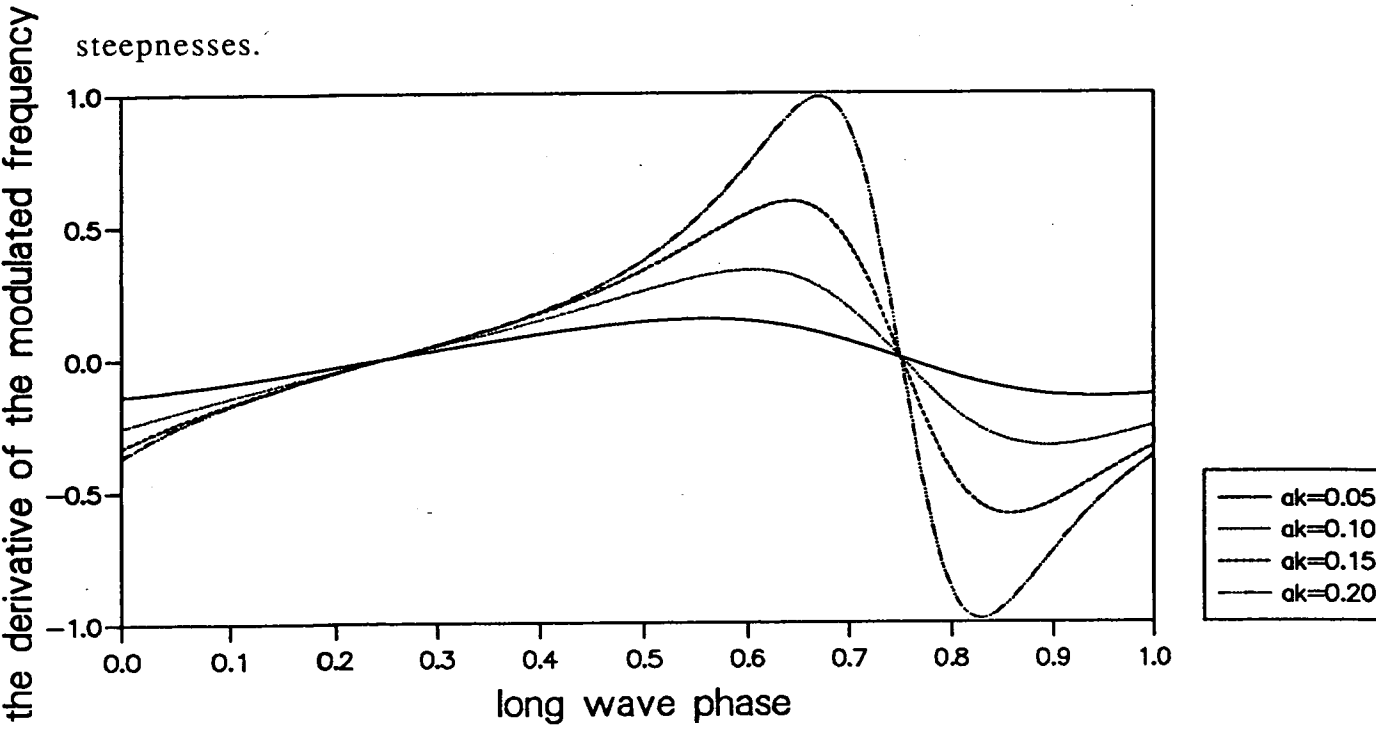

Fig. 5.11: The derivative of the numerical modulated short wave frequency with respect to the long wave phase, as a function of long wave phase, for different long wave steepnesses.

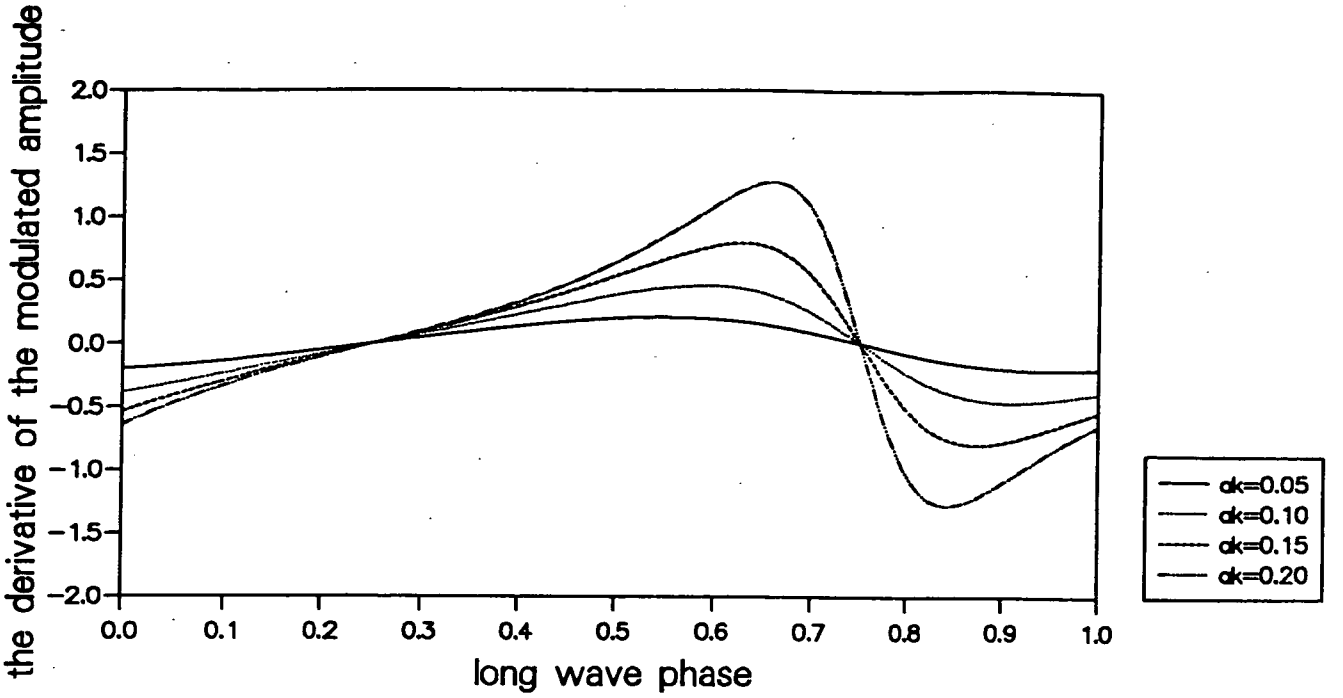

Fig. 5.12: The derivative of the numerical modulated short wave amplitude with respect to the long wave phase, as a function of long wave phase, for different long wave steepnesses.

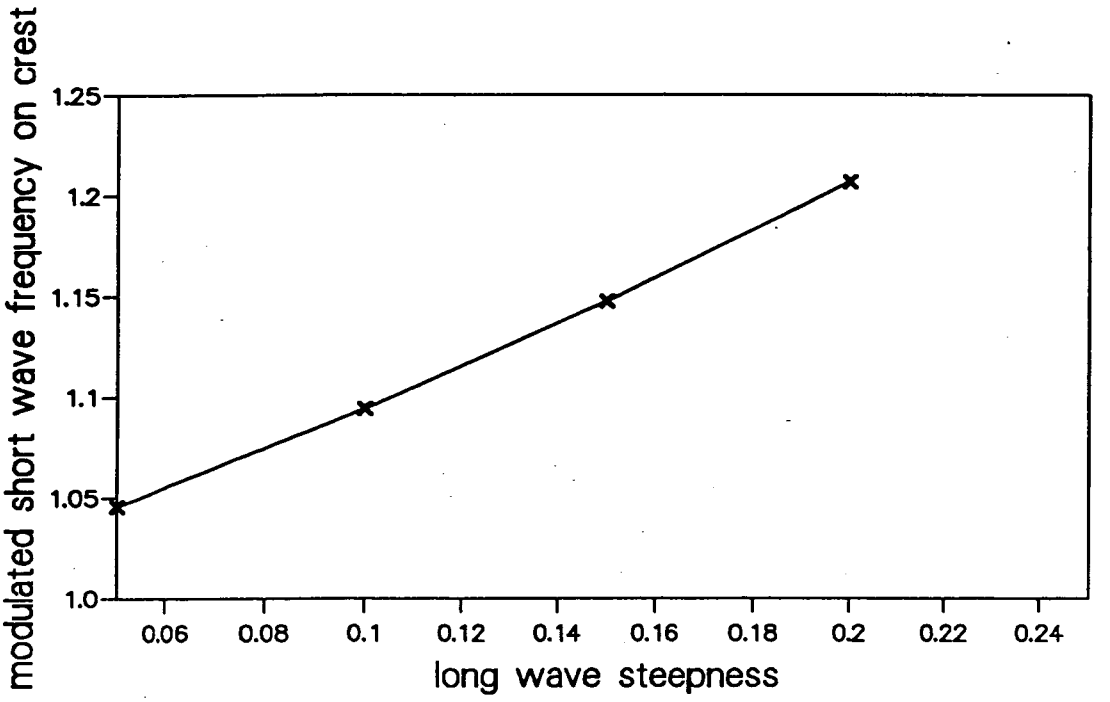

Fig. 5.13: The numerical modulated frequency of short wave riding on long Stokes' wave crest normalized by the value at the trough.

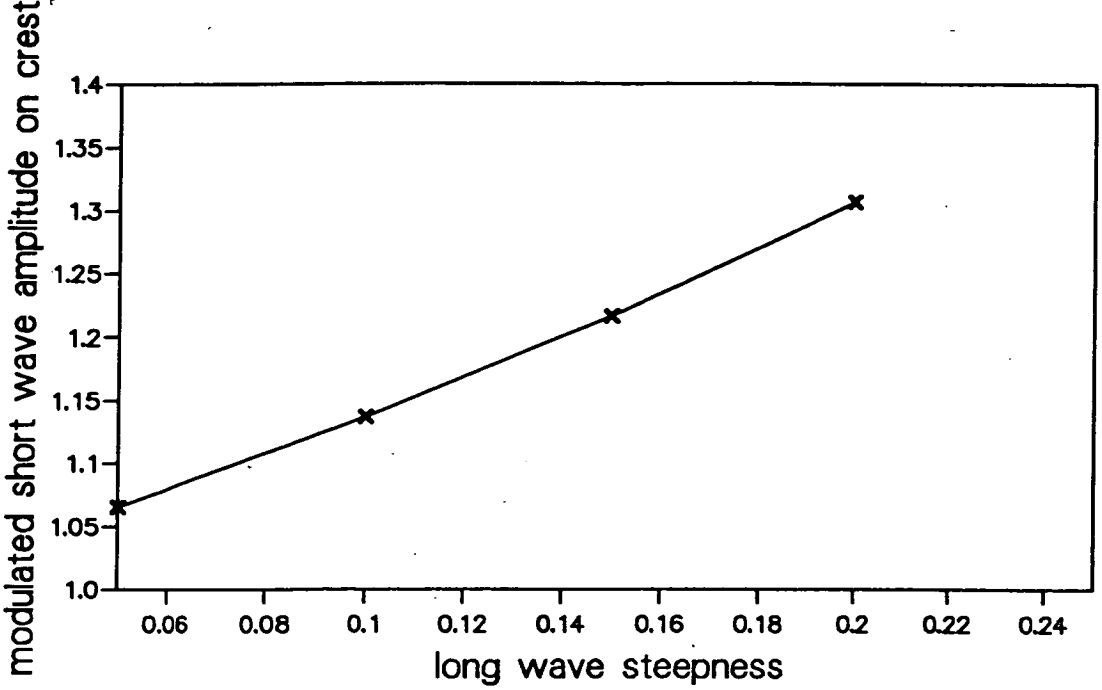

Fig. 5.14: The numerical modulated amplitude of short wave riding on long Stokes' wave crest normalized by the value at the trough.

Figures 5.9 and 5.10 show the modulated frequency and amplitude are periodic functions along the long wave phase and the maximum modulated frequency and amplitude appear on the long wave crest. From figs. 5.11 and 5.12 the anti-symmetry of the modulated frequency and amplitude derivatives are expected, since the modulated frequency and amplitude along the long wave phase are symmetric. Furthermore, in figs. 5.13 and 5.14 the modulated frequency and amplitude riding on the long wave crest increase by increasing long wave steepnesses. The growth of the frequency and amplitude against the long wave steepnesses, both growth rates are in the same order. That is, both the frequency modulation and amplitude modulation of short waves riding long waves are equally significant.

5.2.3 Comparisons

In Section 5.2 the main target is to compare the experimental modulated frequency with the theoretical modulated frequency. It has been demonstrated that the modulated frequency of the short waves riding on Stokes' waves, which represents a narrow periodic strip and is a function of the phase of the monochromatic long wave in different long wave steepnesses. It is found that the maximum/minimum modulated short wave frequency occurs near the crest/trough of the long wave. This is coherent to numerical prediction: the maximum/minimum modulated short wave frequency always occurs at the crest/trough of the long wave. By increasing the long wave steepness, the ratio of the modulated short wave frequency at the crest over the value at the trough of the long wave increases. In the numerical work the wavelength ratio of the long wave to the short wave is near 10 (let $R_c = 4$) at the trough of the long wave and the steady solution is considered. But in the experimental work the wavelength ratio is almost 9 and the experimental modulated frequency is time dependent. The nonlinear modulation and the evolution of frequency play important roles in the experimental approach. Both lead to the difference in quantity between the experimental and numerical work. For the evolution, as Ramamonjiarisoa and Coantic (1976) and Ramamonjiarisoa and Giovanangeli (1978) have researched, a strong tendency for short waves to move with the phase speed of dominant longer waves can be observed. Such tendency, which are involved in the evolution of short waves riding on long waves, needs to be studied in depth. Figure 5.15 shows the comparisons between the theoretical and experimental modulation. The growth of the experimental frequency modulation is faster than that of the theoretical modulation by increasing the long wave steepnesses.

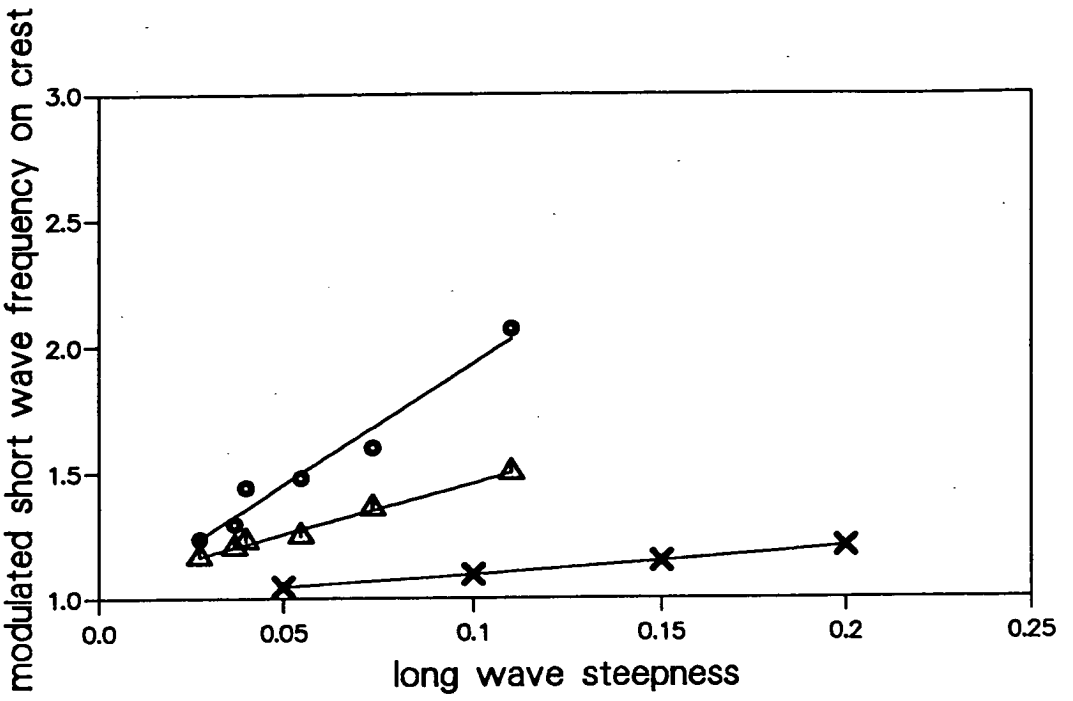

Fig. 5.15: Comparison between the max experimental (•), experimental (Δ) and numerical (x) modulated short wave frequencies riding on the long wave crest, normalized by their respective frequency at the trough.

5.3 Kinematics of Waves

Kinematics were measured using the PIV technique and the prediction were made from the spectra of wave records. The PIV system has a limited dynamic range and is set up to work at the velocities which occur near the crest, as the velocities of the crest are emphasised.

Actually the cut-off frequency of the spectra for wave kinematics is sensitive and depends on the frequency range of the waves involved. A criterion is necessary for choosing the cut-off frequency against various cases of wave kinematics from

moderate to steep waves and from monochromatic to multi-component waves. In this thesis the short wave frequency is close to the third harmonic frequency of long waves, therefore in the following kinematic comparisons the cut-off frequency is chosen under specific requirement. As Sutherland (1992) suggested the cut-off frequency is chosen up to the second harmonics of long waves for the cases of regular waves. For the cases of two-component waves, as mentioned before, there are four main peaks in the spectra. Therefore, under such a circumstance, the cut-off frequency shall be chosen just above the frequency f_s+f_l of the fourth peak, where f_s and f_l are the frequencies of short and long waves.

experiment reference	e5t8	e6t4
long wave amplitude (mm)	40	40
short wave amplitude (mm)	0	10
long wave frequency no.	24	24
short wave frequency no.	73	73
long wave steepness ak	0.147	0.147
short wave steepness ak	0	0.327
relative steepness of long waves	0.72%	0.72%
relative depth of long waves	4.84%	4.84%
relative steepness of short waves	0.00%	1.66%
relative depth of short waves	44.8%	44.8%

Tab. 5.2: The parameters of the cases of regular waves and two-component waves, **e5t8** and **e6t4**, for kinematics comparisons.

The measurements of horizontal velocity for the cases of regular and two-component waves, **e5t8** and **e6t4** tabled in tab. 5.2, taken under the crest of the monochromatic long waves are compared to the horizontal velocity profiles calculated from the measured spectra. Based on the measured spectra, the techniques for wave kinematics are linear theory, Wheeler, Chakrabarti, superposition stretching methods and time-stepping technique.

5.3.1 Comparisons with Linear Theory

As a matter of fact, linear theory is only valid for the waves of infinitesimal amplitude and up to mean water level. However, the case of regular waves **e5t8** in tab. 5.2 being measured are only of 0.72% and 4.84% in the relative steepness and the relative depth. As Dean (1970) also suggested, linear theory fits the medium steepness of waves with finite depth well, so linear theory may be applied to this case of regular waves. Linear theory is also the basis for the following stretching methods which are the modified methods for multi-component waves.

The frequency range for regular waves to sum up Fourier components is from j=16 to j=50. Here j is an intergral input of wave frequency. Wave frequency is obtained by j/25.6 Hz. Also the frequency range for two-component waves to sum up Fourier components is from j=16 to j=100. The comparisons of the horizontal velocity under the crest of regular wave between the PIV measurements and the predictions of linear theory applied to the waves (**e5t8** and **e6t4**) are shown in figs. 5.16.

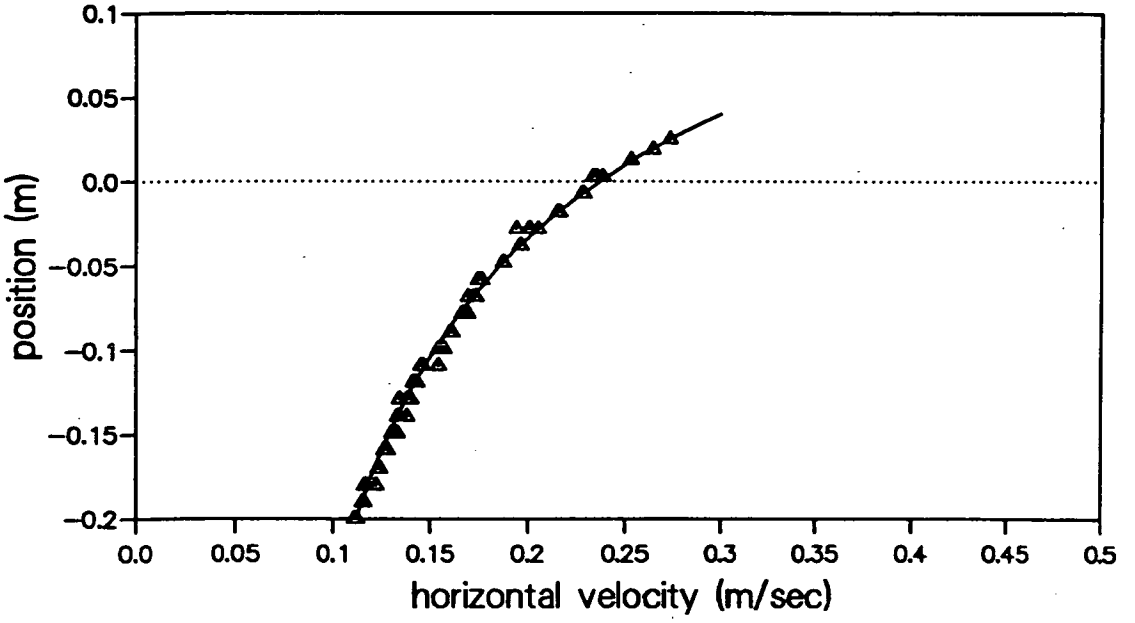

Fig. 5.16(a): Δ measured by PIV; the solid curve calculated from linear theory for the case of **e5t8**; the horizontal dashed line is MWL.

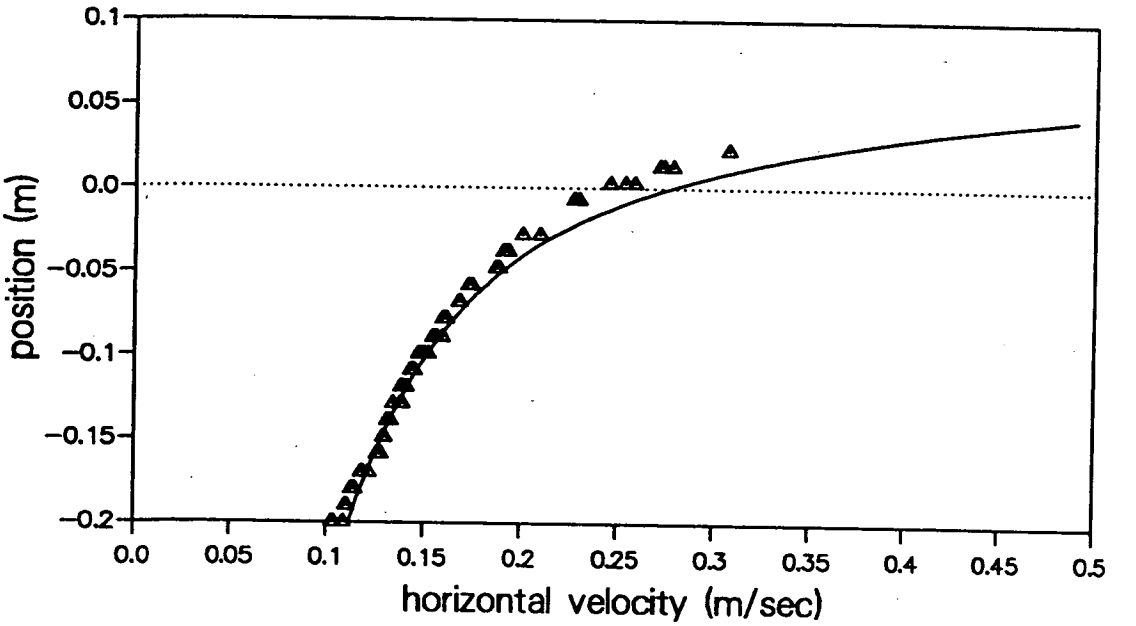

Fig. 5.16(b): Δ measured by PIV; the solid curve calculated from linear theory for the case of **e6t4**; the horizontal dashed line is MWL.

Figs. 5.16: Comparisons of the horizontal velocity under the crest of regular waves between the predictions made by linear theory and the results measured by PIV.

The 1024 sample wave gauge records are Fourier transformed to produce wave amplitude spectra. The output of this process is an amplitude and phase at each of a series of discrete frequencies separated by 1/25.6 Hz. Each one represents the energy contained within the frequency range of 1/25.6 centred on f=j/25.6. The phases are calculated for the start of the record and measured from zero at a long wave crest.

Linear theory provides a good fitting to measured horizontal velocities of the regular wave case, if the second harmonics of long waves is included.

5.3.2 Comparisons with the Wheeler Stretching Method

The Wheeler stretching is one of the well-known and established stretching methods (Wheeler 1969). The main numerical technique is to stretch the vertical co-ordinate from the mean water level to the free surface. The purpose is to equal the calculated velocities from linear theory at the mean water level to that from the Wheeler stretching method at the free surface. The frequency range for regular waves to sum up Fourier components is from j=16 to j=50. Also the frequency range for two-component waves to sum up Fourier components is from j=16 to j=100. The comparisons of the horizontal velocity under the crest of regular waves between the measurements and the Wheeler stretching predictions applied to the waves (**e5t8** and **e6t4**) are shown in figs. 5.17.

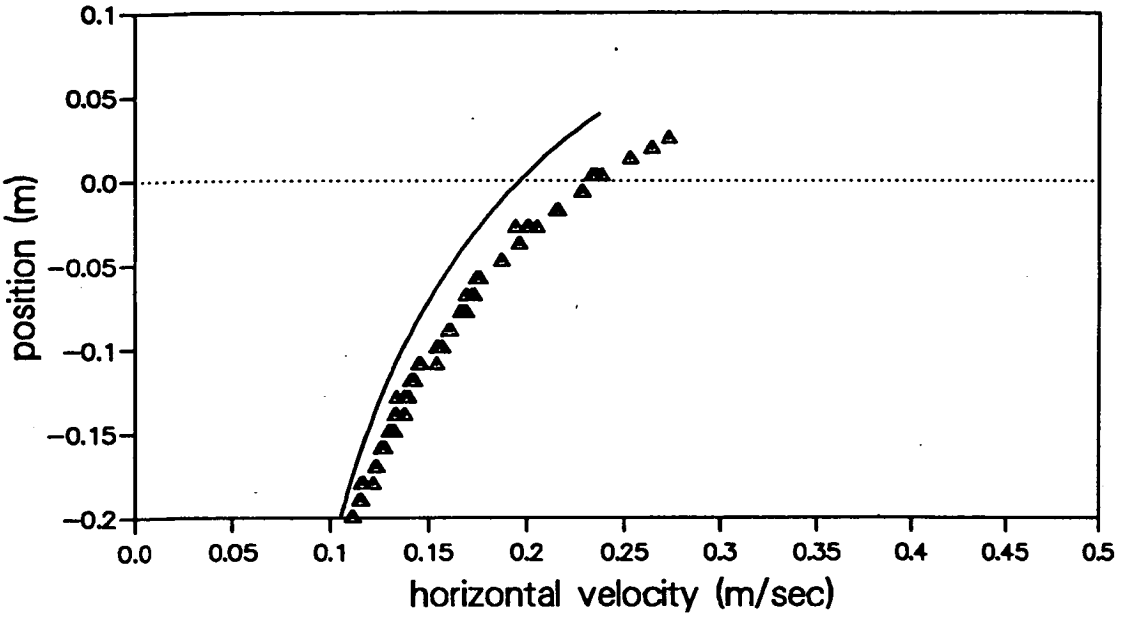

Fig. 5.17(a): Δ measured by PIV; the solid curve calculated from the Wheeler stretching method for the case of **e5t8**; the horizontal dashed line is MWL.

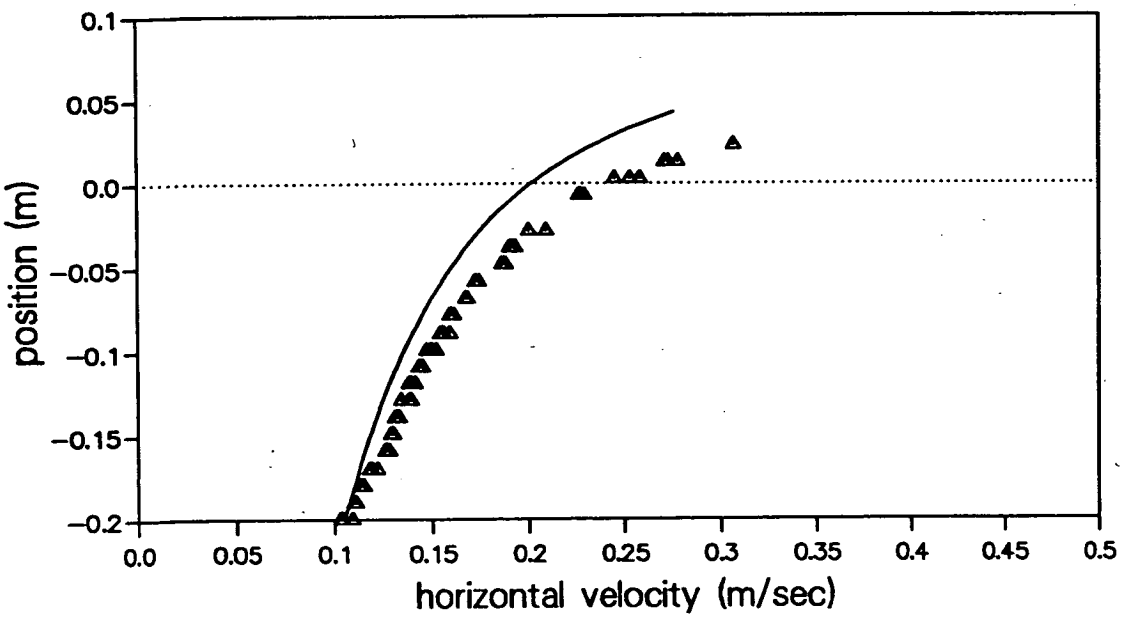

Fig. 5.17(b): Δ measured by PIV; the solid curve calculated from the Wheeler stretching method for the case of **e6t4**; the horizontal dashed line is MWL.

Figs. 5.17: Comparisons of the horizontal velocity under the crest of regular waves between the predictions made by the Wheeler stretching method and the results measured by PIV.

5.3.3 Comparisons with the Chakrabarti Stretching Method

In fact the Chakrabarti stretching method does not stretch the vertical co-ordinate (Chakrabarti 1971). The Chakrabarti stretching method defines the water depth replaced by the distance from the bed to the free surface. Therefore small kinematics are expected under the long wave crest.

The frequency range for regular waves to sum up Fourier components is from j=16 to j=50. The frequency range for two-component waves to sum up Fourier components is also from j=16 to j=100. The comparisons of the horizontal velocity under the crest of regular waves between the PIV measurements and the Chakrabarti stretching predictions applied to the waves (**e5t8** and **e6t4**) are shown in figs. 5.18.

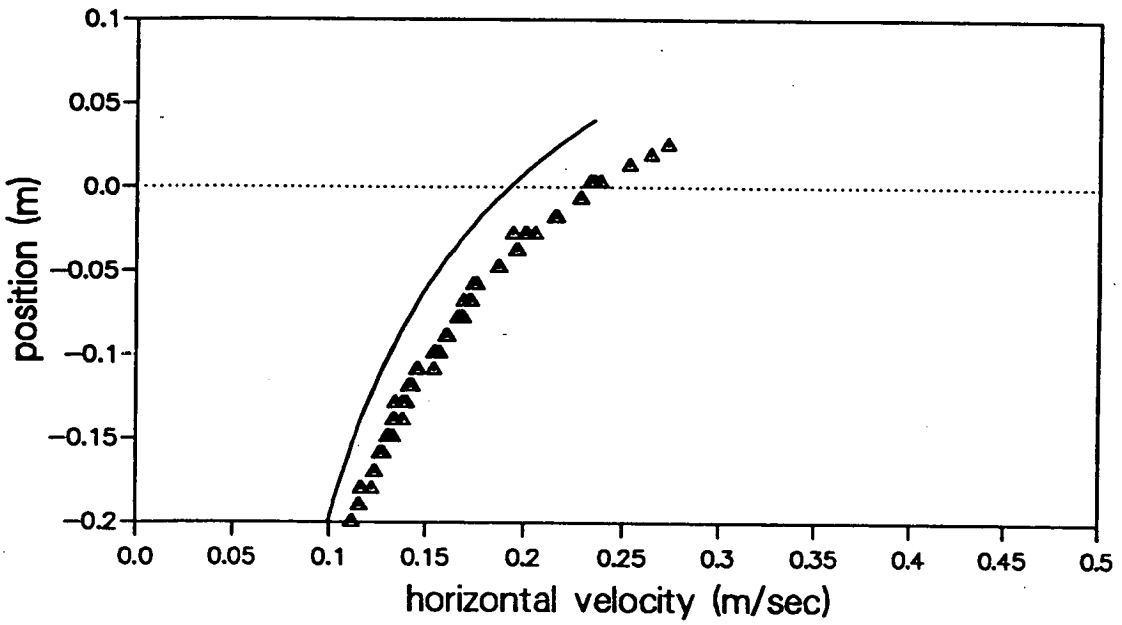

Fig. 5.18(a): Δ measured by PIV; the solid curve calculated from the Chakrabarti stretching method for the case of **e5t8**; the horizontal dashed line is MWL.

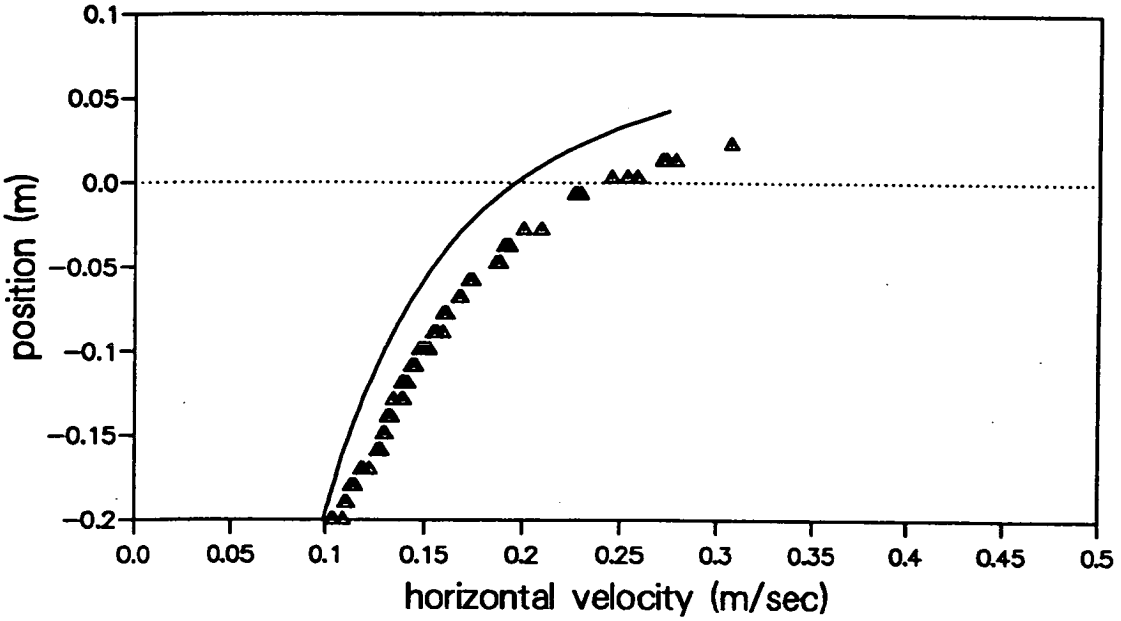

Fig. 5.18(b): Δ measured by PIV; the solid curves calculated from the Chakrabarti stretching method for the case of **e6t4**; the horizontal dashed line is MWL.

Figs. 5.18: Comparisons of the horizontal velocity under the crest of regular waves between the predictions made by the Chakrabarti stretching method and the results measured by PIV.

Both the Wheeler and Chakrabarti stretching theories tend to underpredict measured velocities. In the cases there is a consistent underprediction of the velocities range from 16% at -0.20m to 17% at the level of mean water under the long wave crest.

5.3.4 Comparisons with the Superposition Stretching Method

Superposition stretching method defines the distance of each Fourier component from the bed to the elevation of that component. That is to stretch the vertical co-ordinate with respect to Fourier components.

The frequency range for regular waves to sum up Fourier components is from j=16 to j=50. Also the frequency range for two-component waves to sum up Fourier components is from j=16 to j=100. The comparisons of the horizontal velocity under the crest of regular waves between the PIV measurements and the superposition stretching predictions applied to the waves (**e5t8** and **e6t4**) are shown in figs. 5.19.

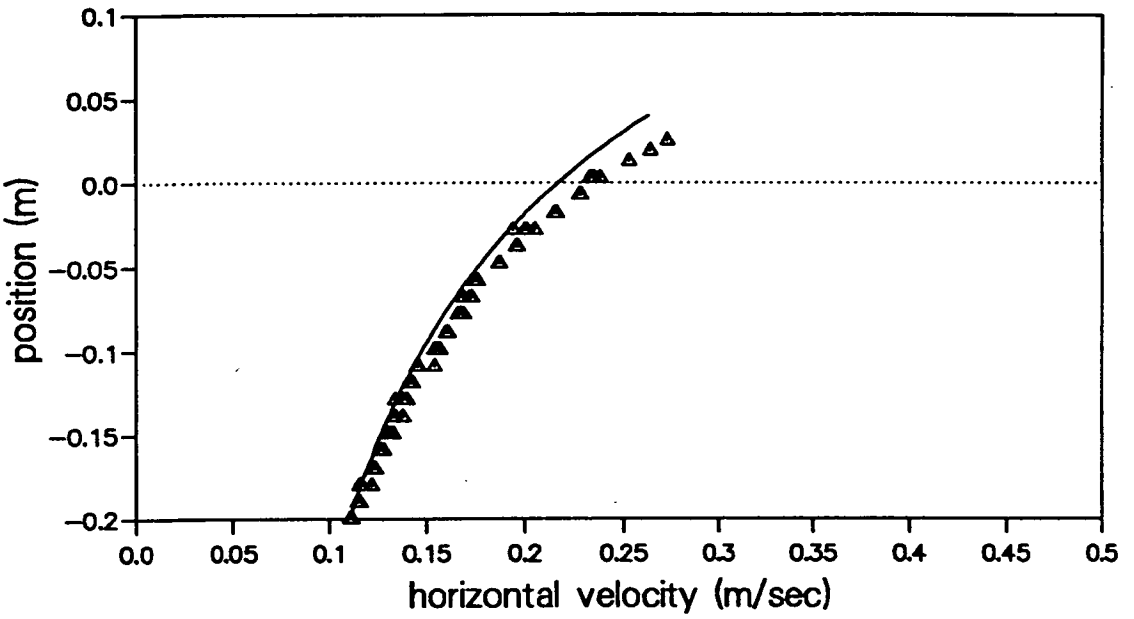

Fig. 5.19(a): Δ measured by PIV; the solid curve calculated from the superposition stretching method for the case of **e5t8**; the horizontal dashed line is MWL.

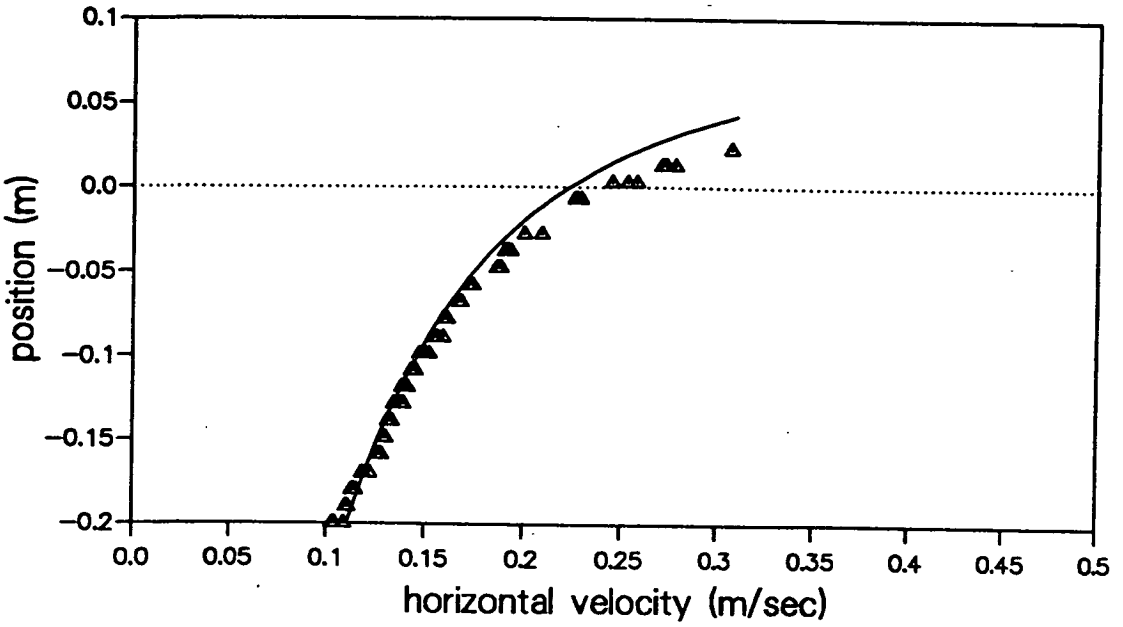

Fig. 5.19(b): Δ measured by PIV; the solid curve calculated from the superposition stretching method for the case of **e6t4**; the horizontal dashed line is MWL.

Figs. 5.19: Comparisons of the horizontal velocity under the crest of regular waves between the predictions made by the superposition stretching method and the results measured by PIV.

5.3.5 Comparisons with the Time-Stepping Technique

The numerical scheme of a two-dimensional numerical wave tank is modeled on the basis of the boundary integral method and developed by She, Easson and Greated (1992). The programme is mounted on a parallel computing machine, AMT DAP-602. The simulation of waves in this numerical tank is generated by a hinged wavemaker at one end and absorbed by a 'damper' at the other end. The inputs for the simulation programme are the number of points for the fluid boundaries, wavemaker frequency, wavemaker amplitude and the dimensions of the tank. The initial conditions are the starting time, x and y positions of the

points, velocity potential and stream function of the fluid boundaries. The wavemaker frequency is of the same as the simulated frequency of waves. Also wave height is a function of wavemaker amplitude with respect to any specific wave frequency. Therefore, a calibration is required for this function. Figure 5.20 shows the sketch of the numerical wave tank. Figure 5.21 shows the calibration between wave height and wavemaker amplitude at f_{24}=0.94 Hz. The comparison of wave elevation along long wave phases between the measurements and the time-stepping prediction applied to the case of regular waves **e5t8** is shown in fig. 5.22. The free surface horizontal velocity along a long wave period calculated by the time-stepping method for the case of regular waves **e5t8** is shown in fig. 5.23. Figure 5.24 shows the comparison of horizontal velocity under the long wave crest between the measurements and the time-stepping prediction applied to the case of regular waves **e5t8**.

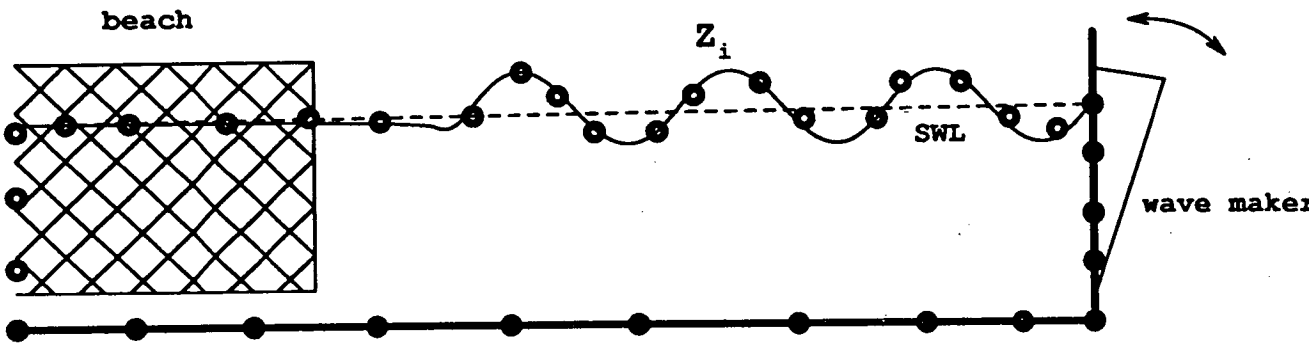

Fig. 5.20: Sketch of the numerical water tank for the time-stepping technique.

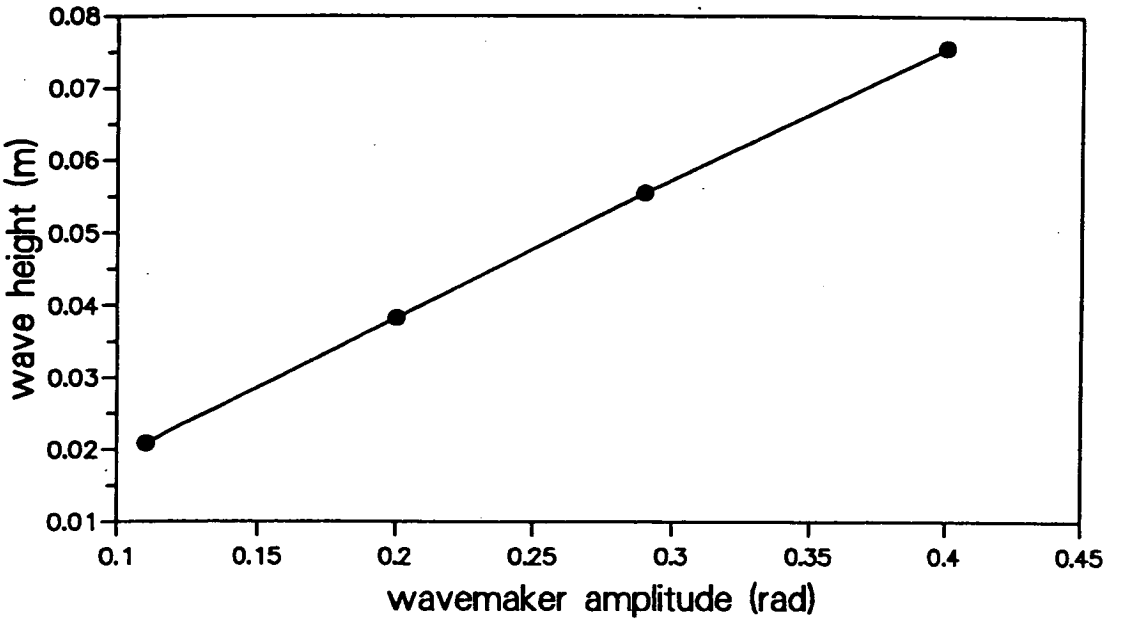

Fig. 5.21: Monochromatic long wave heights as a function of the paddle amplitude at the frequency f_{24}=0.94 Hz.

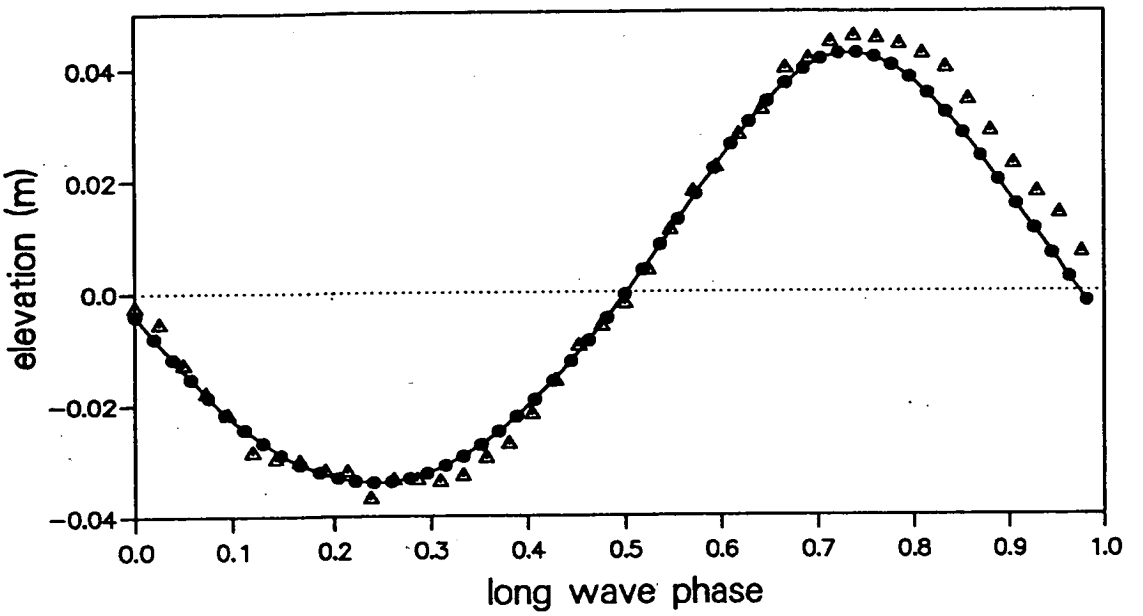

Fig. 5.22: Wave record comparison (Δ measured by gauges; o calculated from time-stepping technique for the case of **e5t8**; the horizontal dashed line is MWL).

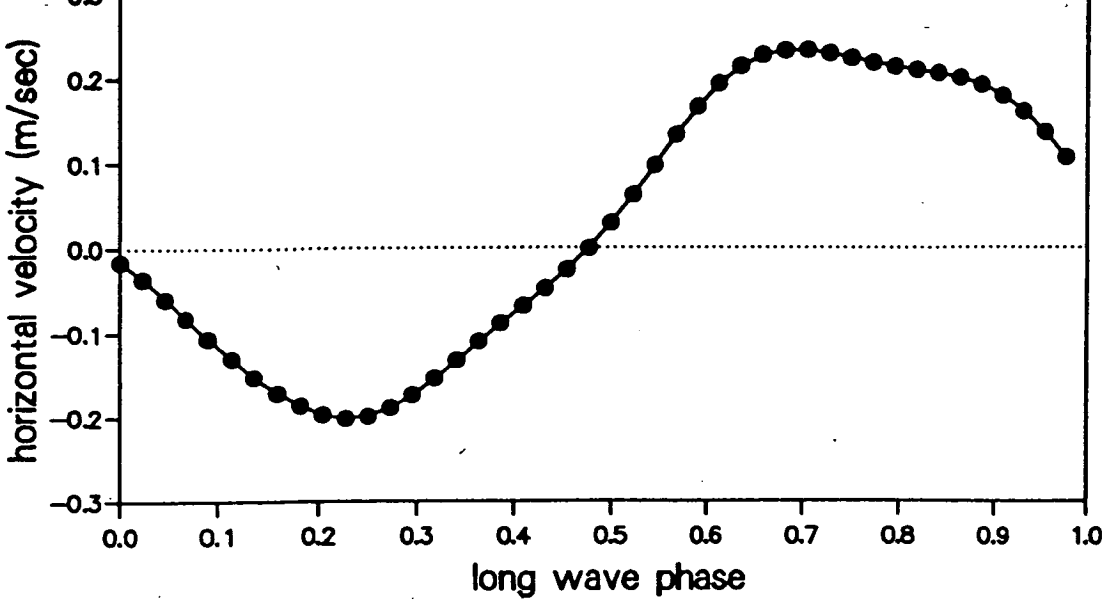

Fig. 5.23: The horizontal free surface velocity distribution along a long wave period (o calculated from the time-stepping technique for the case of **e5t8**; the horizontal dashed line is MWL).

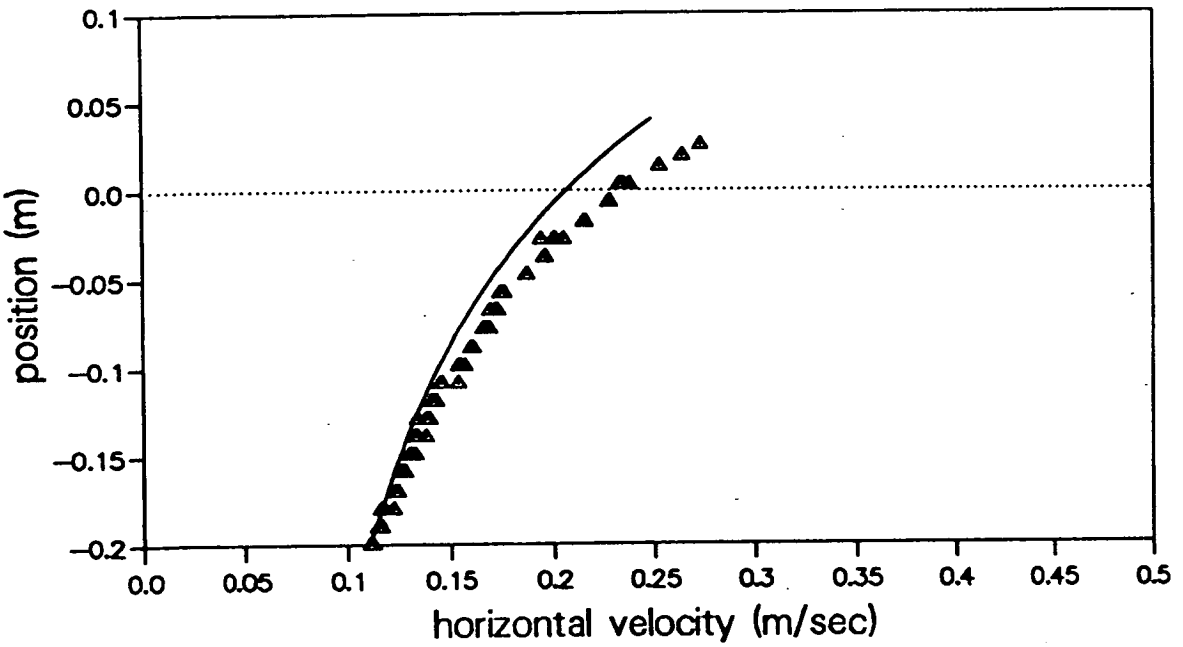

Fig. 5.24: Comparison of the horizontal velocity under the crest of regular waves between the time-stepping prediction and the PIV results (Δ measured by PIV; the solid curve calculated from time-stepping technique for the case of **e5t8**; the horizontal dashed line is MWL).

5.3.6 Comparisons Between Theories

The comparison comprises PIV measurements, linear theory, the Wheeler, Chakrabarti and superposition stretching methods for the cases of regular waves and two-component waves. The frequency range for regular waves to sum up Fourier components is from j=16 to j=50 and the frequency range for two-component waves to sum up Fourier components is from j=16 to j=100 when linear theory, the Wheeler, Chakrabarti and superposition stretching methods are applied. Figures 5.25 give the comparisons of horizontal velocity under the long wave crest for the regular wave case **e5t8** and the two-component wave case **e6t4** among the various predictions and the PIV measurements.

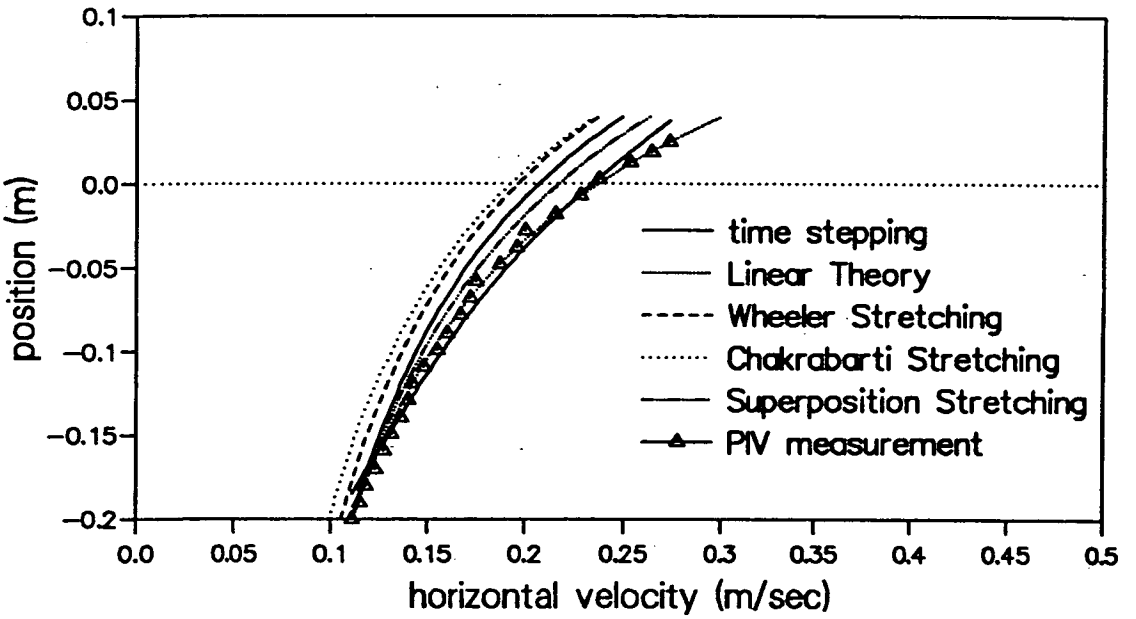

Fig. 5.25(a) The comparisons of the horizontal velocity under the crest of regular waves for the case of **e5t8** (regular waves) among the PIV measurement, linear theory, the Wheeler, Chakrabarti, superposition stretching and the time-stepping predictions (the horizontal dashed line is MWL).

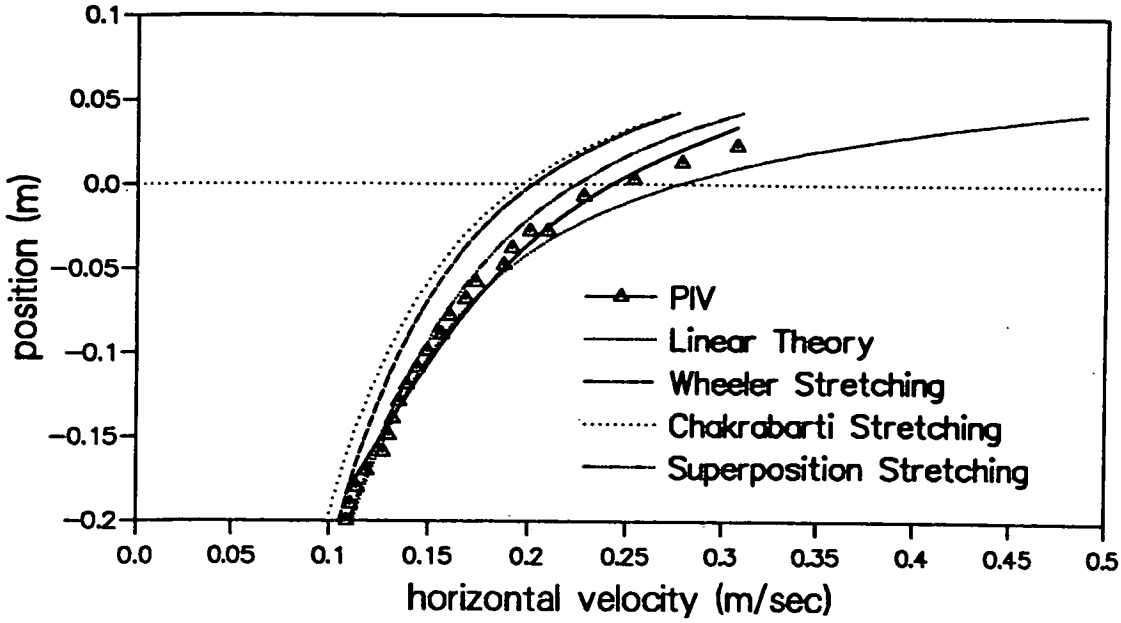

Fig. 5.25(b) The comparisons of the horizontal velocity under the crest of regular waves for the case of **e6t4** (two-component waves) among the PIV measurement, linear theory, the Wheeler, Chakrabarti and superposition stretching predictions (the horizontal dashed line is MWL).

Figs. 5.25: Comparisons of the PIV measurements, linear theory and the various stretching predictions for both cases of long waves and short waves riding on long waves, **e5t8** and **e6t4**, including the time-stepping technique for the case of regular waves **e5t8**.

The summary and conclusion of the kinematics comparisons are given in Chapter 7.

Chapter 6

FURTHER WORK

This chapter contains two sections as extensions of the previous chapters. In Chapter 3 the numerical solution of solitary waves has been presented based on Green's theorem and tailored quadrature weights and abscissas, courtesy of W A B Evans, for solving the integral equation Eqn. (3.42) which is shown in Chapter 3. The first section will discuss the stability of solitary waves based on soft-mode (x-axis) and normal-mode (y-axis) perturbation of free surface and velocity potential. The second section will discuss a new numerical scheme for internal solitary waves based on a generalised Stokes' formula and Green's theorem. The work of these both sections has not appeared in any published paper, although some similar works have been done before, Osborne and Burch (1980). Therefore it is worth writing down the detailed derivations.

6.1 The Stability of Solitary Waves

This section attempts to discuss the normal-mode instability of solitary waves. In other words, the main purpose is to investigate the stability of two-dimensional solitary waves with respect to three-dimensional infinitesimal perturbation.

It is well known that a periodic wave train (Stokes' waves) is unstable with respect to modulated perturbation (Longuet-Higgins 1978 a, b). It is also well proven that the instability of a finite-amplitude periodic wave train will appear, both in deep water and shallow water, under certain circumstances, McLean (1982 a, b). But on the other hand, the stability of solitary waves has not been so explicit like the stability of Stokes' waves. Tanaka (1986) first based on the exact solution of solitary waves of permanent forms and gave the soft-mode stability of solitary waves in the solitary wave travelling direction. Furthermore, the normal-mode perturbation provides a periodic form within the y axis.

The motion of solitary waves is on an inviscid, irrotational and incompressible fluid. $\phi(x, y, z, t)$ and $z = \eta(x, y, t)$ satisfy Laplace's equation and two boundary conditions, dynamic and kinematic.

$$\phi = \Phi + \hat{\phi}, \eta = \bar{\eta} + \hat{\eta} \qquad \text{(EQ 6.1)}$$

where $(\Phi, \bar{\eta})$ and $(\hat{\phi}, \hat{\eta})$ correspond, respectively, to the unperturbed, i.e. permanent, solitary wave and the infinitesimal perturbations of short waves $(\hat{\phi} \ll \Phi, \hat{\eta} \ll \bar{\eta})$. So the first order perturbation equations are given:

$$\nabla^2 \hat{\phi} = 0, 0 < z < \bar{\eta} \qquad \text{(EQ 6.2)}$$

$$\hat{\phi}_t = -\hat{\eta} - \Phi_x \hat{\phi}_x - \Phi_z \hat{\phi}_z - (\Phi_x \Phi_{xz} + \Phi_z \Phi_{zz})\hat{\eta} \text{ at } z = \bar{\eta} \qquad \text{(EQ 6.3)}$$

$$\hat{\eta}_t = -\Phi_x\hat{\eta}_x - \bar{\eta}_x\hat{\phi}_x - (\Phi_{xz}\bar{\eta}_x - \Phi_{zz})\hat{\eta} + \hat{\phi}_z \text{ at } z = \bar{\eta} \qquad \text{(EQ 6.4)}$$

In Eqn. (6.3) and (6.4), the higher order terms (such as $\hat{\phi}_y\hat{\eta}_y$ and $\hat{\phi}_{yz}\hat{\eta}_y\hat{\eta}$) have been ignored.

Differentiating Eqn. (3.41), which is in Chapter 3, with respect to $z_0 = 1 + \bar{\eta}(x_0)$ and using $\Phi_x = \Psi_z$ one obtains

$$\Phi_x =$$

$$-\int_{-\infty}^{\infty} \left((1+\bar{\eta}'(x)^2)\,(F^2 - 2\bar{\eta}(x))\right)^{1/2}$$

$$\left(\frac{\bar{\eta}(x) - \bar{\eta}(x_0)}{(x-x_0)^2 + (\bar{\eta}(x) - \bar{\eta}(x_0))^2} + \frac{2 + \bar{\eta}(x) + \bar{\eta}(x_0)}{(x-x_0)^2 + (2 + \bar{\eta}(x) + \bar{\eta}(x_0))^2}\right)\frac{dx}{2\pi} \qquad \text{(EQ 6.5)}$$

By the same way, differentiating Eqn. (3.41) with respect to x_0 and using $\Phi_z = -\Psi_x$ one obtains

$$\Phi_z =$$

$$\int_{-\infty}^{\infty} \left((1+\bar{\eta}'(x)^2)\,(F^2 - 2\bar{\eta}(x))\right)^{1/2}$$

$$\left(\frac{(x-x_0) - (\bar{\eta}(x) - \bar{\eta}(x_0))\,\bar{\eta}'(x_0)}{(x-x_0)^2 + (\bar{\eta}(x) - \bar{\eta}(x_0))^2} - \frac{(x-x_0) + (2 + \bar{\eta}(x) + \bar{\eta}(x_0))\,\bar{\eta}'(x_0)}{(x-x_0)^2 + (2 + \bar{\eta}(x) + \bar{\eta}(x_0))^2}\right)\frac{dx}{2\pi}$$

(EQ 6.6)

Higher-order derivatives, Φ_{xz} and Φ_{zz}, are obtained by a straightforward application of the chain rule from Eqns. (6.5) and (6.6).

Once the permanent form of solitary waves is given, see Chapter 3, the derivatives of Φ with respect to x and z, i.e. Φ_x, Φ_z, Φ_{xz} and Φ_{zz}, can be obtained through the same set of abscissas and weights, which has been used in Chapter 3, for the above integral equations. The perturbation forms of $\hat{\eta}$ and $\hat{\phi}$ are given:

$$\hat{\eta} = e^{-i\sigma t + iqy}\eta^*(x) \qquad \text{(EQ 6.7)}$$

$$\hat{\phi} = e^{-i\sigma t + iqy}\phi^*(x, z) \qquad \text{(EQ 6.8)}$$

Substitution of Eqns. (6.7) and (6.8) into Eqns. (6.2), (6.3) and (6.4) gives

$$\phi^*_{xx} + \phi^*_{zz} - q^2\phi^* = 0 \qquad \text{(EQ 6.9)}$$

$$\begin{aligned} &i\sigma\eta^*(x) \\ &= \Phi_x\eta^*(x) + \bar{\eta}_x\phi^*_x(x, z) \\ &+ (\Phi_{xz}\bar{\eta}_x - \Phi_{zz})\eta^*(x) - \phi^*_z(x, z) \end{aligned} \qquad \text{(EQ 6.10)}$$

$$\begin{aligned} &i\sigma\phi^*(x, z) \\ &= \eta^*(x) + \Phi_x\phi^*_x(x, z) \\ &+ \Phi_z\phi^*_z(x, z) + (\Phi_x\Phi_{xz} + \Phi_z\Phi_{zz})\eta^*(x) \end{aligned} \qquad \text{(EQ 6.11)}$$

A numerical solution for Eqns. (6.9), (6.10) and (6.11) remains open.

6.2 Internal Solitary Waves

This section discusses the phenomenon of waves along the interface between two fluids. Both fluids have comparable densities. Of course, the density of the lower fluid is larger than that of the upper fluid. In this case, the velocity and dynamic pressure of the upper fluid along the interface can not be ignored. Usually such waves are called 'internal waves'.

Internal waves propagate beneath the sea surface in a medium whose density varies as a function of depth; the density stratification is determined by solar heating from above and by the local salinity content of the water. Osborne and

Burch (1980) provided some useful experimental evidence from their sea-going measurements in the Andaman Sea: (i) the internal solitary waves are long in the sense that their wavelengths (1-3 km) are much greater than average thermocline depth (240 m). (ii) The solitons occur on rather short time scales of five to ten minutes. Thus a high sampling rate is needed for both temperature and velocity measurements. (iii) Packets of solitons occurred almost every 12 hours during the measurement programme. Each packet consisted on the average of about six to eight waves, generally rank-ordered by amplitude, with the largest leading the rest. Also new technology, remote-sensing from satellite photographs, provides graphic evidence of their crest lengths, which range up to 150 km, because internal waves modulate amplitudes of surface waves.

Interest and work on long internal wave motions have been stimulated and achieved in recent years on both theoretical and experimental approaches. The theoretical progress has discovered the inverse scattering transform solutions to several nonlinear wave equations, e.g. KdV equations, which are applicable in describing long internal wave motions in various environments. Experimental progress has been made both in the laboratory and in the field.

6.2.1 Governing Equations

In this scheme, the internal solitary wave with two fluids of densities ρ_1 and ρ_2 ($\rho_1 > \rho_2$) is considered from a co-ordinate (X-Y) moving with this wave, $y_1(x)$ is the elevation of the internal solitary wave profile and $y_2(x)$ is the elevation of the free surface solitary wave profile according to this co-ordinate. Therefore the water in the outskirts of the solitary wave moves with a velocity, $-C\hat{i}$, where C is the solitary wave velocity observed from a fixed co-ordinate. As usual, $\eta_1(x)$ is the internal solitary wave elevation above the undisturbed lower fluid level h_1

and $\eta_2(x)$ is the elevation above the undisturbed upper fluid level $H=h_1+h_2$. That means $\eta_1(x) = y_1(x) - h_1$ and $\eta_2(x) = y_2(x) - H$.

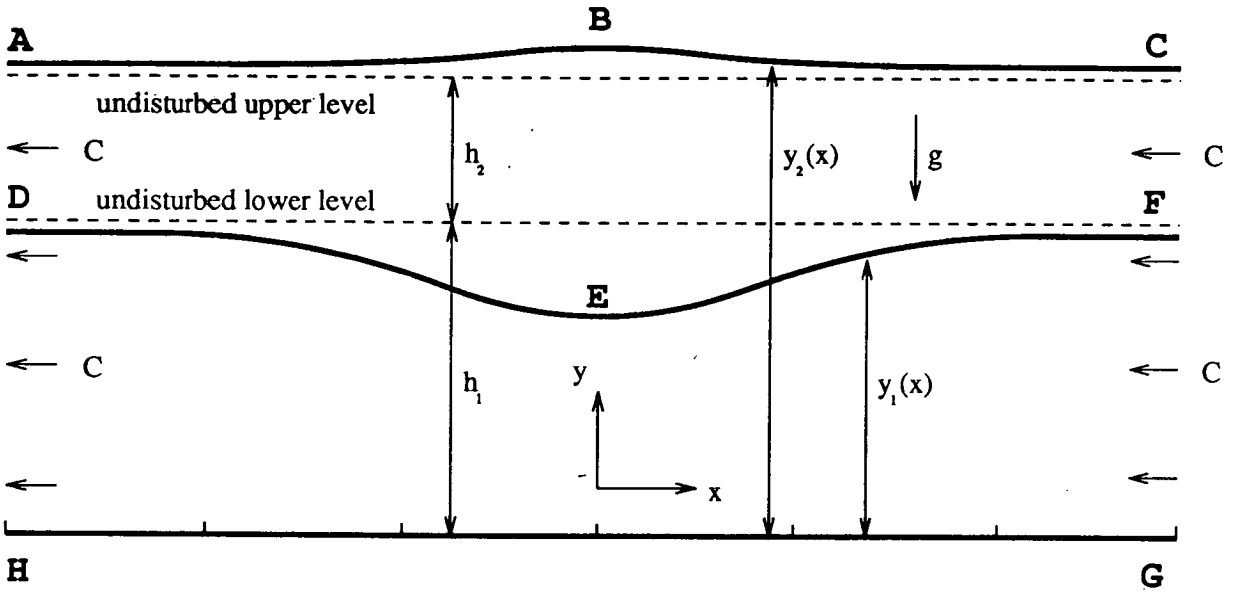

Fig. 6.1: Sketch of the internal solitary wave observed from the co-ordinate moving with the wave.

Either free surface solitary waves or internal solitary waves need their own Stokes' formula in order to build up a relationship between the phase velocity of waves and the decay coefficient μ, which characterizes the profile of solitary waves. In Chapter 3, Stokes' formula for free solitary waves has been introduced. This formula can also be derived from the linear dispersion relation. Let g = h = 1 and $k = i\mu$, then

$$C^2 = \frac{\tan\mu}{\mu} \text{ i.e. } F^2 = \frac{\tan\mu}{\mu} \qquad \text{(EQ 6.12)}$$

That means, it is reasonable to derive the dispersion relation for the generalized Stokes' formula by the same way along the interface between the two fluids.

6.2.1.1 Generalized Stokes' Formula

One dynamic boundary condition and two kinematic boundary conditions are imposed on the interface of the two fluids.

$$\rho_1\left(\frac{\partial\Phi_1}{\partial t} + \frac{1}{2}(\nabla\Phi_1)^2 + g\eta\right) = \rho_2\left(\frac{\partial\Phi_2}{\partial t} + \frac{1}{2}(\nabla\Phi_2)^2 + g\eta\right) \text{ at } y = \eta \qquad \text{(EQ 6.13)}$$

$$\frac{\partial\eta}{\partial t} + \frac{\partial\Phi_1}{\partial x}\frac{\partial\eta}{\partial x} + \frac{\partial\Phi_1}{\partial y}\frac{\partial\eta}{\partial y} - \frac{\partial\Phi_1}{\partial y} = 0 \qquad \text{(EQ 6.14)}$$

$$\frac{\partial\eta}{\partial t} + \frac{\partial\Phi_2}{\partial x}\frac{\partial\eta}{\partial x} + \frac{\partial\Phi_2}{\partial y}\frac{\partial\eta}{\partial y} - \frac{\partial\Phi_2}{\partial y} = 0 \qquad \text{(EQ 6.15)}$$

If the three boundary conditions are linearized by linear theory, then Eqns. (6.13), (6.14) and (6.15) become the following three equations.

$$\rho_1\left(\frac{\partial\Phi_1}{\partial t} + g\eta\right) = \rho_2\left(\frac{\partial\Phi_2}{\partial t} + g\eta\right) \text{ at } y = 0 \qquad \text{(EQ 6.16)}$$

$$\frac{\partial\eta}{\partial t} = \frac{\partial\Phi_1}{\partial y} \qquad \text{(EQ 6.17)}$$

$$\frac{\partial\eta}{\partial t} = \frac{\partial\Phi_2}{\partial y} \qquad \text{(EQ 6.18)}$$

Since Φ_1 and Φ_2 satisfy Laplace's equation and tend to zero as $y \to -h_1$, $y \to h_2$, respectively, the elementary solution takes the form

$$\eta = Ae^{i(kx-\omega t)} \qquad \text{(EQ 6.19)}$$

$$\Phi_1 = B_1 e^{i(kx-\omega t)}\cosh k(h_1 + y) \qquad \text{(EQ 6.20)}$$

$$\Phi_2 = B_2 e^{i(kx-\omega t)} \cosh k(h_2 - y) \qquad \text{(EQ 6.21)}$$

Therefore the dispersion relation is given by

$$\omega^2 = gk \frac{\rho_1 - \rho_2}{\left(\frac{\rho_1}{\tanh kh_1} + \frac{\rho_2}{\tanh kh_2}\right)} \qquad \text{(EQ 6.22)}$$

Let $k = i\mu$ and $g = 1$, then the generalized Stokes' formula is obtained, see Eqn. (6.23).

$$C^2 = \left(\frac{\omega}{k}\right)^2 = \frac{\rho_1 - \rho_2}{\mu\left(\frac{\rho_1}{\tan \mu h_1} + \frac{\rho_2}{\tan \mu h_2}\right)} \qquad \text{(EQ 6.23)}$$

6.2.1.2 Green's Theorem (Curtesy of W A B Evans)

Here it is necessary to recall Green's theorem applied in Chapter 3. Two potential flows are for the two different densities of these two fluids and that pressure is continuous across the interface **DEF** which is a streamline when a steady-state profile is observed with respect to a co-ordinate moving with a specific speed. The velocity potentials and stream functions of the two fluids obey two-dimensional Laplace's equations in both fluid domains. Accordingly, by Green's theorem applied to the stream function gives

$$\Psi(r_0) = \oint (\Psi(r) \nabla (G(r, r_0)) - G(r, r_0) \nabla \Psi) \bullet dA \qquad \text{(EQ 6.24)}$$

where r_0 i.e. (x_0, y_0) is a point within either fluid domain **ABCFED** or **FEDGH** and G(r, r_0) is a chosen Green's function of the two-dimensional Laplace's Equation defined subject to the addition of an arbitrary harmonic function within the domain (complementary function). Equation (6.25) is a good choice for G(r,r_0) according to experience.

$$G(r, r_0) = \frac{1}{2\pi} ln\left(\frac{|r - r_0|}{|r - \bar{r}_0|}\right) \qquad \text{(EQ 6.25)}$$

where $\bar{r}_0=(x_0, -y_0)$ is the image of r_0 in the canal bed (line **GH**). This form of the Green's function evidently vanishes at all points along the canal bed **GH**. Apply Green's theorem to the lower fluid domain **DEFGH** which is equated by Eqn. (6.26). Equation (6.27) is derived from Eqn. (6.26) and the derivation is similar to the technique shown in Chapter 3.

$$\Psi(x, y_1(x_0)-) = 0 = \oint_{DEFGH} dA \bullet (\Psi(r) \nabla G(r, r_0) - G(r, r_0) \nabla \Psi) \qquad \text{(EQ 6.26)}$$

$$Ch_1 + \int_{-\infty}^{\infty} (1 + y_1(x)^2)^{1/2} |v_1(x, y_1(x))| \ln\left(\frac{(x - x_0)^2 - (y_1(x) - y_1(x_0))^2}{(x - x_0)^2 + (y_1(x) + y(x_0))^2}\right) \frac{dx}{4\pi} = 0 \qquad \text{(EQ 6.27)}$$

as the integral equation from the denser fluid domain. Note it depends on the unknown velocity modulus $|v_1|$, in the lower fluid along the interface streamline. For the normal solitary wave, $|v_1|$ would be given by Bernoulli's equation for a free surface and the above would then constitute the integral equation for the normal solitary wave profile.

Then perform the same process for the upper fluid domain **ABCFED**.

$$\Psi(x, y_1(x_0)+) = 0 = \oint_{ABCFED} dA \bullet (\Psi(r) \nabla G(r, r_0) - G(r, r_0) \nabla \Psi) \qquad \text{(EQ 6.28)}$$

Bernoulli's equation applies on the free surface.

$$|v_2(r_{surface})|^2 = C^2 - 2g(y_2(x) - H) \qquad \text{(EQ 6.29)}$$

Furthermore Bernoulli's equation can be used for describing the interfacial boundary condition, since the interface is assumed as a streamline.

Potential flow implies that the streamline constant, $P + \frac{1}{2}\rho|v|^2 + \rho g y$ is constant

throughout each fluid i.e. has same value on each streamline. Also the term P is continuous along the internal surface. In the lower fluid, along the internal streamline, Bernoulli's equation is

$$P + \frac{1}{2}\rho_1 |v_1|^2 + \rho_1 g y = \frac{1}{2}\rho_1 C^2 + \rho_1 g h_1 + \rho_2 g h_2 \qquad \text{(EQ 6.30)}$$

Let ρ_1=1, the density of the lower fluid, and P is the pressure along the interface.

v_1: the local velocity of the lower fluid on the interface.

h_1: the depth of the lower fluid.

In the upper fluid, along the internal streamline, Bernoulli's equation is

$$P + \frac{1}{2}\rho_2 |v_2|^2 + \rho_2 g y = \frac{1}{2}\rho_2 C^2 + \rho_2 g (h_1 + h_2) \qquad \text{(EQ 6.31)}$$

ρ_2: the density of the upper fluid.

v_2: the local velocity of the upper fluid on the interface.

h_2: the depth of the upper fluid.

Thus from Eqns. (6.30) and (6.31) a relation between $|v_1|$ and $|v_2|$ can be built along the interface streamline viz.

$$\rho_1 (C^2 - |v_1|^2 - 2g (y_1(x) - h_1)) = \rho_2 (C^2 - |v_2|^2 - 2g (y_1(x) - h_1)) \qquad \text{(EQ 6.32)}$$

which implies only one of the interface velocity functions need be found to determine the other (assume the lower fluid profile is known). Green's theorem, Eqn. (6.28), gives another integral equation Eqn. (6.33) in the upper fluid.

$$\int_{-\infty}^{\infty} ((1 + y'_2(x)^2)(C - 2g(y_2(x) - H)))^{1/2} \ln\left(\frac{(x - x_0)^2 + (y_2(x) - y_1(x_0))^2}{(x - x_0)^2 + (y_2(x) + y_1(x_0))^2}\right) \frac{dx}{4\pi}$$

$$-\int_{-\infty}^{\infty}(1+y'_1(x)^2)^{1/2}|v_2(x,y_1(x))|\ln\left(\frac{(x-x_0)^2+(y_1(x)-y_1(x_0))^2}{(x-x_0)^2+(y_1(x)+y_1(x_0))^2}\right)\frac{dx}{4\pi} \quad \text{(EQ 6.33)}$$

Furthermore by considering a point just below the free surface for the upper fluid domain, another integral equation Eqn. (6.35) is derived from Eqn. (6.34) in the upper fluid.

$$\Psi(x,y_2(x_0)-) = -Ch_2 = \oint_{ABCFED} dA \bullet (\Psi(r)\nabla G(r,r_0) - G(r,r_0)\nabla\Psi) \quad \text{(EQ 6.34)}$$

$$\Psi(x,y_2(x_0)-) = -Ch_2 =$$

$$((1+y'_2(x)^2)\,(C-2g(y_2(x)-H)))^{1/2}\ln\left(\frac{(x-x_0)^2+(y_2(x)-y_1(x_0))^2}{(x-x_0)^2+(y_2(x)+y_1(x_0))^2}\right)\frac{c}{4}$$

$$-\int_{-\infty}^{\infty}(1+y'_1(x)^2)^{1/2}|v_2(x,y_1(x))|\ln\left(\frac{(x-x_0)^2+(y_2(x)-y_1(x_0))^2}{(x-x_0)^2+(y_2(x)+y_1(x_0))^2}\right)\frac{dx}{4\pi} \quad \text{(EQ 6.35)}$$

Equations (6.27), (6.32) and (6.33), together with the relation Eqn. (6.35) that essentially gives $|v_1|$ in terms of $|v_2|$ or vice-versa, constitute three coupled integral equations for the three unknown functions viz. $y_1(x)$, $y_2(x)$ and either $|v_1|$ or $|v_2|$. These equations are satisfied at any x_0 value along either the internal surface or the free surface.

6.2.1.3 Constrained Flat-Topped Internal Solitary Waves

A simple case of internal waves is the problem with the top-constrained (still) surface i.e. **ABC** is horizontal. In this case, when applying Green's theorem to the upper fluid, it is clearly advantageous to use a Green's function that vanishes on **ABC** i.e. r_0 is now taken as a reflection of r_0 in this top line.

Equations (6.30), (6.31) and hence (6.32) will still be valid. Note: $y_1(x)$ is replaced by $(H-y_1(x))$ in Eqn. (6.33).

$$Ch_2+$$

$$\int_{-\infty}^{\infty} (1+y'_1(x)^2)^{1/2} |v_2(x, y_1(x))| \ln\left(\frac{(x-x_0)^2+(y_1(x)-y_1(x_0))^2}{(x-x_0)^2+(2H-y_1(x)-y_1(x_0))^2}\right)\frac{dx}{4\pi} \quad \text{(EQ 6.36)}$$

In this case the relevant integral equations are Eqns. (6.27) and (6.36) supplemented by the relation Eqn. (6.32). Note that it is necessary to parameterise the two functions $y_1(x)$ and either $|v_1|$ or $|v_2|$, see Eqns. (6.37) and (6.38).

$$\eta(x) = \sum_{m=1}^{NL} a_m e^{-m\mu x} \quad \text{(EQ 6.37)}$$

$$|v_1(x)|^2 = C^2 + \sum_{m=1}^{NL} b_m e^{-m\mu x} \quad \text{(EQ 6.38)}$$

Here $\eta(x)$, $v_1(x)$ and $v_1(x)$ are the internal wave profile and the lower and upper fluid velocity along the internal wave profile. Further computer programming can solve the coefficients a_m and b_m.

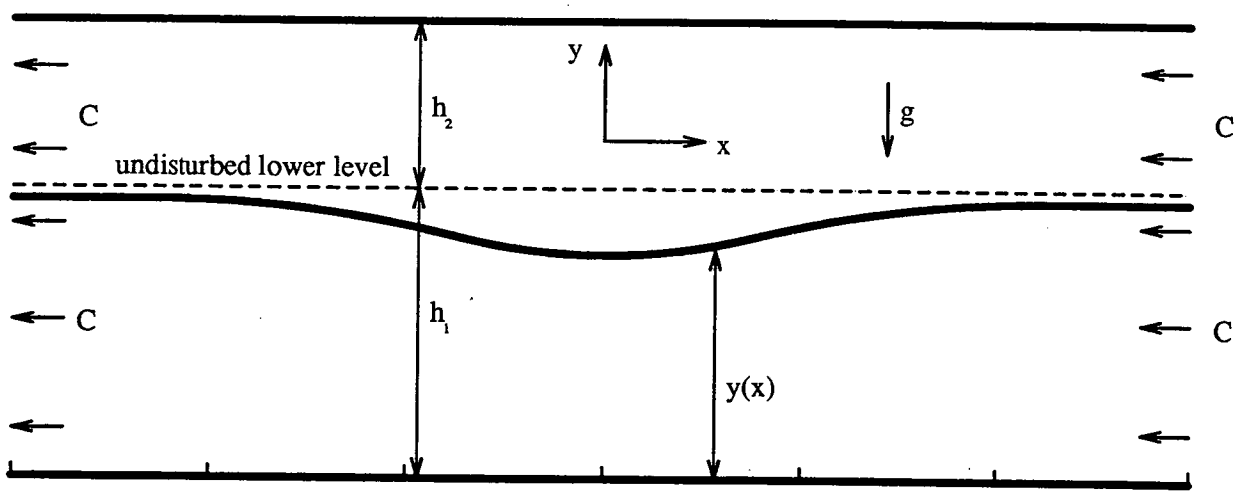

Fig. 6.2: Sketch of the constrained flat-topped internal solitary wave observed from the co-ordinate moving with the wave.

Chapter 7

CONCLUSION

The main purpose of this thesis is to consider the modulation and kinematics of short waves riding on solitary waves and long waves as outlined in Chapter 1. Here it shall be noted that only the time-independent modulation is considered. The evolution of short waves riding on time-dependent non-uniform velocity fields (solitary waves and long regular waves) is beyond the study of the thesis. Through a conformal mapping, the co-ordinates of the non-uniform velocity fields can be described by velocity potential and stream function. Also the free surfaces of these non-uniform velocity fields are streamlines when the fields are time-independent with respect to the co-ordinates moving with the celerity of the non-uniform velocity fields. This chapter consists of two sections: Section 7.1 is a summary of the numerical and experimental results obtained by applying various wave models and experimental measurements, whereas Section 7.2 recommends future potential research areas.

7.1 Summary

In regard to the non-uniform velocity fields, solitary waves and Stokes' waves are chosen as the two main non-uniform velocity fields for the following reasons: solitary waves and Stokes' waves are the most accurately defined waves available and the most-often-studied in the past; their theoretical study and numerical models are well established. Besides, solitary waves and Stokes' waves (monochromatic long waves) represent shallow water waves and deep water waves respectively well.

Kinematic comparisons between waves are presented in Section 5.3. For both cases of regular waves and two-component waves(one train of short waves and one train of long waves), the kinematics under the crests of the long waves are measured by the PIV technique.

Another research aim of this thesis is to perform a relative assessment on the accuracy of various stretching methods in predicting wave kinematics of short waves riding long waves. This assessment has been shown in Section 5.3 in which, the measured velocity profiles for both cases, **e5t8 and e6t4**, are under the crest of long waves. All the stretching methods for wave kinematics prediction use the wave amplitude spectra (time series of FFT) as their inputs. It should be noted that none of the stretching approximations has any real physical definition; they are all empirical adjustments to linear theory.

7.1.1 The Modulation of Short Waves

7.1.1.1 The Modulation of Short Waves Riding on a Long Solitary Wave

The numerical modulation of short waves riding on solitary waves has been discussed in Chapter 3. The modulation consists of wavenumber, frequency and amplitude modulation obtained from the conservations of wave action and phase. Due to the linearization of short waves riding on the free surface of a long solitary wave, the modulation solution is artificially constrained by the parameter ω when $\omega < 0.60$, see Eqn. (3.45), but the physical limitation of the solution for ω is not clear. That is to say, short waves riding on long solitary waves with large amplitude is beyond this study. The main results are:

- Along the free surface of the solitary wave, from the 'outskirts' to the crest, the short wavelength is decreasing, and the short wave amplitude and frequency are increasing. The maximum values for the modulated short wavenumber, frequency and amplitude always occur at the crest of solitary waves.

- On the crest of the solitary wave, the short wavelength becomes significantly smaller, and the amplitude and frequency become larger, as the amplitudes of the solitary waves increase.

The short wavenumber, frequency and amplitude have been confirmed to be strongly modulated by long solitary waves.

7.1.1.2 The Modulation of Short Waves Riding on Long Regular Waves

The time-series wave records of long regular waves and two-component waves have been measured. The elevation differences between the records of long regular waves and two-component waves are used for deriving the experimental

modulated short wave frequency. Meanwhile, the spectra of the time series of long monochromatic waves and two-component waves have been calculated.

The results of the modulation of short waves riding on long waves have been shown in Section 5.2 and lead to the following conclusions:

- The frequency modulation of short waves riding on long waves is a function of the long wave phase for different long wave steepnesses.

- In the empirical modulation of short wave frequency, the minimum modulated short wave frequency appears on the trough of long waves and the maximum modulated short wave frequency occurs somewhere near the crest of long waves (in the preceding trough side). The maximum/minimum modulated short wave frequency always occurs at the crest/trough of the long wave from the theoretical perspective.

- By increasing the long wave steepness, the modulated short wave frequency- which is normalized by the value of the modulated frequency at the long wave trough- increases proportionally at the crest of the long wave.

- The comparison between the numerical and experimental modulation of short waves riding on long regular waves is coherent: the short frequency modulation increases along with increasing the long wave steepnesses.

7.1.2 Wave Kinematics

Wave kinematics predicted by linear theory, the various stretching methods (the Wheeler, Chakrabarti and superposition stretching methods) and the time-stepping technique are compared. The predictions by linear theory and these stretching methods are sensitive to the cut-off frequency for the spectra. The choice of cut-

off frequency, according to the amplitude of wave spectra (both in minimum amplitude and upper limit frequency range used), is important and has been emphasized by Sutherland (1992). The choice of frequency range, in particular whether to include higher order harmonics or not, is of great importance. The kinematic results are strongly related to the use of frequency ranges.

7.1.2.1 Kinematics of Monochromatic Long Waves

The summary on the performance of linear theory, various stretching methods and the time-stepping technique for kinematic comparisons of regular waves, as shown in Section 5.3, is:

Linear theory is found to be the best method to determine the velocities under the crests of regular waves. The prediction by linear theory is generally very accurate and the error is less than 5%.

The Wheeler and Chakrabarti stretching methods tend to be underpredicted under the long wave crest zone. Both stretching methods tend to be of the same values of the horizontal velocity at the free surface. The methods underpredict the measurements.

The superposition stretching method performs very similarly to linear theory in the case of regular waves, since only one narrow-banded component exists significantly. But it is slightly less accurate than linear theory in predicting regular wave kinematics.

The time-stepping technique performs very similarly to linear theory in regular wave environments. The only benefit of this scheme is that it is a direct simulation of the waves in a wave flume.

7.1.2.2 Kinematics of Short Waves Riding on Long Waves

As presented in Section 5.3, the theories- various stretching theories, including linear theory- are compared against measurements of kinematics under short waves riding on long waves. The outcome is different from that obtained in the regular waves.

Linear theory proves to be an accurate theory below the mean water level. It is, however, unable to model the rapid increases in velocities with elevation above the mean water level in the cases of short waves riding on long waves. In such cases it tends to significantly overpredict the kinematics above the mean water level. Therefore linear theory would not be recommended for this kind of two-component wave environments.

The Wheeler and Chakrabarti stretching methods tend to underpredict the velocities in the long wave crests of short wave riding on long waves. For both the Wheeler and Chakrabarti stretching methods, the tendency of underprediction is greatest near the free surface.

The superposition stretching method tends to slightly underpredict the kinematics under the long wave crest for the case of short waves riding on long waves. This method provides a best fit to the experimental results among the several stretching techniques in the case measured here. It is therefore recommended for the case of short waves riding on long waves.

7.1.2.3 General Assessment of Wave Modelling

- In the case of two-component waves, the velocity profile predicted by linear theory under the crests of the long waves shows large differences in crest velocities above the mean water level (MWL). This case of short waves riding on

long regular waves is modelled accurately by using the superposition stretching method.

- No one theory performs better than any of the others in all wave environments. Linear theory performs best for regular waves and neither the Wheeler nor Chakrabarti stretching method is good for the cases of regular waves. The superposition stretching method is suitable for the case of short waves riding on long waves. Unfortunately, the empirical stretching methods do not satisfy Laplace's equation.

7.2 Suggestions for Future Research

Beyond the limited results of the thesis, there are several promising researches that can be embarked upon. One of the main approaches is based on the fact that the waves in the sea are three-dimensional in nature and may be represented by a continuous spectrum. Therefore two uni-directional components cannot fully represent the sea. As the result, more realistic wave spectra should be employed and three-dimensional measurements should be made wherever possible. A further set of experiments, which would be of interest, would be a modelling of an extreme wave group in a two-dimensional tank. This could be done by using a finite number of wave components riding on a non-unform velocity field to model a group of the correct form. An alternative approach would be to model an equivalent group within a sea-state produced by a spectrum.

To sum up the above, a realistic theoretical approach would be to adopt the theory of the Hamiltonian system and the statistical aspect. This will lead to a measurement of the crest velocity under every crest of long waves in irregular short waves riding on long waves by using PIV. The results could be used to form a crest velocity probability density curve. So there are three steps to explore the approach:

(I) The Hamiltonian system: wave motion is very complicated, therefore the study of random short wave interaction riding on long waves can be considered as an infinite-dimensional, nonlinear dynamical system by ignoring viscosity with respect to the non-uniform velocity field of long waves.

(II) The dynamical system and probabilistic method: based on Hamiltonian theory, the combination of both dynamical systems and probabilistic methods might be helpful in solving particular problems given by nonlinear partial differential equations, viewed as infinite-dimensional dynamical systems.

(III) Kinematics measurements: by applying the Particle Image Velocimetry technique, the above mathematical derivations, (I) and (II), can be verified by physical experiments.

On the other hand, the author intends to be involved in the following perspectives after completing this thesis:

- To develop a numerical scheme for the stability of solitary waves. This numerical scheme is based on normal-mode perturbations to steady-state solitary waves. More detailed derivation has been demonstrated in Chapter 6.

- To develop a numerical scheme for internal solitary waves from the scheme for solitary waves used in this thesis. More detailed discussion has been shown in Chapter 6.

- To discuss the evolution of weakly nonlinear short waves riding on long solitary waves and riding on internal solitary waves.

- To adopt an empirical approach for short waves riding on solitary waves and for short waves riding on directional long waves.

Bibilography

Airy, G B, "Tides and waves," **Encyclopaedia Metropolitana**, London, 1845.

Allan, T D, "**Satellite Microwave Sensing**," John Wiley & Sons, 1983.

Baldock, T E and C Swan, "Numerical calculation of large transient water waves," **Applied Ocean Research**, vol. 16, pp. 101 - 112, 1994.

Benjamin, T B and J E Feir, "The disintegration of wavetrains on deep water," **J. Fluid Mech.**, vol. 27, pp. 417 - 430, 1967.

Boussinesq, J, "Theorie de l'intumescence liquid appelee onde solitaire ou de translation se propageant dans un canal rectangulare," **Compte Rendus Acad. Sci. Paris**, vol. 72, pp. 755 - 759, 1871.

Bretherton, F P and C J R Garrett, "Wavetrains in inhomogeneous moving media," **Proc. R. Soc. Lond. A**, vol. 302, pp. 529 - 545, 1968.

Byatt-Smith, J G B, "An exact integral equation for steady surface waves," **Proc. Roy. Soc. Lond. A**, vol. 315, pp. 405 - 418, 1970.

Chakrabarti, S K, "Dynamics of single point mooring in deep water," **J. of Waterways, Port, Coastal and Eng Div.**, vol. 97 (WW3), pp. 588 - 590, 1971.

Chaplin, J R, "Developments of stream function wave theory," **Coastal Engineering**, vol. 3, pp. 179 - 205, 1980.

Chu, Jacob S, Steven R Long, and O M Phillips, "Measurements of the interaction of wave groups with shorter wind-generated wave," **J. Fluid Mech.**, vol. 245, pp. 191 - 210, 1992.

Dean, R G, "Stream function representation of non-linear ocean waves," **J. Geophy. Res.**, vol. 70, no. 18, pp. 4561 - 4572, 1965.

Dean, R G, "Relative validities of water wave theories," **J. Waterways and Harbours Division** , vol. 96, no. WW1, pp. 105 - 118, 1970.

Department of Energy, "Offshore Installations: Guildance on Design and Construction," HMSO, 1986.

Dold, J W and D H Peregrine, "An efficient boundary integral method for steep unsteady water waves," in **Numerical Methods for Fluid Dynamics II**, ed. M J Baines, pp. 671 - 679, Oxford University Press, 1986.

Evans, W A B and M J Ford, "On the shapes and properties of the streamlines of large amplitude solitary water waves," submitted to **Proc. Roy. Soc. Lond. A**, 1994.

Fenton, J A, "A ninth order solution for the solitary wave," **J. Fluid Mech.**, vol. 53, pp. 257 - 271, 1972.

Fenton, J A, "A higher order cnoidal wave theory," **J. Fluid Mech.**, vol. 91, pp. 129 - 161, 1979.

Fenton, J D, "Polynomial approximations and water waves," **Proc. 20th Int. Conf. on Coastal Engineering, ASCE**, vol. 1, pp. 193 - 207, 1986.

Forristall, G Z, "Kinematics in the crests of strom waves," in **International Conference on Coastal Engineering**, ASCE, Berkeley CA, 1986.

Gargett, A E and B A Hughes, "On the interaction of surface and internal waves," **J. Fluid Mech.**, vol. 52, pp. 179 - 191, 1972.

Gray, C, "The Development of Particle Image Velocimetry for Water Wave Studies," PhD thesis, Edinburgh University, 1989.

Gray, C, C A Greated, W J Easson, and N E Fancey, "The application of particle image velocimetry to measurement under waves," in **Proc. 2nd Int. Conf. of Laser Anemometry**, pp. 281 - 287, Strathclyde, Sep. 1987.

Harris, C G and W A B Evans, "Extension of numerical quadrature formulae to cater for end point singular be haviours over finite intervals," **Intern. J. Computer Math.**, vol. 6, pp. 219 - 227, 1977.

Hasselmann, K, T P Barnett, E Bouws, H Carlson, D E Cartwright, K Enke, H Gienapp, D E Hasselmann, P Kruseman, A Meerburg, P Muller,

D J Olbers, K Richter, W Sell, and H Walden, "Measurement of wind-wave growth and swell decay during the Joint North Sea Wave Project (JONSWAP)," **Dtsch. Hydrogr. Z. Suppl. A**, vol. 8, no. 12, 1973.

Hughes, B A and H L Grant, "The effect of internal waves on surface wind waves 1. Experimental measurements," **J. Geophys. Res.**, vol. 83, pp. 443 - 454, 1978.

Huntley, J M, "An image processing system for the analysis of speckle photographs," **J. Physics E: Scientific Instrum.**, vol. 19, pp. 43 - 49, 1986.

Keane, R D and R J Adrian, "Optimization of particle image velocimeters part 2: multiple pulsed systems," **Measurement Science and Technology**, vol. 2, pp. 963 - 974, 1991.

Korteweg, D J and G de Vires, "On the change of form of long wave advancing in a rectangular canal and on a new type of long stationary waves," **Phil. Mag. (5)**, vol. 39, pp. 422 - 443, 1895.

Kuo, C T and S J Kuo, "Effect of wave breaking on statistical distribution of wave heights," **Civil Engineering in the Oceans**, vol. 3, pp. 1211 - 1231, 1974.

Kwoh, D S W, B M Lake, and H Rungaldier, "Microwave scattering from internal wave modulated surface waves: A shipboard real aperture coherent radar study in the Georgia Strait experiment," **J. Geophys. Res.**, vol. 93, pp. 12235 - 12248, 1988.

Lambrako, K F, "Extended velocity potential wave kinematics," **J. Waterway, Port, Coastal and Ocean Div., ACSE**, vol. 107, pp. 159 - 174, 1981.

Laing, A K, "Nonlinear properties of random gravity waves in water of finite depth," **J. Phys. Oceangraphy**, vol. 16, pp. 2013 - 2030, 1986.

Le Méhauté, B, "**An Introduction to Hydrodynamics and Water Waves**," Springer Verlag, Dusseldorf, 1976.

Le Méhauté, B, D Divoky, and A Lin, "Shallow water waves: a comparison of theories and experiments," **Proc. Amer. Soc. Civ. Eng. (11th Conf. Coastal Eng.)**, vol. 1, pp. 86 - 107, 1968.

Lewis, J E, B M Lake, and D R S Ko, "On the interaction of internal waves and surface gravity waves," **J. Fluid Mech.**, vol. 63, pp. 773 - 800, 1974.

Longuet-Higgins, M S, "On the mass, momentum, energy and circulation of a solitary wave," **Proc. Roy. Soc. Lond. A**, vol. 337, pp. 1 - 13, 1974.

Longuet-Higgins, M S, "The instabilities of gravity waves of finite amplitude in deep water. I. Superharmonic," **Proc. R. Soc. Lond. A**, vol. 360, pp. 471 - 488, 1978 a.

Longuet-Higgins, M S, "The instabilities of gravity waves of finite amplitude in deep water. II. Subharmonic," **Proc. R. Soc. Lond. A**, vol. 360, pp. 489 - 505, 1978 b.

Longuet-Higgins, M S, "The propagation of short surface waves on longer gravity waves," **J. Fluid Mech.**, vol. 177, pp. 293 - 306, 1987.

Longuet-Higgins, M S and E D Cokelet, "The deformation of steep surface waves on water---I. A numerical method of computation," **Proc. R. Soc. Lon. A**, vol. 350, pp. 1 - 26, 1976.

Longuet-Higgins, M S and J D Fenton, "On the mass, momentum, energy and circulation of a solitary wave II," **Proc. Roy. Soc. Lond. A**, vol. 340, pp. 471 - 493, 1974.

Longuet-Higgins, M S and R W Stewart, "Changes in the form of short gravity waves on long waves and tidal currents," **J. Fluid Mech.**, vol. 8, pp. 565 -583, 1960.

Longuet-Higgins, M S and R W Stewart, "The changes in amplitude of short gravity waves on steady non-uniform currents," **J. Fluid Mech.**, vol. 10, pp. 529 - 549, 1961.

Longuet-Higgins, M S and R W Stewart, "Radiation stress and mass transport in gravity waves, with application to 'surf beats'," **J. Fluid Mech.**, vol. 13, pp. 481 - 504, 1962.

Longuet-Higgins, M S and R W Stewart, "Radiation stress in water waves: a physical discussion with application," **Deep Sea Res.**, vol. 11, pp. 529 - 562, 1964.

McLean, J W, "Instabilities of finite-amplitde water waves," **J. Fluid Mech.**, vol. 114, pp. 315 - 330, 1982 a.

McLean, J W, "Instabilities of finite-amplitde gravity waves on water of finite depth," **J. Fluid Mech.**, vol. 114, pp. 331 - 341, 1982 b.

Miller, Sarah J, Omar H Shemdin, and M S Longuet-Higgins, "Laboratory measurements of modulation of short-wave slopes by long surface waves," **J. Fluid Mech.**, vol. 233, pp. 389 - 404, 1991.

Morison, J R, M P O'Brien, J W Johnson, and S A Schaaf, "The force exerted by surface waves on piles," **Petorleum Transactions AIME**, vol. 189, pp. 149 - 154, 1950.

Naciri, M and C C Mei, "Evolution of a short surface wave on a long surface wave of finite amplitude," **J. Fluid Mech.**, vol. 235, pp. 415 - 452, 1992.

Osborne, A R and T L Burch, "Internal Solitons in the Andaman Sea," **Science**, vol. 208, pp. 451 - 460, 1980.

Pawsey, S F and F J Dello Stritto, "Improved wave kinematics from wave staff arrays," in **Offshore Technology Conference**, p. OTC 4587, Houston, Texas, 1983.

Phillips, O M, "**Flow Res. Rep.**," Flow Research Co. Divison of Flow Industries Inc., 1979.

Phillips, O M, "The dispersion of short wavelets in the presence of a dominant long wave," **J. Fluid Mech.**, vol. 107, pp. 465 - 485, 1981.

Pierson (Jr), W J and L Moskowitz, "A proposed spectral form for fully developed wind seas based on the similarity theory of S A Kitaigorodskii," **J. Geophys. Res.**, vol. 69, pp. 5181 - 5190, 1964.

Queen, P A, D J Skyner, C Gray, C A Greated, and W J Easson, "A critical assessment of the particle image velocimetry technique as applied to water waves," **Applied Scientific Research**, 1992.

Ramamonjiarisoa, A and M Coantic, "Loi experimental de dispersion des vagues produites par le vent sur une faible longueur d'action," **C. A. Acad. Sci. Paris**, vol. B282, pp. 111 - 113, 1976.

Ramamonjiarisoa, A and J P Giovanageli, "Observations de la vitesse de propagation des vagues engendrees par le vent au large," **C. A. Acad. Sci. Paris**, vol. B287, pp. 133 - 136, 1978.

Rayleigh, Lord, "On Waves," **Phil. Mag. (5)**, vol. 1, pp. 257 - 279, 1876.

Rodenbusch, G and G Z Forristall, "An empirical for random directional wave kinematics near the free surface," in **Offshore Technology Conference**, p. OTC 5097, Houston, Texas, 1986.

Scott-Russell, J, **14th meeting of the British Association Report**, pp. 311 - 390, York, 1844.

Salter, S H, "Absorbing wavemakers and wide tanks," **Proc. Conf. Directional Wave Spectra Applications (A.S.C.E.)**, pp. 185 - 200, 1982.

Schwartz, L W, "Computer extension and analytic continuation of Stokes' expansion for gravity waves," **J. Fluid Mech.**, vol. 62, pp. 553 - 578, 1974.

She, K, C A Greated, and W J Easson, "Development of a two-dimensional numerical wave tank," **Proc. 2nd Conf. Int. Offshore and Polar Eng.**, vol. 3, pp. 102 -113, San Francisco, CA, 1992.

Shen, I-Fan, W A B Evans, W J Easson, and C A Greated, "The modulation of short waves riding on solitary waves," **Physics of Fluids**, vol. 6, no. 10, pp. 3317 - 3323, 1994.

Skyner, D J, "The Mechanics of Extreme Water Waves," PhD thesis, Edinburgh University, 1992.

Sleath, J F A, "**Sea Bed Mechanics**," John Wiley & Son, 1984.

Sobey, R J, "Wave theory predictions of crest kinematics," In **Water Wave Kinematics**, eds Torum & Gudmestad, NATO ASI Ser, pp. 215 - 231, 1990.

Sobey, R J, "A local Fourier approximation method for irregular wave kinematics," **Applied Ocean Research**, vol. 14, pp. 93 - 105, 1992.

Stewart, R H, "**Methods of Satellite Oceanography**," University of California Press, 1985.

Stokes, G G, "On the theory of oscillatory waves," **Trans. Camb. Phil. Soc.**, vol. 8, pp. 441 - 455, 1847.

Sutherland, J, "The Dynamics of Nonlinear Water Wave Groups," PhD thesis, Edinburgh University, 1992.

Sutherland, J, W J Easson, and C A Greated, "The effect of frequency spreading on a two-component sea state," in **Environmental Forces on Offshore Structures and Their Prediction**, Kluwer Academic Publishers, 1990.

The Swamp Group: Ocean Wave Modelling, Plenum Press, New York, 1985.

Tanaka, Mitsuhiro, "The stability of solitary waves," **Phys. Fluids**, vol. 29, no. 3, pp. 650 - 655, 1986.

Unna, P J, "White horses," **Nature Lond.**, vol. 148, pp. 226 - 227, 1941.

Unna, P J, "Waves and tidal streams," **Nature Lond.**, vol. 149, pp. 219 - 220, 1942.

Watson, K M and B J West, "A transport-equation description of nonlinear ocean surface wave interaction," **J. Fluid Mech.**, vol. 70, pp. 815 - 826, 1975.

West, B J, K A Brueckner, and R S Janda, "A new numerical method for surface hydrodynamics," **J Geophys. Res.**, vol. 92, no. C11, pp. 11803 - 11824, 1987.

Wheeler, J D, "Method for calculating forces produced by irregular waves," **J. Petroleum Tech.**, pp. 359 - 367, 1969.

Whitham, G B, "A general approach to linear and nonlinear dispersive using a Lagrangian," **J. Fluid Mech.**, vol. 22, pp. 273 - 283, 1965.

Zakharov, V E, "Stability of periodic waves of finite amplitude on the surface of a deep fluid," **J. Appl. Mech. Tech. Ph.**, vol. 2, pp. 190 - 194, 1968.

Zhang, J, "Nonlinear Interaction Between Surface Water Waves," PhD thesis, MIT, 1987.

Zhang, J and W K Melville, "Evolution of weakly nonlinear short waves riding on long gravity waves," **J. Fluid Mech.**, vol. 214, pp. 321 - 346, 1990.

Zhang, J and W K Melville, "On the stability of weakly nonlinear short waves on finite-amplitude long gravity waves," **J. Fluid Mech.**, vol. 243, pp. 51 - 72, 1992.

Zhang, J, R E Randall, and C A Spell, "On wave kinematics approximate methods," in **Offshore Technology Conference**, p. OTC 6522, Houston, Texas, 1991.

Appendix A

The Conservations

In this appendix A the derivations are going to show for those equations, which are originally related to the conservation theory and are shown in Chapter 3.

A.1 The Phase Conservation

The wave-train is assumed to remain 'coherent' which is a definition from optics: that is, it can be always described, locally, in terms of a single wave-mode of wavenumber $\vec{k}$. The frequency relative to the fixed co-ordinates is $\omega = \sigma + \vec{U} \bullet \vec{k}$, where ω satisfies the linear dispersion relation. σ is the local frequency as seen by an observer moving with the current velocity $\vec{U}$. If the variational principle is valid, then $\frac{\partial \vec{k}}{\partial t} + \nabla \omega = 0$.

$$\frac{\partial \vec{k}}{\partial t} + \nabla (\sigma + \vec{U} \bullet \vec{k}) = 0 \qquad \text{(EQ A1)}$$

(A1) is called the equation of conservation of phase or wave crests.

Since the steady state is considered and $H_0 = U_0/C$, the time derivative of (A1) has to be ignored. It is convenient to consider the conservation theory for one wave train with respect to another potential flow, which is constructed by the velocity potential and the stream function Φ and Ψ, therefore an orthogonal co-ordinate (s-n) has been defined.

$$s \equiv \frac{\phi}{C}, n \equiv \frac{\Psi}{C} \qquad \text{(EQ A2)}$$

$$\frac{\partial}{\partial s}[\sigma + kH_0U_0] = 0 \qquad \text{(EQ A3)}$$

$$\frac{\partial}{\partial s}[kH_0U_0] = -\frac{\partial \sigma}{\partial s} \qquad \text{(EQ A4)}$$

Let (A4) be divided by kH_0U_0, and then

$$\frac{1}{kH_0U_0}\frac{\partial}{\partial s}(kH_0U_0) = -\frac{1}{kH_0U_0}\frac{\partial \sigma}{\partial s} \qquad \text{(EQ A5)}$$

(A6) provides the dispersion relation and substitutes into (B5).

$$\sigma^2 = H_0^2 g_1 k \qquad \text{(EQ A6)}$$

$$\frac{\partial}{\partial s} lnk + \frac{\partial}{\partial s} lnH_0U_0 = -\frac{1}{\frac{\sigma^2}{H_0^2 g_1} H_0U_0}\frac{\partial \sigma}{\partial s} \qquad \text{(EQ A7)}$$

$$= -\frac{H_0 g_1}{\sigma U_0}\frac{\partial}{\partial s} ln\sigma \qquad \text{(EQ A8)}$$

$$= -\frac{H_0 g_1}{2\sigma U_0}\frac{\partial}{\partial s} lnH_0^2 g_1 k \qquad \text{(EQ A9)}$$

$$= -\frac{1}{2R_c}\frac{\partial}{\partial s} lnH_0^2 g_1 - \frac{1}{2R_c}\frac{\partial}{\partial s} lnk \qquad \text{(EQ A10)}$$

where $R_c = C\frac{\sigma}{g_1}$

$$(1 + \frac{1}{2R_c})\frac{\partial}{\partial s} lnk = -\frac{1}{2R_c}\frac{\partial}{\partial s} lnH_0^2 g_1 - \frac{\partial}{\partial s} lnH_0U_0 \qquad \text{(EQ A11)}$$

$$\frac{1}{k}\frac{\partial k}{\partial s} = -\frac{2}{H_0}\frac{\partial H_0}{\partial s} - \frac{1}{2g_1(R_c + \frac{1}{2})}\frac{\partial g_1}{\partial s} \qquad \text{(EQ A12)}$$

A.2 The Conservation of Wave Action

The definition for wave action $A \equiv E/\omega$ is necessary. Wave action conservation was first introduced by Whitham (1965). For coherent wave-trains, the function Θ satisfies a variational principle with respect to variations in amplitude a and phase $\chi = \hat{k} \bullet \hat{x} - \omega t + \Delta$, namely

$$\frac{\partial \Theta}{\partial a}, \frac{\partial}{\partial t}\left(\frac{\partial \Theta}{\partial \chi_t}\right) + \nabla \bullet \frac{\partial \Theta}{\partial (\nabla \chi)} - \frac{\partial \Theta}{\partial \chi} = 0 \qquad \text{(EQ A13)}$$

Because of the averaging Θ is independent of χ. Also, by definition, $\chi_t = -\omega$ and $\nabla\chi = \hat{k}$ and so the latter equation is

$$\frac{\partial A}{\partial t} + \nabla \bullet B = 0, A = \frac{\partial \Theta}{\partial \omega}, B = -\frac{\partial \Theta}{\partial \hat{k}} \qquad \text{(EQ A14)}$$

The equation $\partial\Theta/\partial a = 0$ yields a nonlinear dispersion relation and the linear one is recovered on letting $a \rightarrow 0$. In the presence of a slowly-varying mean flow $\vec{U}$, the latter dispersion relation has the form $\omega = \vec{U} \bullet \hat{k} + \Omega(\hat{k})$ relating $\hat{k}$ to ω. Accordingly,

$$B = -\frac{\partial \Theta}{\partial \hat{k}} = -\frac{\partial \Theta \partial \omega}{\partial \omega \partial \hat{k}} = A(\vec{U} + C_g) \qquad \text{(EQ A15)}$$

where $C_g = \partial\Omega/\partial\hat{k}$, and a result of the form for wave action conservation (B15) is established.

$$\frac{\partial A}{\partial t} + \nabla \bullet ((\vec{U} + C_g)A) = 0 \qquad \text{(EQ A16)}$$

For a linear wave,

$$A = \frac{1}{2}\bar{g}|a_d|^2, C_g = \frac{\sigma}{2k_d} \qquad \text{(EQ A17)}$$

where $|a_d|$ is the local amplitude of short waves, $\bar{g} = g\cos\theta$, and $k_d = H_0 k$.

A.3 Dean's Stream Function

There are two applications of this method, both described explicitly in the original paper (Dean 1965). First, Dean's case A examplifies the solution to the problem of a wave of steady, defined surface profile. Secondly, Dean's case B provides a solution to the design wave problem. Both solutions proceed in a similar way. The stream function is described as an expansion in sinusoidal forms. The coefficients for these sinusoidal terms are then derived by reducing the errors between the numerical prediction and the values for the boundary conditions. Dean's methods (case A and B) have been extended to very high order by Chaplin (1980) whose programs are now commercially available as **MSTR56**.

Figure A.1 gives the comparison of horizontal velocity profiles under the long wave crest for the regular wave case **e5t8** with Dean's solution, which is obtained from **MSTR56**, and the PIV measurement. Furthermore, a method by Longuet-Higgins and Stewart (1964), who first introduced radiation stresses in water waves, is employed for predicting the kinematics of short waves riding on long waves, see fig. A.2.

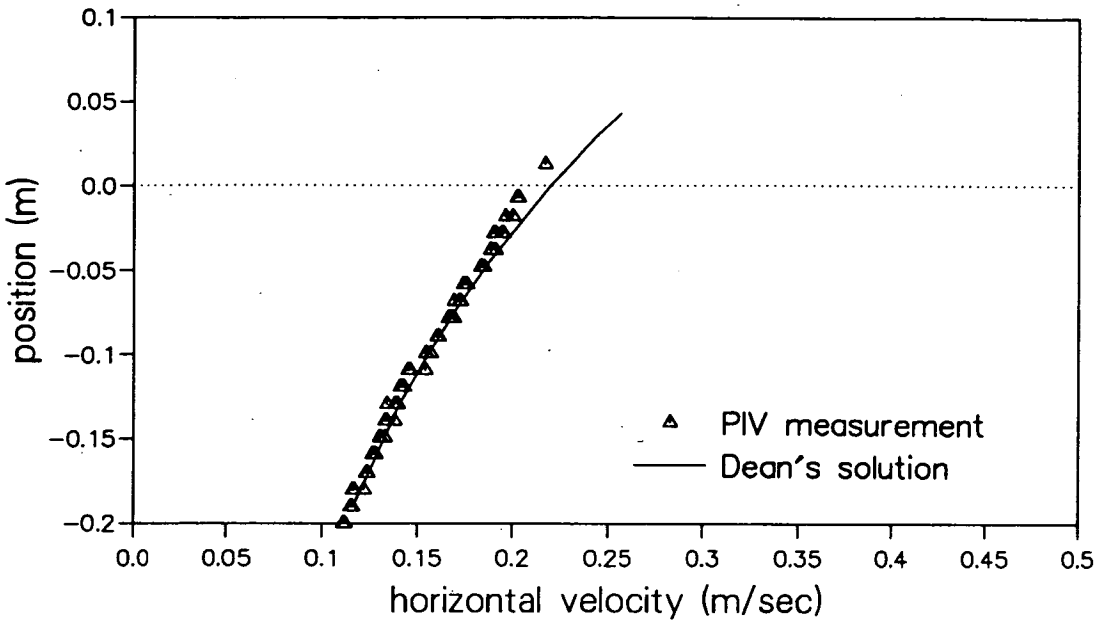

Fig. A.1 The comparison of the horizontal velocity under the crest of regular waves for the case of **e5t8** (regular waves) between the PIV measurement and Dean's solution (the horizontal dashed line is MWL).

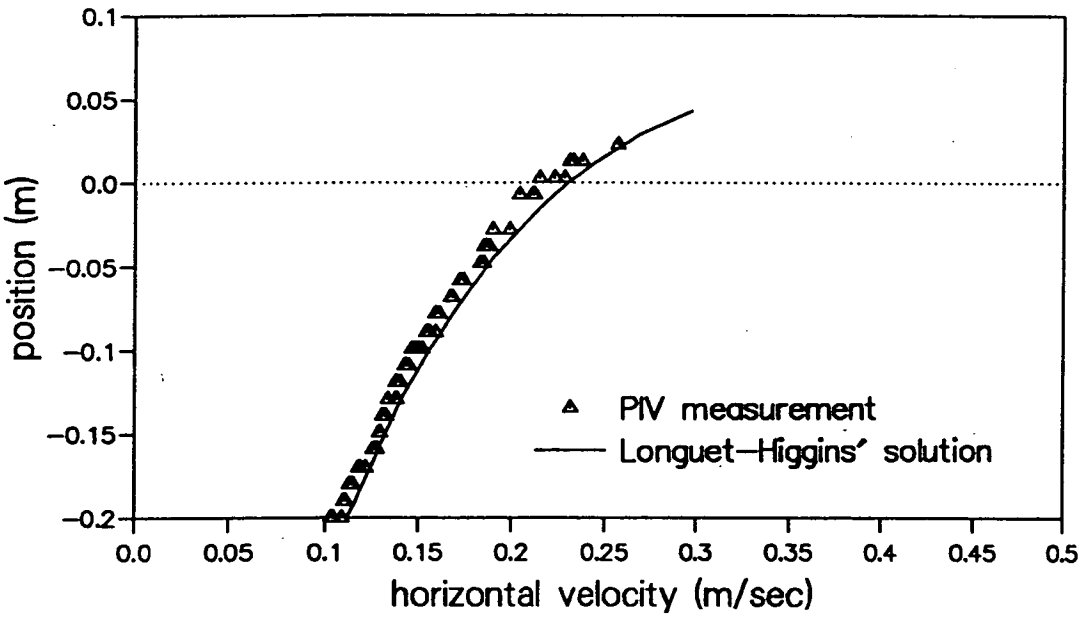

Fig. A.2 The comparisons of the horizontal velocity under the crest of regular waves for the case of **e6t4** (two-component waves) between the PIV measurement and Longuet-Higgins' solution (the horizontal dashed line is MWL).

The solution of **MSTR 56** are only based on wave height and period. For the case of regular waves, Dean's case A, it gives a good prediction. Longuet-Higgins' method considers the kinematics contribution of short waves by the equation of radition stress, while short waves riding on long waves, and fig. A.2 shows that the prediction of Longuet-Higgins and Stewart (1964) fits the PIV measurement very well.